THE EFFECT OF DIETARY ADDED SUGAR INTAKE ON CEREBROVASCULAR FUNCTION AND BRAIN HEALTH

by

Faria Sanjana

A dissertation submitted to the Faculty of the University of Delaware in partial fulfillment of the requirements for the degree of Doctor of Philosophy in Applied Physiology

Summer 2023

© 2023 Faria Sanjana
All Rights Reserved

THE EFFECT OF DIETARY ADDED SUGAR INTAKE ON CEREBROVASCULAR FUNCTION AND BRAIN HEALTH

by

Faria Sanjana

Approved: _____

David G. Edwards, Ph.D.
Chair of the Department of Kinesiology and Applied Physiology

Approved: _____

William B. Farquhar, Ph.D.
Dean of the College of Health Sciences

Approved: _____

Louis F. Rossi, Ph.D.
Vice Provost for Graduate and Professional Education and
Dean of the Graduate College

I certify that I have read this dissertation and that in my opinion it meets the academic and professional standard required by the University as a dissertation for the degree of Doctor of Philosophy.

Signed: _____

Christopher R. Martens, Ph.D.
Professor in charge of dissertation

I certify that I have read this dissertation and that in my opinion it meets the academic and professional standard required by the University as a dissertation for the degree of Doctor of Philosophy.

Signed: _____

Shannon L. Lennon, Ph.D.
Member of dissertation committee

I certify that I have read this dissertation and that in my opinion it meets the academic and professional standard required by the University as a dissertation for the degree of Doctor of Philosophy.

Signed: _____

William B. Farquhar, Ph.D.
Member of dissertation committee

I certify that I have read this dissertation and that in my opinion it meets the academic and professional standard required by the University as a dissertation for the degree of Doctor of Philosophy.

Signed: _____

Curtis L. Johnson, Ph.D.
Member of dissertation committee

ACKNOWLEDGMENTS

My passion for the life sciences began in middle school and carried over throughout my higher education. Following my Master's degree, I found myself in a research assistant position in an integrative physiology laboratory at the New Jersey Veterans Affairs Medical Center. It was in this laboratory under the mentorship of Dr. Jorge Serrador that I discovered a real love of physiology, particularly cerebrovascular physiology, which was an area that I wanted to explore for a PhD education. As luck would have it, I was recruited in Dr. Chris Martens' Neurovascular Aging (NOVA) Laboratory for my PhD in applied physiology. Thank you, Dr. Martens for believing in me to become one of your first PhD students. The list of things I learnt from you is extensive among which setting up a new laboratory, a multitude of laboratory techniques, scientific writing and oral presentation skills, are a few examples. You always encouraged and pushed me into exploring new territories (e.g., learning all things MRI) and knew that I would find my way at times when I thought I would not be able to, all while offering me much needed guidance and support.

Thank you to my committee members, Dr. Curtis Johnson, who played an integral role in supporting me from my first year as a PhD student as I picked up my MRI skills, Dr. Shannon Lennon, who offered guidance on my dissertation as an expert in nutrition and vascular physiology, and Dr. William Farquhar who offered advice based on his years of expertise in vascular physiology and controlled-feeding studies. To current and former NOVA lab members: Ted- thank you for being the go-to person to answer my spur-of-the-moment questions and for assisting me with study

visits during times when we did not have a big lab; Josh- thank you for making participant recruitment easy during my first few years at the NOVA lab. To the newer NOVA lab members: Kevin and Nick – I cannot thank you enough for sacrificing your sleep and time to spend 6 hours on my dissertation study visits; Fiona- thank you for offering your pets as my stress relief; Cat- thank you for taking over liquid nitrogen and food transport and for assisting me with the last few participants' recruitment. A huge thank you goes to members of the Johnson lab- Peyton and Mary who offered tremendous support in helping me learn MRI and with analyzing MRE data and to Dr. Alex Cerjanic who helped me set up the ASL protocol for my dissertation project. My sincerest gratitude goes to Wendy, our research nurse, Elizabeth, NOVA lab research assistant, Kristina, our research dietician, and Seran, COBRE wet lab coordinator, Trevor (and other CBBI staff) – my dissertation would not have progressed without your assistance and expertise.

Lastly, I would like to dedicate my dissertation to my mom who always inspired me to dream big and told me that I could achieve anything at a very young age. I would not be here without my dad from whom I inherited my love for science and my sister and brother-in-law who are stellar examples in my life. To my husband, Rakean- we went through a long-distance marriage, a pandemic, and cancer during my PhD journey, and you were there with me every step of the way with your unwavering support and belief that I could finish this. Thank you to my in-laws for their encouragement and patience and to my kitty-Lizzy who I fell in love with while fostering during the last few months of my PhD. It truly takes a village to complete a PhD and I could not be more grateful for mine!

TABLE OF CONTENTS

LIST OF TABLES ix
LIST OF FIGURES x
ABSTRACT xiv

Chapter

1 REVIEW OF LITERATURE 1

1.1 Introduction 1
1.2 Cerebrovascular System: Cerebrovascular Anatomy 3
1.3 The Blood-Brain Barrier (BBB) 5
1.4 Regulation of Cerebral Blood Flow 6

1.4.1 Assessment of Cerebral Blood Flow: Arterial-Spin Labeling 7
1.4.2 Regulation of Cerebral Blood Flow by Carbon Dioxide 10

1.4.2.1 Cerebrovascular Reactivity to Carbon Dioxide 12
1.4.2.2 Stimulus Delivery for Cerebrovascular CO_2 Reactivity 14

1.5 The Hippocampus: Structure and Function 15

1.5.1 Assessment of Hippocampal Tissue Structural Properties: Magnetic Resonance Elastography 16
1.5.2 Relation between Cerebral Blood Flow and Brain Tissue Viscoelastic Properties 18

1.6 Diet and Brain Health 18

1.6.1 Fructose Transport and Metabolism 20
1.6.2 Fructose-Induced Hypertriglyceridemia 23
1.6.3 Triglyceride-Rich VLDL Transport and Metabolism 24
1.6.4 Hypertriglyceridemia-Induced Peripheral Vascular Endothelial Dysfunction 25
1.6.5 Fructose-Induced Hyperuricemia, Oxidative Stress and Lipid Accumulation 28

1.6.6 Uric Acid-Induced Peripheral Vascular Endothelial Dysfunction....29

1.7 Effect of Acute Added Sugar Intake on Peripheral Vascular Endothelial Function....31
1.8 Effect of Acute Added Sugar Intake on Cerebral Blood Flow....32
1.9 Peripheral vs. Cerebrovascular Endothelial Function....33
1.10 Conclusion....35

2 ASSOCIATION AMONG BLOOD LIPIDS, HIPPOCAMPAL TISSUE VISCOELASTIC PROPERTIES, AND CEREBROVASCULAR FUNCTION....36

2.1 Introduction....36
2.2 Methods....37

2.2.1 Study Participants....38
2.2.2 Blood Lipids Analysis....39
2.2.3 Hippocampal Tissue Viscoelastic Properties....39
2.2.4 Cerebrovascular Reactivity....40

2.2.4.1 Cerebral Perfusion Quantification....41

2.2.5 Statistical Analysis....43

2.3 Results....44

2.3.1 Blood Lipids and Hippocampal Tissue Viscoelastic Properties....47
2.3.2 Cerebrovascular Function and Hippocampal Tissue Viscoelastic Properties....49
2.3.3 Cerebrovascular Function as Mediator of Blood Lipids on Hippocampal Tissue Viscoelastic Properties....50

2.4 Discussion....54
2.5 Conclusions....60

3 ACUTE EFFECTS OF DIETARY ADDED SUGARS ON CEREBROVASCULAR FUNCTION AND BRAIN TISSUE VISCOELASTIC PROPERTIES....62

3.1 Introduction....62
3.2 Methods....65

3.2.1 Study Protocol....65

3.2.2 Study Participants....66
3.2.3 Study Meals....67
3.2.4 Blood Analysis....68
3.2.4.1 Measurement of Oxidative Stress....68
3.2.4.2 Measurement of Total Antioxidant Capacity....69
3.2.5 Cerebrovascular Reactivity....69
3.2.5.1 Measurement of Cerebral Perfusion....70
3.2.6 Brain Tissue Viscoelastic Properties....72
3.2.7 Cognitive Tasks....72
3.2.8 Statistical Analysis....73
3.3 Results....74
3.3.1 Serum Lipids and Uric Acid....79
3.3.2 Oxidative Stress and Total Antioxidant Capacity....81
3.3.3 Vascular Properties and Cerebrovascular Reactivity....83
3.3.4 Whole Brain and Hippocampal Tissue Viscoelastic Properties....86
3.3.5 Cognitive Tasks....88
3.3.6 Responsiveness to Meals....89
3.4 Discussion....90
3.5 Conclusions....98
4 CONCLUSION....99
4.1 Summary....99
4.2 Perspectives....101
REFERENCES....103
Appendix
IRB APPROVAL LETTER....133

LIST OF TABLES

Table 2.1 Screening characteristics 45

Table 2.2 Baseline blood chemistries 46

Table 2.3 Bivariate correlation between serum lipids and hippocampal tissue viscoelastic properties 47

Table 2.4 Bivariate correlation matrix between cerebrovascular measures and hippocampal viscoelastic properties 50

Table 3.1 Screening characteristics 76

Table 3.2 Baseline blood chemistries 77

Table 3.3 Dietary intake 78

Table 3.4 Serum lipids 80

Table 3.5 Cerebrovascular variables 85

LIST OF FIGURES

Figure 1.1 Cerebrovascular anatomy. Blood is supplied to the brain by two pairs of major arteries that branch into cerebral arteries and forms the Circle of Willis at the base of the brain. Figure from file freely available through public domain (Medical News Today) 4

Figure 1.2 Arterial spin-labeling. Hydrogen nuclei in blood water are labeled at the neck vessels by radiofrequency pulses and carried upstream. The labeled blood-water is allowed to sufficiently perfuse into the brain tissue for acquisition after a post-labeling delay. A control image, obtained without labeling, is subtracted from the labeled image that suppresses the static tissue signal to form a perfusion-weighted image, which is quantitatively proportional to cerebral blood flow. Figure from Ferre et al., Diagn Interv Imaging, 2013 (54). Originally published by and used with permission from Elsevier. 8

Figure 1.3 Metabolism of fructose vs. glucose. Fructose is oxidized to CO_2 and fatty acids in the liver, while glucose is either released into the circulation or converted into glycogen. Figure from Tappy and Le, Physiol Rev, 2010 (180). Originally published by and used with permission from American Physiological Society. 21

Figure 1.4 Fructose to uric acid metabolism. Rapid phosphorylation of fructose leads to degradation of ATP to AMP, which activates AMP deaminase and converts AMP to IMP and ultimately uric acid. Figure from Johnson et al., J Am Soc Nephrol, 2010 (195). Originally published by and used with permission from Wolters Kluwer Health, Inc.....22

Figure 1.5 Pathophysiology of triglyceride-rich lipoproteins (TRLs) in endothelial dysfunction and inflammation. TRLs enter the subendothelial space and contributes to endothelial dysfunction. TRLs are also taken up by macrophages which combine with monocytes and release inflammatory products to form foam cells. Further cholesterol loading causes these foam cells to become atherosclerotic plaques. Figure from Toth, Vasc Health Risk Manag, 2016 (235). Originally published by and used with permission from Dove Medical Press Ltd. 27

Figure 1.6 Possible mechanism of uric acid-induced endothelial dysfunction. Xanthine oxidase facilitates the conversion of hypoxanthine and xanthine to uric acid after ATP is degraded due to fructose phosphorylation. This process reduces oxygen to superoxides that scavenge nitric oxide leading to the production of peroxynitrites and reduced nitric oxide bioavailability. Figure from Maruhashi et al., Atherosclerosis, 2018 (245). Originally published by and used with permission from Elsevier. 30

Figure 2.1 Association between serum triglycerides and (**A**) hippocampal stiffness (clinically high TG participant included); N=21; (**B**) hippocampal damping ratio (clinically high TG participant included); N=21; (**C**) hippocampal stiffness (clinically high TG participant removed); N=20; (**D**) hippocampal damping ratio (clinically high TG participant removed); *p < 0.05; N=20; dashed lines represent 95% confidence interval. 49

Figure 2.3 Mediation models between LDL-C and hippocampal stiffness showing no mediating effect of (A) gray matter perfusion and (B) hippocampal perfusion; *p < 0.05; N=21 51

Figure 2.4 Mediation models between triglycerides and hippocampal damping ratio showing no mediating effect of (A) gray matter perfusion and (B) hippocampal perfusion; *p < 0.05; N=20 52

Figure 2.5 Mediation models between LDL-C and hippocampal stiffness showing no mediating effect of (A) gray matter cerebrovascular reactivity and (B) hippocampal cerebrovascular reactivity; *p < 0.05; N=21.....53

Figure 2.6 Mediation models between triglycerides and hippocampal damping ratio showing no mediating effect of (A) gray matter cerebrovascular reactivity and (B) hippocampal cerebrovascular reactivity; *p < 0.05; N=20 54

Figure 3.1 (**A**) Triglyceride concentration at baseline and 3-hours postprandial following high-sugar and low-sugar meal. (**B**) Change in triglyceride concentration following high-sugar and low-sugar meal. HS: high-sugar meal; LS: low-sugar meal; PRE: baseline; POST: postprandial; *p < 0.05; N=22.....80

Figure 3.2 (**A**) Uric acid concentration at baseline and 3-hours postprandial following high-sugar and low-sugar meal. (**B**) change in uric acid concentration following high-sugar and low-sugar meal. HS: high-sugar meal; LS: low-sugar meal; PRE: baseline; POST: postprandial; *p < 0.05; N=22.....81

Figure 3.3 Superoxide (**A**) concentration and (**B**) number following high-sugar and low-sugar meal. HS: high-sugar meal; LS: low-sugar meal; PRE: baseline; POST: postprandial; *p < 0.05; N=22 82

Figure 3.4 (**A**) Total antioxidant capacity at baseline and 3-hours postprandial following high-sugar and low-sugar meal. (**B**) change in total antioxidant capacity following high-sugar and low-sugar meal. HS: high-sugar meal; LS: low-sugar meal; *p < 0.05; N=20 83

Figure 3.5 Systolic (**A**) and diastolic (**B**) blood pressure at baseline and 3-hours postprandial following high-sugar and low-sugar meal. HS: high-sugar meal; LS: low-sugar meal; PRE: baseline; POST: postprandial; *p < 0.05; N=22.....84

Figure 3.6 (**A**) Gray matter and (**B**) hippocampal cerebrovascular reactivity at baseline and 3-hours postprandial following high-sugar and low-sugar meal. CBF: cerebral blood flow; GM: gray matter; HC: hippocampus; HS: high-sugar meal; LS: low-sugar meal; PRE: baseline; POST: postprandial; *p < 0.05; N=20.....86

Figure 3.7 Whole brain (**A**) stiffness and (**B**) damping ratio at baseline and 3-hours postprandial following high-sugar and low-sugar meal. HS: high-sugar meal; LS: low-sugar meal; PRE: baseline; POST: postprandial; *p < 0.05; N=17.....87

Figure 3.8 Hippocampal (**A**) stiffness and (**B**) damping ratio at baseline and 3-hours postprandial following high-sugar and low-sugar meal. HS: high-sugar meal; LS: low-sugar meal; PRE: baseline; POST: postprandial; *p < 0.05; N=17.....88

Figure 3.9 (**A**) Pattern Comparison Processing Speed (**B**) Dimensional Change Card Sort (**C**) Flanker Inhibitory Control and Attention test corrected T-scores at baseline and 3-hours postprandial following high-sugar and low-sugar meal. HS: high-sugar meal; LS: low-sugar meal; PRE: baseline; POST: postprandial; *p < 0.05; N=10 89

Figure 3.10 Association between baseline triglycerides and 3-hours postprandial changes in triglyceride concentration following a high-sugar and low-sugar meal; HS: high-sugar meal; LS: low-sugar meal; TG: triglycerides; *p < 0.05; N=22 90

ABSTRACT

Alzheimer's disease (AD) is the most common form of dementia and the fifth leading cause of death in the United States. AD shares many of the same modifiable risk factors as cardiometabolic diseases, which includes aberrant blood lipids such as increased blood triglycerides (TGs), which are associated with reduced brain tissue microstructural integrity and poor memory performance. Additionally, a high consumption of added sugars typically from a Western diet, is associated with elevated cardiometabolic parameters that likely contribute to cognitive aging. Increased added sugar intake acutely raises blood TGs and uric acid and is associated with reduced peripheral vascular endothelial function via the production of reactive oxygen species (ROS). Limited research suggests that acute added sugar intake may be associated with reduced cerebral blood flow. As such, repetitive acute insults to the cerebrovasculature from increased added sugar consumption may result in long-term reductions in brain tissue properties through sustained reductions in cerebrovascular function. **OBJECTIVES**: To evaluate the associations among habitually elevated blood lipids, acute dietary added sugar intake, cerebrovascular function, and brain tissue viscoelastic properties in humans through the following aims: 1) Determine whether habitually elevated blood lipids are cross-sectionally associated with lower hippocampal (HC) tissue properties and assess whether this relation is moderated by cerebrovascular function. 2) Determine whether acute consumption of a high-sugar (HS) meal is associated with a transient reduction in cerebrovascular function, brain tissue properties and cognitive (executive) function compared to a low-sugar (LS)

meal, and assess whether these reductions are correlated to an increase in blood lipids, uric acid and markers of ROS. **HYPOTHESES**: 1) Elevated blood lipids will be associated with lower HC tissue properties and this relation will be mediated by reduced cerebrovascular function. 2) Acute consumption of a HS meal will be associated with a transient reduction in cerebrovascular function, brain tissue properties and cognitive (executive) function compared to a LS meal, and these reductions will be correlated to an increase in blood lipids, uric acid and markers of ROS. **METHODS**: Healthy young and mid-life adults were enrolled in a randomized-controlled crossover trial that consisted of a single meal high in added sugars (HS: 61 g) and a single meal low in added sugars (LS: 16 g). Serum lipids and uric acid were assessed at baseline and 3 hours postprandial following both meals. ROS levels were measured as superoxide concentration and assessed with electron paramagnetic resonance. Cerebral perfusion and cerebrovascular reactivity to hypercapnia was assessed using arterial-spin labeling coupled with prospective end-tidal targeting. Brain tissue viscoelastic properties were assessed using magnetic resonance elastography. **RESULTS**: Twenty-two participants [9M/13F, age: 48±12 y (range: 30-64 y), BMI: 24.7±2.8 kg/m^2, BP: 116±11/73±6 mmHg) were included in this study. Baseline LDL-C was significantly associated with HC stiffness ($r=-0.42$, $p=0.049$) while baseline TG was significantly associated with HC damping ratio ($r=0.46$, $p=0.04$). These associations were not mediated by cerebrovascular function. Serum TG concentration was higher following both meals (Time: $p<0.0001$; Meal: $p=0.29$; Interaction: $p=0.07$) where the increase tended to be greater following the HS meal ($p=0.06$). Serum uric acid concentration was reduced following both meals (Time: $p<0.0001$; Meal: $p=0.80$; Interaction: $p=0.0003$) and the reduction was greater

following the HS meal ($p<0.001$). ROS concentration was reduced following both meals (Time: $p=0.002$; Meal: $p=0.14$; Interaction: $p=0.32$). There was no significant change in cerebrovascular function following either meal. Whole brain damping ratio was higher (Time: $p=0.0007$; Meal: $p=0.55$; Interaction: $p=0.21$) and HC stiffness was lower (Time: $p=0.02$; Meal: $p=0.11$; Interaction: $p=0.095$) following both meals. In a subset of participants, executive function increased following both meals, whereas participants' measures of attention and inhibitory control were increased following the HS meal and was decreased following the LS meal. **CONCLUSIONS**: Habitually elevated LDL-C and TGs are associated with a reduction in brain tissue properties, however, this association is not mediated by a reduction in cerebrovascular function. Habitually elevated LDL-C and TGs are associated with a reduction in brain tissue properties, however, this association is not mediated by a reduction in cerebrovascular function. Acute high dietary added sugar intake tends to lead to a greater increase in serum TG concentration and a greater reduction in serum uric acid concentration. There is also a reduction in postprandial ROS concentration following both meals. Brain tissue properties, but not cerebrovascular function, are reduced following both meals, regardless of added sugar content.

Chapter 1

REVIEW OF LITERATURE

1.1 Introduction

Alzheimer's Disease (AD), the most common form of age-related dementia, is a major health concern characterized by neurodegeneration and irreversible memory loss (1). As the number of older adults increases globally, the incidence of AD cases is projected to more than double by 2050 if preventive measures are not undertaken (2). This will not only continue to add to the burden of the disease on the patients themselves, but it will also continue to be a burden on the patients' caregivers in terms of their economic, physical and emotional well-being. Moreover, there is mounting concern over the increasing cost associated with caring for AD patients, which is already at a staggering rate of $305 billion annually and is projected to surpass $1 trillion by 2050 as the population ages (3).

Growing evidence suggests AD and/or age-related cognitive decline share many of the same modifiable risk factors as cardiometabolic and cerebrovascular diseases (4), especially when they develop earlier in life prior to clinically relevant memory loss. These risk factors include elevated blood triglycerides (TGs), low-density lipoprotein cholesterol (LDL-C), and reduced high-density lipoprotein cholesterol (HDL-C) (5). We have recently shown that aberrant blood lipids are cross-sectionally associated with reduced memory performance and neuronal tissue viscoelastic properties of the hippocampus (6), a brain structure essential for memory encoding and recall (7). Despite these associations, the underlying mechanisms linking

elevated blood lipids to brain health, are not completely understood in humans. Elevated blood concentrations of TGs and other lipid particles contribute to peripheral vascular endothelial dysfunction through the promotion of oxidative stress and systemic inflammation (8–12). This is important because peripheral endothelial dysfunction is associated with the development of atherosclerosis as well as an increased risk of age-related cognitive decline (13,14). Relatedly, peripheral vascular endothelial function is known to be correlated with cerebrovascular endothelial function (15,16), and impaired cerebrovascular function is a hallmark of cognitive aging (17,18). Additionally, previous studies have observed that an acute increase in cerebral blood flow (CBF) via hypercapnia results in a transient increase in the overall stiffness of brain tissue, a mechanical property correlated with microstructural integrity (19,20). Therefore, one possible mechanism by which increased blood lipids impact brain health may be through impaired cerebrovascular function.

Consumption of a Western diet (5,21), which is high in added sugars and saturated fat and low in fiber, also contributes to elevated cardiometabolic risk parameters (8), including elevated blood lipids. Elevation of serum TGs and uric acid is consistently observed in individuals who consume foods and beverages high in added sugars (22,23). Fructose, a typical component of added sugars, is especially known to acutely increase postprandial blood TG concentration via *de novo* lipogenesis (24). Reductions in CBF and peripheral vascular endothelial function have been observed following acute added sugar intake (25–33), however, these studies have largely focused on the immediate hyperglycemic response to sugar-sweetened beverages (SSBs) on the vasculature or have studied other pathways of the brain related to appetite and reward behavior. As such, the direct effects of acute added

sugar intake from a Western-style diet on cerebrovascular function are not fully understood. Repetitive acute insults to the cerebral vasculature resulting from a Western diet may culminate in the long-term loss of brain tissue integrity via sustained reductions in CBF, and ultimately lead to cognitive impairment. Therefore, causal evidence for a link between habitually elevated blood lipids, acute added sugar intake and brain health is necessary to prevent loss of brain structure and function in late life. The overall objective of this dissertation is to evaluate the influence of blood lipids and acute added sugar intake on cerebrovascular function and hippocampal tissue viscoelastic properties in humans. This review will focus on the current literature that has examined the effects of added sugar consumption and subsequent increase in blood lipids and uric acid on vascular function.

1.2 Cerebrovascular System: Cerebrovascular Anatomy

The brain is a neurovascular organ that needs a highly developed vascular component to control CBF with exact precision to maintain proper functioning of the neural component. Delivery of oxygen and other substrates, elimination of waste, control of acid-base balance, maintenance of cerebral metabolism, and buffering of the transmission of pressure waves to the cerebral micro-vessels are some of the functions that are carried out by the cerebrovasculature (34).

CBF is supplied by a bilateral pair of extracranial arteries branching off from the aortic root – the internal carotid arteries (ICA) and vertebral arteries (VA). The ICA supplies the anterior portion of the brain, passing through the Foramen Lacerum, proceeding onto the base of the brain, and branching into the middle cerebral arteries (MCA), anterior cerebral arteries (ACA), anterior choroidal, and posterior communicating arteries. The ICA bilaterally supplies ~70% of the brain's total CBF

(35). The VAs enter the cranium posteriorly through the Foramen Magnum and converge into the basilar artery (BA), which divides into a bilateral pair of posterior cerebral arteries (PCA) that serve ~30% of the brain's total CBF. The MCA, ACA, and PCA along with the communicating arteries conjoin to form an anastomotic ring called the Circle of Willis (34). Approximately 50% of individuals have an unconventional or incomplete configuration of the Circle of Willis as it varies among individuals (36).

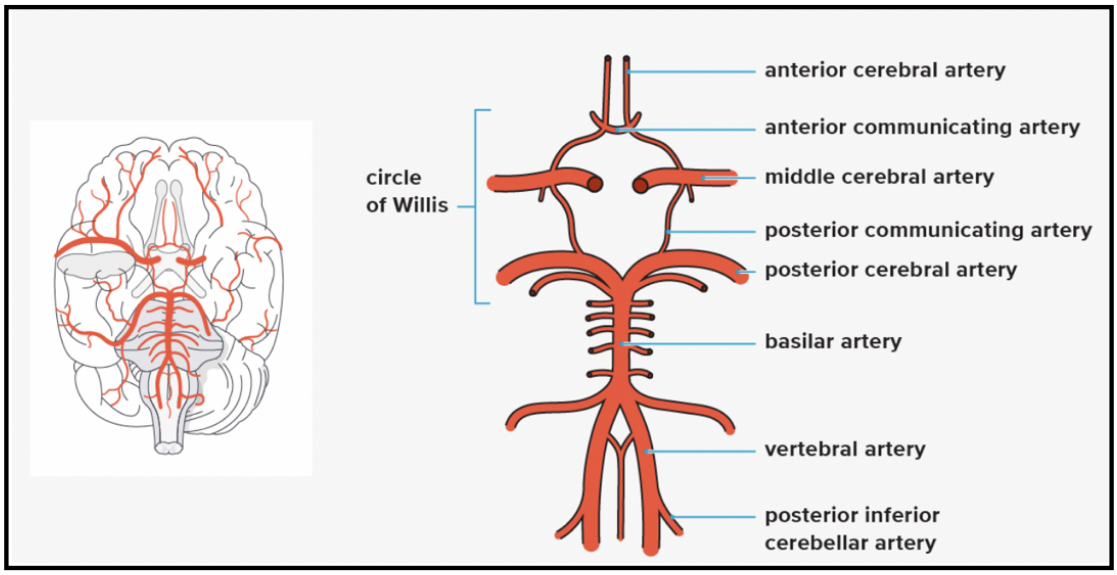

Figure 1.1 Cerebrovascular anatomy. Blood is supplied to the brain by two pairs of major arteries that branch into cerebral arteries and forms the Circle of Willis at the base of the brain. Figure from file freely available through public domain (Medical News Today)

The MCA, ACA, and PCA are major arteries that bifurcate into smaller arteries after branching out from the Circle of Willis (34). These smaller arteries lie adjacent to the parenchyma of the brain, where they are called the pial arteries. These

pial arteries form penetrating arterioles that supply blood to the cortex as they enter the parenchyma (37). As these arterioles enter the parenchyma, they become enclosed by the astrocytic end feet, which envelop all cerebral blood vessels and provide support in controlling CBF.

1.3 The Blood-Brain Barrier (BBB)

The blood-brain barrier (BBB) is a diffusion barrier that prevents entry of most compounds from the blood into the brain. It provides a surface area of ~18 to 25 m^2 for blood-brain exchange (38). The BBB is comprised of three elements of the brain microvasculature – endothelial cells, astrocytic end feet, and pericytes (39). Tight junctions line the endothelial cells and limit paracellular transport of large hydrophilic molecules. Conversely, small lipophilic molecules such as oxygen and carbon dioxide (CO_2) are able to diffuse across the BBB down their concentration gradient (40). Nutrients like glucose and amino acids are also allowed to enter via transporters, while uptake of larger molecules such as insulin and leptin occur via receptor-mediated endocytosis (41). This form of transcellular transport maintains a highly regulated mode of exchange between the blood and the brain.

A capillary basement membrane surrounds the endothelial cell layer (39). Pericytes are embedded in the basement membrane, which is also surrounded by astrocytic end feet that enclose the blood vessels and maintain the integrity of the tight junction barrier. This type of structural placement allows for interaction between the BBB, astrocytes, and pericytes for the proper regulation of BBB function. Disruption of BBB function is attributed to the pathogenesis of many brain-related diseases including stroke and dementia (42).

1.4 Regulation of Cerebral Blood Flow

Proper CBF regulation is achieved when there is a balance between cerebral perfusion pressure and cerebral vascular resistance (34). Cerebral perfusion pressure (CPP) is defined as the amount of blood pressure needed to maintain CBF and it is the net pressure gradient that drives the movement of blood through the cerebral circulation to the tissue. CPP is determined by the difference between mean arterial pressure (MAP) and intracranial pressure (ICP) (43). ICP is the pressure exerted inside the intracranial space and on cerebral tissue by fluids such as the cerebrospinal fluid (CSF). Cerebral vascular resistance is determined by the viscosity of blood (η), length of the vessel (L), and radius of the artery (r). Poiseuille's Law describes laminar flow of a fluid in a rigid cylindrical structure by relating pressure gradient, fluid viscosity, and the length and the radius (or diameter) of the vessel. Accordingly, blood flow (Q) is correlated to the pressure gradient across the vessel and the vessel radius to the fourth power (44). Therefore, according to Poiseuille's Law, CBF is equal to the quotient of CPP divided by cerebrovascular resistance and is represented in the following equation:

$$CBF = \frac{CPP.\pi r^4}{8L\eta}$$

Variable resistance to flow is mostly experienced in the cerebral arteriolar and capillary bed. Conversely, the large cerebral arteries and veins are noncompliant and act mostly as a conduit for pulsatile blood flow from the aorta to the brain (45). CBF needs to be dynamically adjusted to changes in perfusion pressure, brain metabolic activity, autonomic nerve activity and humoral factors in order to protect the cerebral circulation from these changes and to maintain constant perfusion to the brain. There are a number of regulatory mechanisms that carry out CBF regulation. For the purpose of this proposal, CBF regulation by CO_2 will be reviewed in the upcoming sections.

1.4.1 Assessment of Cerebral Blood Flow: Arterial-Spin Labeling

The first experiment to measure CBF in humans was developed by Kety and Schmidt using the arteriovenous dynamics of a freely diffusible tracer, inert nitrous oxide (N_2O), which was passed into the arterial system (46,47). Regional CBF was estimated using a modified Fick's principle in which the concentration of tracer absorbed by the tissue per unit time was equal to the arteriovenous difference of the tracer concentration with the venous concentration being corrected for the difference in blood and tissue water contents. This method is rarely used in patients today but the Kety-Schmidt theory has been applied in numerous imaging techniques such as single-photon emission computed tomography (SPECT) and positron emission tomography (PET) imaging (48). Arterial-spin labeling (ASL) techniques to assess CBF do not use an extrinsic tracer. ASL is a non-invasive magnetic resonance imaging (MRI) technique for measuring tissue perfusion, which uses magnetically labeled blood water protons as an endogenous tracer (49).

ASL MRI perfusion produces a "labeled" or "tag image" and a "control image" in which the static tissue signals are identical but the magnetization of the inflowing blood is different (50). ASL, for the purpose of brain imaging, involves a radiofrequency (RF) pulse that magnetically inverts hydrogen nuclei in water of the blood in the neck, which is known as labeling (51). A tracer that is composed of labeled blood-water is therefore, created by this process. The RF labeling continues for a pre-specified duration, known as the labeling duration. A delay, called post-labeling delay (PLD), is added between labeling and image acquisition to allow the labeled blood-water to pass through the vasculature into the brain tissue and accumulate sufficiently enough to measure as the perfusion signal (50,52). A control image, in which no RF labeling occurs, is subsequently acquired. Tag and control

images are thus acquired in a temporally interleaved manner (53). Labeled images are subtracted from control images, which eliminates the static tissue signal and the remaining signal becomes a relative measure of perfusion proportional to CBF (52). CBF maps are generated when multiple labeled-control image pairs are acquired.

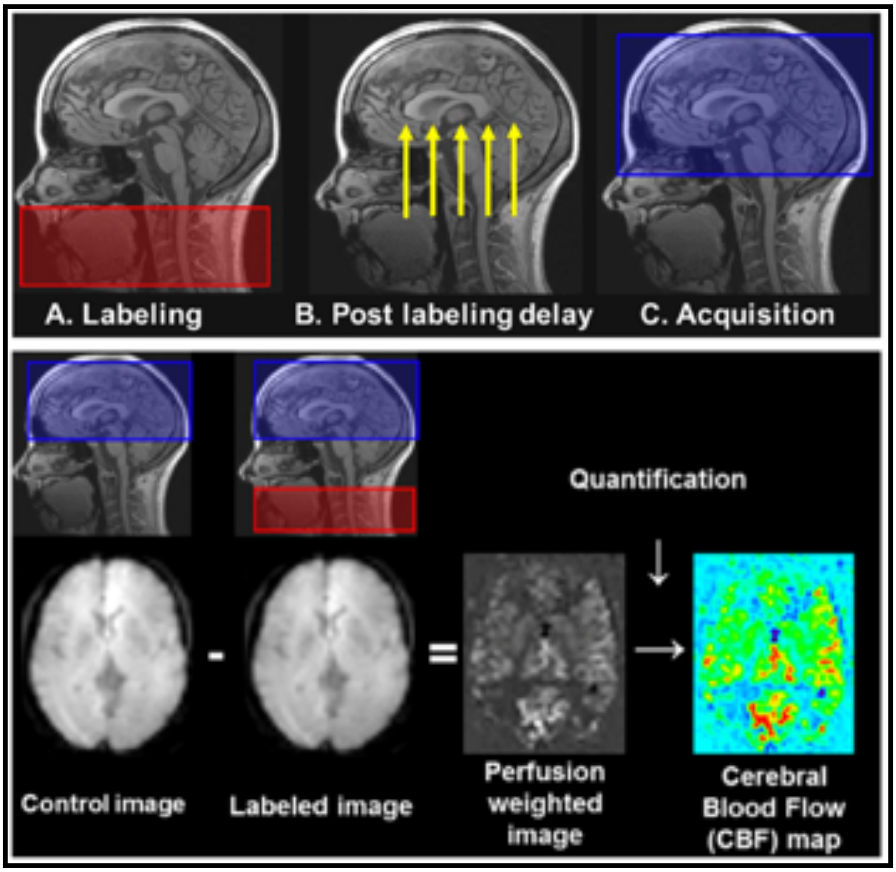

Figure 1.2 Arterial spin-labeling. Hydrogen nuclei in blood water are labeled at the neck vessels by radiofrequency pulses and carried upstream. The labeled blood-water is allowed to sufficiently perfuse into the brain tissue for acquisition after a post-labeling delay. A control image, obtained without labeling, is subtracted from the labeled image that suppresses the static tissue signal to form a perfusion-weighted image, which is quantitatively proportional to cerebral blood flow. Figure from Ferre et al., Diagn Interv Imaging, 2013 (54). Originally published by and used with permission from Elsevier.

Evaluation of cerebrovascular diseases is one of the most frequent clinical applications of perfusion imaging (55). As decreased perfusion is the most common underlying cause of all ischemic strokes, ASL can be applied to study acute stroke in both adult and pediatric populations (49,56). ASL techniques can be used to depict areas of hemispheric perfusion deficits, post ischemic hyperperfusion or perfusion-diffusion mismatches. As such, ASL is a predictor of recurrent strokes. Previous studies have also shown ASL's ability to detect regional hypoperfusion in frontotemporal dementia, AD and mild cognitive impairment (MCI) (57). Moreover, ASL techniques may predict cognitive decline and the conversion from MCI to AD (58). Other clinical applications of ASL include epilepsy (59), arteriovenous malformations (60) central nervous system (CNS) neoplasms (61) and infections (52).

A limitation of ASL is its low signal-to-noise ratio (SNR) and temporal resolution, which results in noise contribution to the control image that may introduce variation in perfusion calculations (62). This limitation is, however, resolved by increasing the repetition time (TR) and using a high magnetic field strength scanner (i.e., 3T) (49). Access to MRI equipment can be difficult and expensive; while many studies use Transcranial Doppler (TCD) ultrasound as an alternative method to quantify CBF, it must be noted that the TCD provides an estimation of CBF because it is not possible to image blood vessel diameters with only the TCD (63). As such, it is assumed that the diameters of large cerebral arteries do not change and CBF velocity is used as a surrogate for CBF (64). However, it has been observed that MCA diameters do change during hypercapnia (between 9-15 mmHg increase in end-tidal partial pressure of CO_2) (65,66), which makes the estimation of CBF from TCD measures unreliable. TCD is also highly operator dependent and is limited to

measuring velocities in large basal arteries (MCA, ACA and the PCA). Hence, using MR-based techniques such as ASL for quantification of CBF appears to be most advantageous.

1.4.2 Regulation of Cerebral Blood Flow by Carbon Dioxide

CO_2 is a potent vasodilator and is a key molecule that regulates blood flow allowing the brain to be constantly perfused. CBF is sensitive to fluctuations in the arterial partial pressure of CO_2 ($PaCO_2$), which has an impact on the respiratory central chemoreceptor stimulus and maintains central pH (43). An increase in $PaCO_2$ is called hypercapnia and results in dilation of the cerebral blood vessels, while a decrease in $PaCO_2$ is called hypocapnia, resulting in cerebrovascular constriction (67). Recent data suggest that the entire cerebral circulation is vasoactive (34) with an increase in $PaCO_2$ between 5-7% resulting in a ~75% increase in CBF (68). Regulation of cerebrovascular resistance during $PaCO_2$ manipulations occur in the large cerebral arteries along with the pial and penetrating micro-vessels (65,66,69–71). This intrinsic sensitivity to $PaCO_2$ makes cerebral vessels unique to those in the periphery (72).

The mechanism of action of CO_2-induced vasodilation is not fully understood. Some evidence suggests that an elevated partial pressure of CO_2 in arterial blood leads to vascular smooth muscle (VSM) relaxation of the cerebral vasculature. A high blood concentration of CO_2 results in a reduction in pH that leads to the activation of ATP-sensitive K^+ and voltage-gated K^+ channels (73) in the VSM, which in turn leads to cerebral vasodilation (74). K^+ efflux, occurring as a result of open K^+ channels, results in hyperpolarization of cerebrovascular endothelial cells (75). Vasodilation occurs when voltage-gated Ca^{2+} channels are closed as a result of hyperpolarizing currents

being transmitted to the VSM. The closure of voltage-gated Ca^{2+} channels lead to a reduction in intracellular Ca^{2+} concentration, and ultimately to relaxation of the vasculature. Additionally, hyperpolarizing currents are also transmitted to neighboring endothelial cells that allow conduction over longer distances along the cerebrovascular endothelium.

Another hypothesis for the mechanism of action of CO_2-induced vasodilation lies in alterations of CO_2/pH-induced vasoactive factors such as the shear-stress mediated vasodilator, nitric oxide (NO) and prostaglandins (PGs) (76,77). NO is synthesized from the amino acid, L-arginine by the enzyme, nitric oxide synthase (NOS). It has been observed in animal models that changes in pH levels can influence NOS activity on the VSM and endothelial cells (78). Endothelial (eNOS) and neuronal (nNOS) NOS are two major isoenzymes of NOS. Even though both of these enzymes are found in astrocytes and neurons (79), nNOS appears to be the modulator of cerebral arterial pH reactivity in perivascular nerves (80). Alternatively, several animal studies have used NOS inhibitors to examine the role of NO in cerebral vasodilation. The majority of these studies found that NOS inhibitors tend to attenuate CBF increases elicited by hypercapnia (81–84), therefore, providing evidence that NO is a major regulator of CO_2-induced vasodilation.

Evidence in human endothelial cells corroborate findings in animal models as robust NO increases are observed under hypercapnic conditions while decreases in NO levels are seen under hypocapnic conditions (85). *In vitro* models of cerebral artery endothelial cells demonstrate increased NO bioavailability when exposed to shear stress (86). Human studies have shown that NO plays a role in CO_2-dependent vasodilation as measured by plasma nitrate (87) and in presence of exogenous NO

donors such as sodium nitroprusside (SNP) (88). Human studies have also found initial evidence of shear-mediated CBF regulation as demonstrated by dilation of the ICA in the presence of transient (~30 s) hypercapnia (89–91). Shear-mediated dilation of CO_2 reactivity is affected by pharmacological blockade of NO/NOS as vasodilatory responses in the ICA (89,91) and MCA (69) are either delayed by ~60 s or do not occur at all (92).

PGs appear to have a role in vasodilation of endothelial and smooth muscle cells in the cerebral circulation of humans and animals. Exogenous PGs added to *in vitro* tissue baths have been observed to dilate larger intracranial arteries such as the MCA, VA and the BA, along with the pial arterioles in humans and animals (93–96). However, the vasodilatory effect of prostaglandin-E_2 (PGE_2) appears to be specific to the anterior circulation as seen by MCA dilation (93). Studies of *in vivo* arachidonic acid (from which PGs are produced) have shown increased PG production and subsequent pial vessel dilation in animals (97–99) and in cultured endothelial cells (100). Conversely, when PG synthesis was inhibited by administration of indomethacin, a cyclooxygenase (COX) inhibitor, a significant reduction in cerebrovascular reactivity (CVR) in humans (96,101–103) and in animals (77,98) was observed. Despite variability in the mechanism of action in CBF regulation, it is clear that vasodilation due to CO_2 causes CBF to increase while vasoconstriction decreases CBF.

1.4.2.1 Cerebrovascular Reactivity to Carbon Dioxide

CVR is represented as the proportion of change in CBF to the change in a vasoactive stimulus (104). Because of its vasodilatory capability, CO_2 is often used as a controlled and repeatable stimulus. CVR measures are used to assess

cerebrovascular health and to indicate the cerebral vasculature's response to normal physiological demands. CVR can be quantified as both the absolute and relative (%) change in CBF. A decrease in CVR to hypercapnia is predictive of stroke and stenotic arterial lesions in clinical populations (105–109). A reduction in CVR is also associated with neurodegenerative disorders such as AD (17,18) and multiple sclerosis (110,111), and metabolic disorders such as diabetes (112,113) and obesity (114). Furthermore, CVR has been reported to be linked with peripheral vascular endothelial function (15,16).

Mediators of cerebral vasodilation have a greater influence on intracranial vascular tone in the hypercapnic range compared to the hypocapnic range (87), which might explain why CVR is usually higher in the hypercapnic range (115–117). In the anterior and posterior circulation, regional differences have been observed in the magnitude of CVR in which the anterior circulation's absolute CVR is about 50% higher compared to the posterior circulation (70,101). However, this difference appears to be minimized when CVR is represented as % change. In fact, relative CVR is similar between the MCA and BA (118). Blood velocity reactivity of the MCA and PCA appear to be similar during end-tidal forcing in an extreme $PaCO_2$ range between 15-65 mmHg (70). Additionally, regional differences in CVR have been observed between the gray and white matter in which the gray matter possesses a two- to threefold greater absolute CVR compared to the white matter as measured by PET (119), blood oxygenation level-dependent (BOLD)-MRI (120,121), and ASL (122).

Apart from the regional differences present in CVR mentioned above, other variables such as neuronal activity and wakefulness have an impact on CVR. As such, CVR has been shown to be reduced with sleep (123) and elevated during exercise

(124,125). CVR also appears to follow a distinct circadian rhythm in which it is lower in early morning than in late afternoon (15,126). Potential clinical implications of wakefulness and circadian-related alterations in CVR is shown by 20-40% occurrences of strokes at night (127) and a rise in cerebrovascular events in early morning (128,129).

1.4.2.2 Stimulus Delivery for Cerebrovascular CO_2 Reactivity

The magnitude of the stimulus and characteristics of the cerebrovascular response can vary depending on the method that is used to induce changes to $PaCO_2$ to assess CVR in humans (34). In order to minimize test-retest variability, precise control of delivering changes in $PaCO_2$ is required. In this regard, simple respiratory circuits that deliver a fixed concentration of inspired gases, such as non-rebreathing valves (130) and an inspired gas reservoir (131) are often used (132). These methods provide constant inspired fractional concentrations of CO_2 ($FiCO_2$) and O_2 (FiO_2). However, a fixed $FiCO_2$ does not yield a standardized $P_{ET}CO_2$ because of differences in metabolism and variable alveolar ventilations from variable respiratory chemoreflex ventilatory response to CO_2 among different individuals (133). Hence, an unknown gradient between $P_{ET}CO_2$ and $PaCO_2$ exists from which a target value of either is unable to be achieved from a $FiCO_2$.

Computerized gas control systems, such as dynamic end-tidal forcing (134) and prospective end-tidal targeting (135), can provide precise and repeatable sequences of $P_{ET}CO_2$ and $PaCO_2$ followed with low breath-to-breath variability. The prospective end-tidal targeting method works by employing sequential breathing that equalizes $P_{ET}CO_2$ and $PaCO_2$ (136,137). A variety of stimulus patterns along with rapid changes in end-tidal gases can be produced to induce the necessary $P_{ET}CO_2$ and

$P_{ET}O_2$ targeting. These systems, however, are expensive and require participant cooperation (i.e., breathing at their preferred resting rate or higher at a controlled rate) to obtain consistent end-tidal gas targeting.

1.5 The Hippocampus: Structure and Function

The hippocampus (HC) is a brain structure that has been studied in detail after the release of the 1957 case study report of patient H.M., who could not form new, declarative memories after his HC was surgically removed (138). The HC, in humans, is an elongated structure embedded deep in the brain's medial temporal lobe (7,139). It consists of several sub-regions or subfields – the dentate gyrus (DG), cornu ammonis (CA1-3), and the subiculum, each of which have distinct roles in memory processing (140). Cross-sectional anatomy of the HC shows three synaptic loops that make up the HC connectivity (139). The entorhinal cortex (EC) provides major cortical input with projections to the DG, the DG then forms projections with the CA3 via the mossy fiber pathway, and the CA3 projects to the CA1 via the Schaffer Collateral pathway, which in turn projects back to the EC via the subiculum, completing the loop.

In terms of function, the HC and its adjacent regions are essential for the making of new, declarative memories, which consist of episodic and semantic memories (7,139). Episodic memory refers to the recall of a specific event related to a specific time and place, whereas semantic memory refers to an individual's recollection of general knowledge. The HC is particularly important for forming new episodic memories (139) along with selective retrieval of old episodic memories (141). Patients with damage to their HC in early life were observed to have problems remembering their life's daily events but had little trouble learning languages and factual knowledge. Amyloid plaques and neurofibrillary tangles observed in brains of

AD patients are typically identified first in the HC and its surrounding EC region. Interestingly, alterations in the generation of new HC neurons have been shown to take place much earlier than clinical presentation of lesions or neuronal loss that are characteristic of AD (142). Therefore, this presents a need to examine the early loss of HC neuronal microstructural integrity to better understand the mechanism behind cognitive aging.

1.5.1 Assessment of Hippocampal Tissue Structural Properties: Magnetic Resonance Elastography

Magnetic Resonance Elastography (MRE) is a novel and noninvasive imaging modality that is used to assess brain tissue viscoelastic properties in humans and animal models (143). MRE measures of viscoelastic properties reflect the distribution and organization of neurons, axons, and glial cells (144–146), thereby providing an insight into brain tissue microstructural integrity. Declines in neuronal tissue microstructure, measured by MRE, correlates with aging (147–149), increased inflammation (150) and several neurodegenerative diseases that include AD (151–153), Parkinson's disease (154,155), multiple and amyotrophic lateral sclerosis (156–158). Specifically, changes to HC viscoelastic properties have been shown to be strongly associated with episodic memory performance (159,160).

Application of MRE is performed through a pneumatic actuator system and a soft pillow driver (161). The actuator sends vibrations to the participant's head at 50 Hz from which motion is sampled in the X, Y, and Z direction. The resulting displacement data is then input into a nonlinear inversion algorithm and is combined with soft prior regularization from which complex shear modulus maps are estimated (162,163). In order to obtain information of the HC shear modulus, bilateral HC masks

are obtained from a T1-structural MRI scan and subsequently segmented and registered from the T1 anatomical space to the MRE space (6). The complex shear modulus maps are utilized to determine the mechanical viscoelastic properties that consists of shear stiffness and damping ratio (159,160,164–166).

Shear stiffness describes a material's resistance to deformation due to applied loading (144). It is related to the speed of propagation of the shear waves, where waves are transmitted faster through a stiffer material compared to a softer material. In terms of brain tissue properties, stiffness corresponds to the density of neurons, neuronal myelin content, and the network strength of neurons in animals (144,167,168). As such, a higher HC stiffness is depictive of a higher number of neurons meshed in a strong cellular matrix and is indicative of a better HC tissue integrity (144). Damping ratio, on the other hand, relates to a material's relative attenuation of deformation from external vibrations. A higher damping ratio means that the material has undergone rapid attenuation, exhibiting the behavior of a viscous fluid. In contrast, a lower damping ratio indicates that the material has undergone a slower attenuation, exhibiting the behavior of a more elastic solid. In animal models, damping ratio is proposed to reflect the density of neuronal connections along with neuronal organization (145,146). As such, a lower HC damping ratio reflects a tissue that is more elastic, and is likely packed with dense neuronal connections, indicative of a better HC tissue integrity. Alternatively, a higher HC damping ratio represents a more viscous fluid likely with fewer neuronal connections, indicative of poorer HC tissue integrity. Collectively, a lower HC stiffness and higher HC damping ratio are suggestive of poorer HC tissue integrity and have been associated with advancing age (148), memory impairment (159,160), and potentially the transition to AD (169).

1.5.2 Relation between Cerebral Blood Flow and Brain Tissue Viscoelastic Properties

Recent studies have identified that acute manipulations of CBF can transiently alter brain tissue viscoelastic properties. In healthy individuals, 5 minutes of CO_2-induced CVR resulted in an increase in brain stiffness assessed from viscoelastic properties through MRE (20). Using trans-temporal ultrasound time-harmonic elastography (THE), it was shown that brain stiffness was increased during the first 2 minutes of 5% CO_2 inhalation and the post-hypercapnic recovery of brain stiffness was delayed by an average of 2.7 minutes (19). When a Valsalva maneuver was used as the stimulus for CVR, it was observed that brain stiffness was also increased when assessed via THE (170). While the relevance of these acute studies to long term brain health are not clear, they highlight a potentially important link between CBF and brain tissue viscoelastic properties that may have implications for cognitive aging.

1.6 Diet and Brain Health

Dietary interventions have recently emerged as potential strategies to combat cognitive aging. Researchers had found that the Mediterranean (171) and the Dietary Approaches to Stop Hypertension (DASH) diets (172) were successful at slowing the progression of age-related cognitive decline (173,174). Both these diets are characterized by increased consumption of fruits, vegetables, nuts, whole-cereal products, moderate consumption of fish and dairy products, and low consumption of red meat. However, neither diet was specifically designed to prevent the onset of AD and/or age-related cognitive decline. Hence, the Mediterranean and DASH diets were modified to emphasize nutrients that provided the most compelling evidence in the delay and prevention of cognitive aging, e.g., increased consumption of green leafy vegetables and berries was associated with slower cognitive decline. This modified

diet was called the Mediterranean-DASH diet intervention for neurodegenerative delay (MIND) and its uniqueness was that it specified the consumption of green leafy vegetables and berries (175). In retrospective analyses of a cohort of over 950 older individuals from the Rush Memory and Aging Project, it was observed that individuals who consumed more components of the Mediterranean and MIND diet, had a significant slower rate of cognitive decline (175) and high to moderate adherence to the MIND diet substantially reduced AD risk (176).

Conversely, consumption of a Western diet (WD) is associated with an increased risk of cognitive aging and AD (177–179). A WD typically consists of increased amounts of added sugars and saturated fats. Increased added sugar consumption has been observed to be associated with a greater risk of cardiovascular disease (CVD) (22) and other metabolic diseases like diabetes and obesity (180,181). Added sugars consist of sugars and syrups (i.e. caloric sweeteners) that are added to food or beverages during preparation, processing, or at the table. Consumption of soft drinks, fruit drinks, desserts, candy and ready-to-eat cereals account for the major sources of energy consumed from added sugars (22). The most common form of added sugar found in the WD diet is fructose, a monosaccharide, whose chemical formula is identical to glucose but differs by the fact that fructose contains a ketone functional group while glucose contains an aldehyde functional group (182). Fructose also differs from glucose by how it is metabolized which is discussed in the following section. Fructose is added to processed foods and beverages in the form of high-fructose corn syrup (HFCS), which is composed of either 42% or 55% of fructose and is similar to sucrose (table sugar) in composition. The following sections will review

the metabolic effects of these sugars and impact of its metabolites (i.e. triglycerides and uric acid) on vascular function.

1.6.1 Fructose Transport and Metabolism

Fructose arrives in the gut from pure fructose or HFCS ingestion or from sucrose digestion, and is transported to enterocytes (cells of the intestinal lining) via a fructose transporter, GLUT5 (180). GLUT2 transporters, on the basolateral side of enterocytes, mediate the transport of fructose and allow it to diffuse into the blood vessels (183,184). Fructose absorption by the gut is limited compared to glucose (185,186). In addition, fructose absorption has been shown to be modulated by non-carbohydrate contents of the diet. For example, in rats, intestinal fructose absorption is enhanced by co-ingestion with saturated fats (187). After absorption, the fructose present in the portal blood is taken up by the liver via GLUT2 (188,189) where most of it is phosphorylated to fructose-1-phosphate by fructokinase C (190,191). Fructose-1-phosphate is then broken down to glyceraldehyde and dihydroxyacetone-phosphate (DHAP) by aldolase B (192). DHAP is then isomerized into glyceraldehyde-3-phosphate, which is a triose-phosphate, and enters the glycolytic pathway to be converted into pyruvate, which is subsequently oxidized to acetyl-coenzyme A (CoA). Acetyl-CoA is either oxidized in the Kreb's cycle or used for the synthesis of fatty acids (193). Glyceraldehyde-3-phosphate also contributes to fatty acid synthesis through the formation of glycerol-3-phosphate, which serves as a backbone for TGs (194).

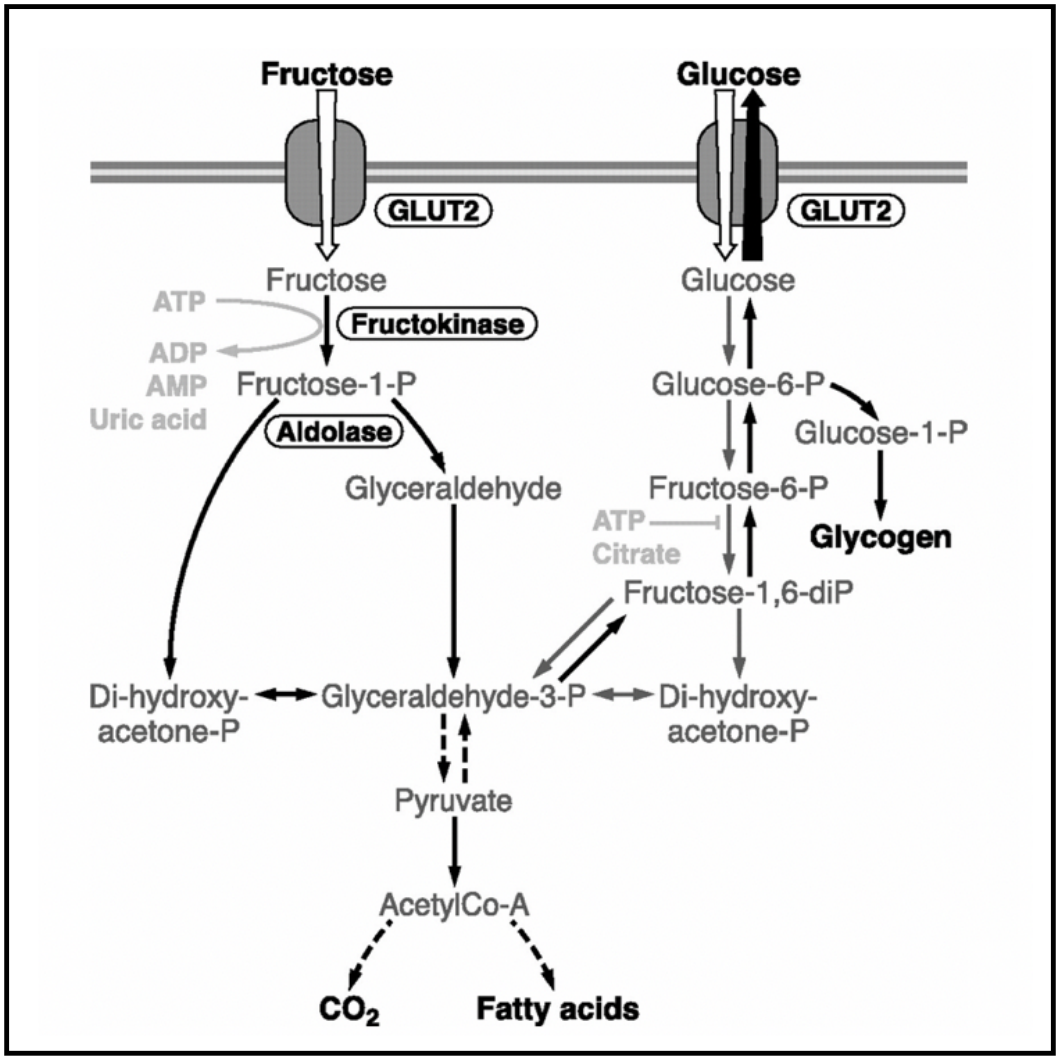

Figure 1.3 Metabolism of fructose vs. glucose. Fructose is oxidized to CO_2 and fatty acids in the liver, while glucose is either released into the circulation or converted into glycogen. Figure from Tappy and Le, Physiol Rev, 2010 (180). Originally published by and used with permission from American Physiological Society.

Unlike glucose metabolism where its phosphorylation is tightly regulated and adenosine triphosphate (ATP) is never depleted, the phosphorylation of fructose by fructokinase C results in the depletion of ATP and a reduction in the intracellular

phosphate concentration (10,23). As a result, the attenuation of intracellular phosphate concentration leads to activation of adenosine monophosphate (AMP) deaminase, which in turn breaks down the resulting AMP substrate and produces inosine monophosphate (IMP). IMP is broken down further to xanthine and hypoxanthine by xanthine oxidase. Uric acid is ultimately generated from xanthine and hypoxanthine. Fructose-induced hyperuricemia and its subsequent effects resulting in uric acid-mediated oxidative stress and vascular endothelial dysfunction is discussed in later sections.

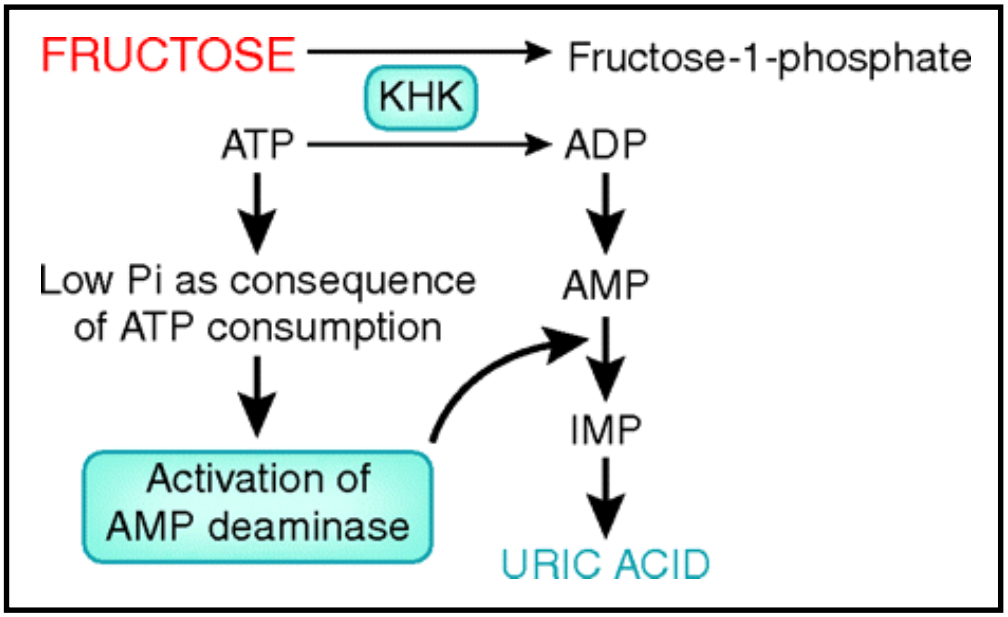

Figure 1.4 Fructose to uric acid metabolism. Rapid phosphorylation of fructose leads to degradation of ATP to AMP, which activates AMP deaminase and converts AMP to IMP and ultimately uric acid. Figure from Johnson et al., J Am Soc Nephrol, 2010 (195). Originally published by and used with permission from Wolters Kluwer Health, Inc.

1.6.2 Fructose-Induced Hypertriglyceridemia

Multiple studies suggest that long-term consumption of either an isocaloric or a hypercaloric high-sugar diet plays a role in the acceleration of hepatic *de novo* lipogenesis to induce increased concentration of TGs in the blood (known as hypertriglyceridemia) in humans (196–202). Interestingly, it appears that high fructose consumption acutely leads to substantial postprandial increases in plasma TGs (203–210). This effect is observed when either pure fructose, HFCS, glucose and fructose mixtures, or sucrose is ingested, suggesting that collectively, increased level of fructose-containing added sugars lead to elevated TG concentration from hepatic *de novo* lipogenesis, which results in both increased TG production and reduced TG clearance.

The hepatic *de novo* lipogenesis pathway was initially identified in rats *in vivo* (211) and in isolated rat hepatocytes (212,213), where the administration of [^{14}C]-labeled fructose resulted in ^{14}C being incorporated in liver lipids. In this pathway, high levels of ingested fructose contribute to the synthesis of very-low-density lipoprotein (VLDL)-TGs. In humans, it has been shown that an acute administration of fructose, or fructose-glucose mixtures, lead to the incorporation of ^{13}C-labeled acetate into VLDL-palmitate (11,214). Acute fructose administration results in the production of increased levels of hepatic triose-phosphates, which then become precursors for the synthesis of fatty acids (24,214). Some *in vitro* data suggest that instead of triose-phosphates, lactate is the primary lipogenic precursor for fatty acid synthesis and that the activation of pyruvate dehydrogenase from a high-fructose diet is the key regulatory step in this process (215–217). Simultaneously, fructose also inhibits hepatic lipid oxidation, therefore, promoting fatty acid re-esterification and further VLDL-TG synthesis (212).

Another mechanism by which fructose has been shown to increase hepatic lipogenesis is by inducing the expression of the transcription factor, sterol regulatory element binding protein (SREBP-1c) (218,219). SREBP-1c controls expression of lipogenic enzymes involved in *de novo* lipogenesis and it has been shown that fructose induces its expression independent of the action of insulin. Fructose also increases the expression of glucose-6-phosphate dehydrogenase, that is proposed to trigger carbohydrate-responsive element binding protein's (ChREBP) activation. ChREBP is a hepatic transcription factor that increases the expression of acetyl-CoA carboxylase and hepatic fatty acid synthase for the synthesis of fatty acids (220,221).

1.6.3 Triglyceride-Rich VLDL Transport and Metabolism

TGs are lipid esters formed from glycerol and fatty acids. VLDL-TGs are a type of TG-rich lipoproteins (TRLs) that transport TGs along with cholesterol from the liver and deliver to either muscle tissue for oxidation or in adipose tissue for storage (222). VLDL assembly starts in the lumen of the endoplasmic reticulum (ER), from which it is transferred by microsomal triglyceride transfer protein (MTP), incorporating a small number of TGs in apolipoprotein B-100 (apoB-100), which are specific proteins present on the surface of lipoprotein particles (223). Additional TGs are packaged into nascent apoB-100 particles as they traverse from the ER to the Golgi apparatus to form VLDL particles (224). VLDL particles are then secreted by a vesicle-mediated mechanism.

Once inside the plasma, VLDL-TGs adhere to glycosaminoglycan molecules on endothelial cells of muscle, capillaries, lung or adipose tissue, where they are hydrolyzed by lipoprotein lipase (LPL) to glycerol and free fatty acids (FFAs) and also form smaller and denser VLDL remnants called intermediate-density lipoproteins

(IDLs) (12). IDLs cannot be extracted by the liver but can undergo further hydrolysis by hepatic lipase to form cholesteryl-ester-rich low-density lipoproteins (LDLs). LDLs are generally cleared from the circulation by binding to hepatic LDL receptors.

1.6.4 Hypertriglyceridemia-Induced Peripheral Vascular Endothelial Dysfunction

Hypertriglyceridemia occurs when there is overproduction or reduced clearance of TGs. Increased blood TG concentration is a well-established risk factor of CVD as it is involved in the progression of endothelial dysfunction, which is an early step in the development of atherosclerosis (225,226).

The vascular endothelium is comprised of a layer of endothelial cells (EC) that line the luminal surface of the vasculature (227). The endothelium releases various vasoactive factors that regulate vascular tone and homeostasis in response to mechanical and chemical stimuli. Alterations in endothelial physiology due to aging and poor lifestyle factors are known as endothelial dysfunction, and is characterized by a reduction in bioavailability and/or production of vasodilators, including NO (228,229). In a healthy blood vessel, an increase in shear stress or stimulation by certain vasoactive molecules such as acetylcholine results in the production of NO by eNOS, which diffuses into the adjacent VSM cells where it causes relaxation and induces vasodilation (228,230). A decline in endothelial function, on the other hand, occurs when chronic inflammation causes activation of central inflammatory mediators such as nuclear factor kappa-beta (NFkB) and promotes the release and synthesis of circulating inflammatory cytokines and reactive oxygen species (ROS) (14,231). The ROS scavenge NO, reducing its bioavailability, thus leading to endothelial dysfunction.

Increased concentration of TRLs, due to increased TG transport, activates the cholesteryl ester transfer protein (CETP), which facilitates the exchange of TGs and cholesteryl esters between TRLs and LDL, leading to the formation of more TG-rich LDLs (226). Accumulation of these TRLs in the vascular wall's intimal layer leads to the recruitment of circulating monocytes (232). TG-rich LDLs are hydrolyzed by hepatic lipase to smaller and denser LDL particles that can be easily oxidized. Oxidized LDL is engulfed by macrophages that differentiate from monocytes, which subsequently leads to the formation of foam cells (233,234). Additionally, these macrophages release proinflammatory cytokines such as interleukin-6 (IL-6) and tumor necrosis factor alpha (TNF-α), thereby promoting plaque formation and atherosclerotic progression.

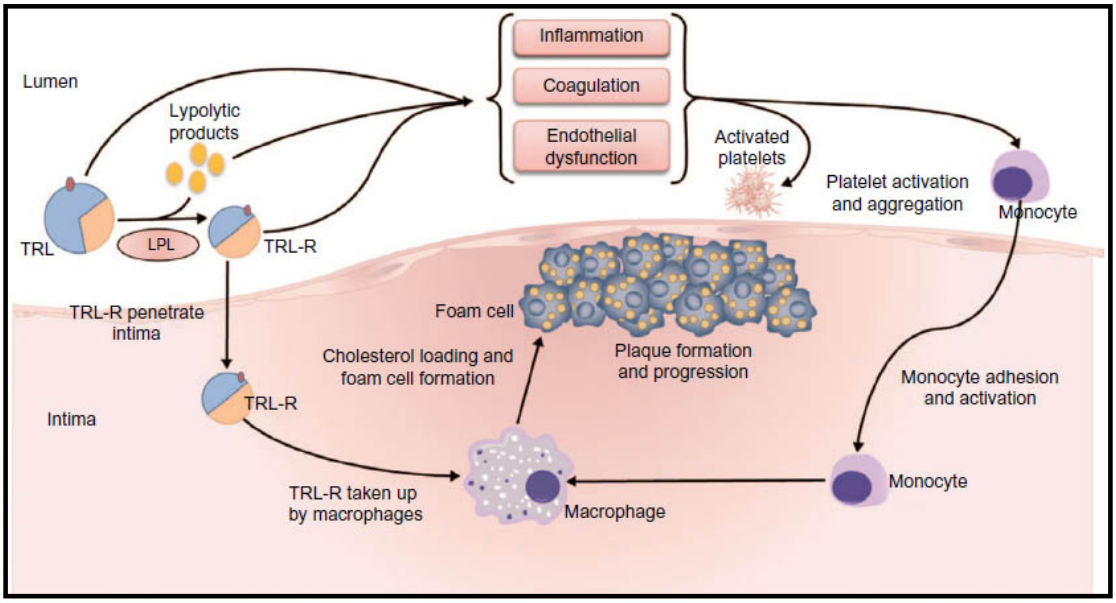

Figure 1.5 Pathophysiology of triglyceride-rich lipoproteins (TRLs) in endothelial dysfunction and inflammation. TRLs enter the subendothelial space and contributes to endothelial dysfunction. TRLs are also taken up by macrophages which combine with monocytes and release inflammatory products to form foam cells. Further cholesterol loading causes these foam cells to become atherosclerotic plaques. Figure from Toth, Vasc Health Risk Manag, 2016 (235). Originally published by and used with permission from Dove Medical Press Ltd.

Apolipoprotein C-III (apoC-III) in VLDL-TGs also promote atherosclerosis by activating proinflammatory toll-like receptor 2 (TLR2) signaling, which in turn leads to the activation of NFkB (12). NFkB activation results in vascular cell adhesion molecules such as VCAM1 to be upregulated and bind monocytes to endothelial cells and release proinflammatory cytokines, thus causing endothelial dysfunction.

1.6.5 Fructose-Induced Hyperuricemia, Oxidative Stress and Lipid Accumulation

As mentioned in section 1.6.1, activation of AMP deaminase from the fall in intracellular ATP levels during fructose metabolism results in uric acid generation. Fructose-induced uric acid generation not only results in oxidative stress but is also instrumental in causing lipogenesis and a lowering of energy production. Uric acid, in combination with a fall in ATP levels, initiates the mitogen-activated protein kinase (MAPK) and nicotinamide adenine dinucleotide phosphate (NADPH) oxidase cascades that lead to the production of ROS and oxidative stress, particularly in the mitochondria (8,236,237). Mitochondrial oxidative stress leads to the accumulation of citrate as a result of reduced activity from aconitase-2 enzyme in the Kreb's cycle. Citrate then travels to the cytoplasm, where it activates fatty acid synthase, ATP citrate lyase, and acetyl CoA carboxylase, which have implications in hepatic fatty acid synthesis (236). Uric acid generation further causes a reduction in the activity of the enzyme enoyl CoA hydratase which in turn blocks fatty acid beta-oxidation and causes a shift to glycolysis, which results in further oxidative stress and lipid accumulation in hepatocytes (236,238).

Another mechanism by which uric acid may increase hepatic lipid accumulation is from the increased expression of fructokinase C that drives uric acid production from fructose (8). It has been shown that elevated intracellular uric acid production activates further expression of fructokinase C, which produces more uric acid, which in turn, activates ChREBP, leading to an increased TG accumulation in response to fructose metabolism (238). Hepatic lipid accumulation is linked to insulin resistance (239), and uric acid may also induce insulin resistance on adipocytes, which is further linked to oxidative stress and inflammation. Uric acid, transported to

adipocytes, induces oxidative stress through NADPH oxidase activation, and generates oxidized lipids and inflammatory mediators such as monocyte chemoattractant protein-1 (MCP-1) (240,241).

1.6.6 Uric Acid-Induced Peripheral Vascular Endothelial Dysfunction

Uric acid, while an antioxidant in extracellular environments, is a pro-oxidant and a pro-inflammatory substance in intracellular environments including endothelial cells, VSM cells, and adipocytes (8). Some studies have suggested xanthine oxidase as the driver of endothelial dysfunction as it generates oxidants in addition to uric acid as products of its oxidation of hypoxanthine and xanthine (8,9). Oxygen is reduced to superoxide (O_2^-) or hydrogen peroxide (H_2O_2) in xanthine oxidase-catalyzed reactions (242,243). George et al. (2006) observed that introduction of high-dose allopurinol, an inhibitor of xanthine oxidase improved endothelial dysfunction in individuals with heart failure while lower uric acid concentration with probenecid showed no favorable outcomes (244). However, this effect of allopurinol is mostly attributed to its ability to block uric acid production from xanthine oxidase as it has been found that in the presence of allopurinol, elevated levels of uric acid increases hepatic fat accumulation (238).

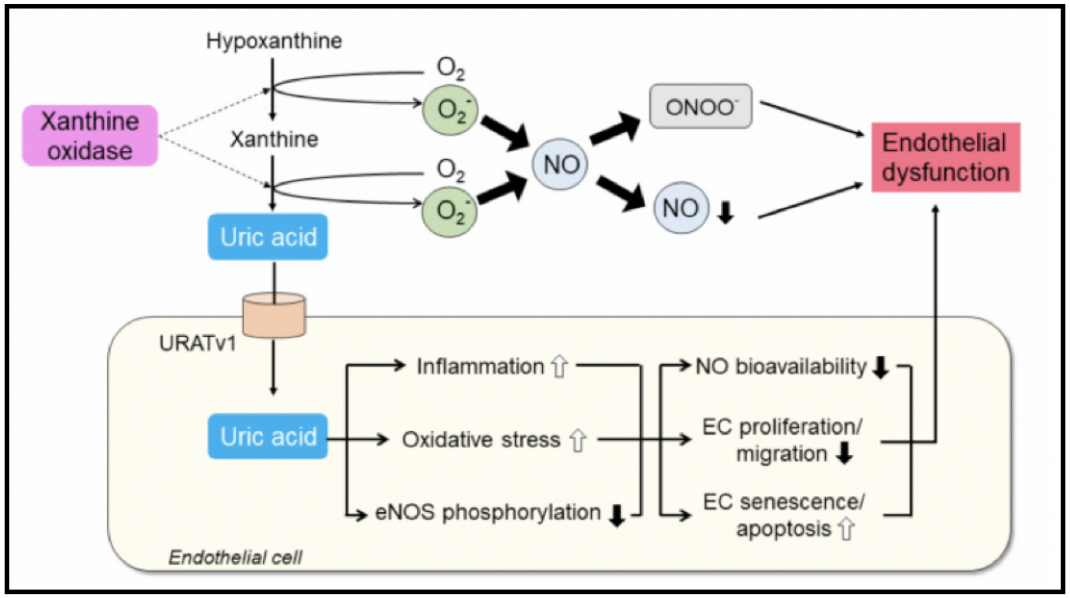

Figure 1.6 Possible mechanism of uric acid-induced endothelial dysfunction. Xanthine oxidase facilitates the conversion of hypoxanthine and xanthine to uric acid after ATP is degraded due to fructose phosphorylation. This process reduces oxygen to superoxides that scavenge nitric oxide leading to the production of peroxynitrites and reduced nitric oxide bioavailability. Figure from Maruhashi et al., Atherosclerosis, 2018 (245). Originally published by and used with permission from Elsevier.

There is evidence that uric acid generates aminocarbonyl radicals along with alkylating species upon reaction with peroxynitrite ($ONOO^-$) that directly inactivates or scavenges NO (246–248). Excess ROS generation from uric acid impairs eNOS activity and NO bioavailability, thus affecting endothelium-dependent vasodilation. Other mechanisms by which uric acid reduces endothelial NO is by blocking the uptake of L-arginine and by stimulating the degradation of L-arginine by arginase (249,250). Aminocarbonyl radicals can accelerate oxidative damage through the oxidation of lipozomes, LDL-C and other lipid hyperoxides (251). Oxidized LDL and

lipid particles subsequently create an inflammatory response as described in section 1.6.4.

Insulin resistance induced by uric acid may also affect the vasculature as insulin is an essential hormone that stimulates the release of NO from endothelial cells, which causes dilation of the vasculature so that glucose can be effectively delivered to skeletal muscle. As such, uric acid-induced insulin resistance is also attributed to inhibition of endothelial NO generation, leading to endothelial dysfunction (237).

1.7 Effect of Acute Added Sugar Intake on Peripheral Vascular Endothelial Function

Thus far, evidence of how lipids and uric acid metabolized from added sugars, particularly, from fructose, affect peripheral vascular endothelial function has been presented. It should be noted that these effects usually must occur repeatedly over a long period of time to impair vascular function. However, some studies suggest that even a single meal containing high added sugars can acutely impair vascular endothelial function in healthy individuals and in individuals with cardiometabolic disease. In this regard, a randomized, single-blind, cross-over trial showed that acute consumption of a single sugar-sweetened beverage reduced both macrovascular and microvascular endothelial function in young healthy men (25). It was also shown that a single bout of aerobic exercise was able to reverse the transient endothelial dysfunction elicited by acute added sugar intake (26,28). Similarly, a single bout of endurance exercise, performed 17 h prior to ingestion of a candy bar and sugary drink, attenuated the reduction of macrovascular endothelial function in healthy individuals compared to those who did not perform the exercise (252). In nondiabetic obese

individuals, another randomized, cross-over trial showed that consumption of a meal with a high glycemic index acutely impaired macrovascular endothelial function (29). Furthermore, in newly diagnosed type 2 diabetics, it was observed that endothelial function was significantly reduced 120 minutes after ingestion of a single cookie (253).

Although, there is significant evidence of added sugars acutely impairing vascular endothelial function, most researchers have studied this in relation to the postprandial hyperglycemic response of glucose ingestion (mostly via oral glucose tolerance tests) on vascular function (27); however, as mentioned previously, dietary added sugars predominantly contain fructose, whose direct acute effects on both the peripheral and cerebral vasculature are largely unknown, specifically in healthy mid-life individuals with a range of cardiometabolic risk parameters.

1.8 Effect of Acute Added Sugar Intake on Cerebral Blood Flow

Few studies have examined the effect of acute added sugar intake on the cerebral vasculature. Similar to studies that primarily examined the effect of acute hyperglycemia on peripheral vascular function, most studies that have looked at acute effects of added sugar intake on CBF have done so in relation to the acute hyperglycemic response of glucose. In rats that were in a chronically induced hyperglycemic state, acute intraperitoneal injection of glucose significantly reduced CBF in multiple brain regions including the HC (254). When examining solely the effect of acute hyperglycemia, intraperitoneal glucose injection in rats demonstrated a decrease in cortical CBF 20 minutes after glucose injection (255,256). The mechanism behind CBF reduction due to acute hyperglycemia was attributed to increased serum osmolality that may have increased blood viscosity and therefore, reduced flow.

Whether cerebrovascular endothelial dysfunction due to acute hyperglycemia plays a role in CBF reduction is yet to be determined from these studies.

In humans, studies examining the acute hyperglycemic response on CBF have assessed their findings in relation to appetite and reward behavior (257). These studies measured CBF in the hypothalamus as it is the brain structure that regulates appetite (258). Hypothalamic CBF, indirectly measured from BOLD-fMRI, was attenuated either during an acute glucose injection or 60-min after acute glucose ingestion (257,259–261). The reduction in CBF was attributed to an inhibitory hypothalamic response, which occurs when participants reach satiety as a result of glucose ingestion (257). When some of these studies investigated how fructose affects CBF acutely, it was observed that cortical BOLD signal was reduced due to a 60-min infusion of 0.3 mg/kg fructose (30). In a study that measured CBF using ASL to assess acute fructose intake, CBF was reduced in the HC 60 minutes after ingestion of a fructose drink (31). The mechanism behind CBF reduction due to acute fructose ingestion has also been explained in terms of appetite behavior in which fructose has been shown to elicit a hunger and binging response as opposed to glucose that elicits a satiating response (262). However, CBF reduction in the HC and in cortical regions of the brain after acute fructose consumption has not been explained in terms of cerebrovascular endothelial dysfunction, which likely has a substantial role in cognitive aging.

1.9 Peripheral vs. Cerebrovascular Endothelial Function

Endothelial function in the periphery is commonly assessed non-invasively by flow-mediated dilation (FMD) of the brachial artery, which quantifies endothelium-dependent vasodilation by the percent change in diameter from baseline following several minutes of occlusion of a cuff placed on the distal part of the artery (% FMD)

(263). As mentioned in section 1.4.2.1, CO_2- induced CVR has been applied in clinical settings to evaluate cerebrovascular function (105,107). Even though the similarity between regulation of the peripheral vasculature and the cerebral vasculature is not fully understood, evidence suggests that there is a close link between peripheral and cerebrovascular endothelial dysfunction and age-related cognitive impairment and/or AD (17,264). The exact mechanism behind CVR to hypercapnia is unclear but there is increased possibility that it is at least partially NO-dependent (43). Reduced cerebral NO bioavailability is thought to precede histological and angiographic evidence of AD (265), which supports the importance of investigating cerebrovascular endothelial function as a marker of future cognitive impairment.

Brachial artery FMD has been found to be correlated with a decrease in CVR to hypercapnia, suggesting that peripheral and cerebrovascular endothelial function may share similar mechanisms (15). Individuals with known endothelial dysfunction in the form of a cardiometabolic disease (i.e., hypertension and diabetes) were observed to have impaired CVR compared to healthy controls (16). Additionally, in older adults with a range of cardiometabolic risk factors, reduced FMD was found to be associated with increased white matter hyperintensities (WMH) (266). Presence of WMH has been documented to be correlated with a reduction in CVR due to CO_2 and acetazolamide (267,268). Therefore, these studies suggest that a relation exists between the peripheral and cerebral vasculature. Since it is known that fructose and its metabolites negatively affect peripheral blood vessels and there is some evidence of acute added sugar intake blunting peripheral vascular endothelial function and CBF, additional research is needed to examine the effects of acute added sugar intake and subsequent increases in blood lipids on cerebrovascular function.

1.10 Conclusion

Elevated blood lipids, including TGs, are known risk factors for cardiometabolic disease as well as age-related cognitive decline (4,5). Aberrant blood lipids have been found to be associated with reduced HC tissue integrity and memory performance (6). This relationship may be mediated by the negative effects of lipids on the cerebrovasculature. Increased added sugar consumption is known to acutely raise blood lipid concentration (203,206,208,210,214) and impair peripheral vascular endothelial function and CBF (25–33). However, the direct effects of acute added sugar intake from solid foods present in a Western-style meal and subsequent increase in blood lipids on cerebrovascular function and HC tissue properties are currently unknown in humans. Therefore, there is an urgent need to examine the mechanism behind added sugar consumption and elevated blood lipids on brain health in order to prevent future loss brain structure and function and risk of acquiring neurodegenerative diseases such as AD.

Chapter 2

ASSOCIATION AMONG BLOOD LIPIDS, HIPPOCAMPAL TISSUE VISCOELASTIC PROPERTIES, AND CEREBROVASCULAR FUNCTION

2.1 Introduction

Alzheimer's disease (AD), the most common form of dementia, is the fifth leading cause of death in adults 65 years and older in the United States (1,2). As the global population grows older, the incidence of AD is projected to more than double in the next thirty years (2,269). This is set to increase the burden on AD patients and caregivers as well as total healthcare costs, which equals up to $305 billion annually (3). Moreover, current AD drug trials have a 2% success rate (270). These factors highlight the importance of alternative approaches for the prevention and treatment of cognitive aging that includes targeting of modifiable lifestyle factors.

One important modifiable risk factor for brain aging is dyslipidemia, including high blood triglycerides (TG), low-density lipoprotein cholesterol (LDL-C) and low high-density lipoprotein cholesterol (HDL-C) (5). We have shown that elevated TGs and a high TG/HDL-C ratio, are associated with reduced memory performance and lower tissue integrity of the hippocampus (HC), a brain structure essential for memory encoding and recall (6). More importantly, these changes to HC tissue properties have been observed prior to clinically relevant brain structural changes such as HC tissue atrophy, which likely provides evidence into early events linking changes in blood lipids to loss of HC tissue integrity. However, the underlying mechanism linking elevated blood lipids to reductions in brain health in humans remain unclear.

One possible mechanism may be related to an association between circulating lipids and the cerebrovascular system. In order to supply the brain with adequate nutrients and to ensure efficient removal of waste products, cerebral blood flow (CBF) needs to be tightly regulated (70). Cerebrovascular reactivity (CVR) to carbon dioxide (CO_2) partially reflects endothelial-dependent dilation of cerebral blood vessels (43) and its reduction is associated with an increased risk of age-related cognitive decline (17,18). In healthy adults, it has been observed that CO_2-induced CVR results in a transient increase in brain tissue viscoelastic properties (19,20). Therefore, the possible contribution of attenuated cerebrovascular function to the reduction of HC tissue properties in individuals with habitually elevated blood lipids needs to be examined. The purpose of this study was to determine if cerebrovascular function mediates the relation between habitually elevated blood lipids and reduced HC tissue properties. We hypothesized that reduced cerebrovascular function would mediate the association between increased blood lipids and reduced HC tissue properties.

2.2 Methods

All experimental procedures and protocols outlined in this study conformed to the standards outlined in the latest revisions of the Declaration of Helsinki (revised 1983). The study was approved by University of Delaware's (UD) Institutional Review Board (1718585). Data reported in this study are part of a registered clinical trial (ClinicalTrials.gov Identifier: NCT05408338). The study purpose, along with the possible benefits and risks, were explained to all study participants and written and verbal informed consent was obtained from participants prior to participation. All measurements were made in the Neurovascular Aging Laboratory and the Center for Biomedical and Brain Imaging between June 2022 and April 2023.

2.2.1 Study Participants

Twenty-one young and mid-life adult men and women (8M/13F) between the ages of 30 – 64 years were recruited from the greater Newark/Wilmington, DE area for this study. Participants completed medical history, family history, MRI safety and menstrual history (females only) questionnaires during the screening visit. Height (cm) and body mass (kg) were measured using a stadiometer and electronic scale from which body mass index (BMI; kg/m^2) was calculated. Seated resting blood pressures were assessed after 10 minutes of quiet rest using a semi-automated blood pressure device (ADView 2®, American Diagnostic Corporation, Hauppauge, NY). Participants' non-dominant arm was used to make repeat measurements with 2 min of quiet rest between each measurement until three blood pressure values were within 5 mmHg of each other. The values were averaged to determine resting systolic and diastolic blood pressure (SBP, DBP). Participants were generally healthy with normal liver and renal function and without stage 2 hypertension (SBP < 140 mmHg; DBP < 90) and morbid obesity (BMI < 40 kg/m^2). Participants were also free from chronic diseases (e.g., heart disease, kidney disease, type 1 or 2 diabetes, cancer) and major psychological and neurological disorders as assessed by their medical history, complete blood count, and comprehensive metabolic panel. We excluded participants who were smokers and/or tobacco product users, who were on lipid-lower medications (e.g., statins), who were unable to have an MRI scan (e.g., metal implants) and females who were pregnant or breastfeeding. Participants were asked to refrain from over-the-counter medications for 48 h, vigorous aerobic exercise and alcohol for 24 h and food and beverages (except water), including caffeine for 12 h before the experimental visits of the clinical trial.

2.2.2 Blood Lipids Analysis

Blood was drawn from participants' antecubital vein by a phlebotomy-trained laboratory member. A standard serum lipid panel (Labcorp, Burlington, NC) consisting of total cholesterol, TG, LDL-C, HDL-C and very low-density lipoprotein cholesterol (VLDL-C), were measured at baseline following a 12 h overnight fast during each phase of the randomized-controlled crossover clinical trial referenced in section 2.2. The values reported in this study are averages of the two baseline blood lipids from the experimental visits of the clinical trial.

2.2.3 Hippocampal Tissue Viscoelastic Properties

All scans were performed with a 3T Magnetom Prisma MRI scanner (Siemens, Erlangen, Germany) using a 64-channel head coil. A T_1-weighted magnetization-prepared rapid echo (MPRAGE) scan (repetition time (TR)/echo time (TE): 2300/2.32 ms; flip angle: 8°; 240 x 240 mm^2 FOV; 256 x 256 matrix; 192 slices; slice thickness: 0.9 mm) was acquired first to generate bilateral HC masks segmentations to provide information about the HC tissue viscoelastic properties. The viscoelastic properties of the whole brain were measured with a high-resolution 3D multiband, multishot spiral MRE sequence. We used a 1.25 mm^3 isotropic resolution that required a total MRE scan time of 4 minutes and 29 seconds. The imaging parameters were: TR/TE: 140/76 ms; flip angle: 90°; 240 x 240 mm^2 field-of-view (FOV); 160 x 160 matrix; 80 slices; slice thickness: 1.5 mm. Shear waves were generated synchronously with the scan at 50 Hz through a pneumatic actuator system (Resoundant, Rochester, MN) and a soft pillow driver to the participant's head (161). The motion was sampled using motion-encoding gradients in three cardinal directions. The resulting displacement data was input into a nonlinear inversion (NLI) algorithm, combined with soft prior

regularization (SPR), to estimate maps of the viscoelastic complex shear modulus calculated using the formula: $G = G' + iG''$ (162,163). The quality of the MRE data was assessed using octahedral shear-strain based signal-to-noise ratio (OSS-SNR) as previously described by McGarry et al. (2011) (271).

Bilateral HC masks were segmented from the MPRAGE structural scan using FreeSurfer 6.0 (6). The segmented images were then registered from the T_1 anatomical space into the MRE space using the FLIRT tool in FSL (FMRIB Software Library v. 6.0.0) (272). The maps of the complex shear modulus were used to calculate the viscoelastic properties that include shear stiffness (μ) and damping ratio (ξ) (159,160,164–166). Shear stiffness (μ) is a viscoelastic property of brain tissue that describes its resistance to deformation due to applied loading and is calculated using the formula: $\mu = 2(|G|^2)/(G' + |G|)$ (144). An increased brain tissue stiffness indicates increased number of neurons within a strong cellular matrix. Damping ratio (ξ) relates to the relative attenuation of brain tissue from deformation due to external vibrations. Damping ratio (ξ) is calculated using the formula: $\xi = G''/2G'$. A lower damping ratio indicates a more elastic solid. Collectively, a higher stiffness and lower damping ratio indicates better brain tissue viscoelastic properties. Values presented here are averages of the baseline measures from both experimental visits of the clinical trial.

2.2.4 Cerebrovascular Reactivity

Cerebrovascular Reactivity (CVR) was assessed as the maximal change (from rest) in cerebral perfusion measured with arterial-spin labeling (ASL) during 3-minutes of hypercapnia [+9 mmHg increase in end-tidal partial pressure of carbon dioxide ($P_{ET}CO_2$)]. Hypercapnia was induced using an MR-compatible prospective

end-tidal targeting system which allows for precise and repeatable manipulation of $P_{ET}CO_2$ on a breath-by-breath basis using a computerized gas blender (RespirAct™, Thornhill Research, Ontario, Canada) (132,136,273). Four input gases were supplied to the gas blender from customized gas tanks (Airgas, Air Liquide, Radnor, PA): (1) gas A 10/90% O_2/N_2; (2) gas B 10/90% O_2/CO_2; (3) pure oxygen (100% O_2); (4) calibration gas (10/9% CO_2/O_2/balance N_2). A rubber face-mask was fitted onto the participants' face with adhesive tape (Tegaderm, 3M, St. Paul, MN) prior to the ASL scan to ensure there were no air leaks. After the face-mask was connected to the gas-delivery system, participants were asked to breathe at a steady rate (15 breaths per minute) for ~ 3 minutes to allow oxygen (O_2) consumption and CO_2 production to achieve a steady state. Target $P_{ET}CO_2$ was set at 9 mmHg above resting values, whereas $P_{ET}O_2$ remained at resting levels. ASL images were acquired over 9 minutes including 3 minutes of resting, 3 minutes of hypercapnia, and 3 minutes of recovery scans. CVR was calculated using the formula:

$$CVR = \frac{CBF_{hypercapnia} - CBF_{resting}}{CBF_{resting}\,(P_{ET}CO_{2.hypercapnia} - P_{ET}CO_{2.resting})} \times 100\%$$

2.2.4.1 Cerebral Perfusion Quantification

A pseudo-continuous arterial spin labeling (PCASL) scan used to quantify cerebral perfusion (274). The scan sequence was obtained from the Human Connectome Project (275) and modified according to Alsop et al.'s (2015) "white paper" for clinical ASL implementations (276). Imaging parameters used for the scan were: TR/TE: 4510/20 ms; voxel size: 2.5 x 2.5 x 2.3 mm^3; flip angle: 90°; 215 x 215 mm^2 FOV; 86 x 86 matrix; 60 slices; slice thickness: 2.27 mm; labeling duration: 1.8

s; post-labeling delay (PLD): 1.8 s; 60 pairs of control/label images; total acquisition time: 9 minutes and 27 seconds. Signal readout was implemented using multi-band 2D gradient echo-planar imaging (EPI) using partial Fourier = 6/8 and SMS acceleration factor = 6. Two equilibrium echo magnetization (M_0) images were acquired at the end of the scan and were averaged to produce a calibration image.

The T_1 MPRAGE image, collected prior to the MRE scan (described in section 2.2.3), was segmented into individual gray matter (GM) and white matter (WM) structures, cortical and subcortical structures using the "recon-all" function in FreeSurfer 6.0. The segmented images were registered onto the ASL space using the FLIRT tool in FSL. Perfusion was quantified with a standard kinetic- model inversion using the Bayesian algorithm (277). Perfusion maps were calibrated onto the proton density-weighted M_0 image using voxel-wise calibration mode with a sequence TR=8 s and a calibration gain of 1. Motion correction and spatial regularization of the estimated perfusion image were used on the ASL time-series (278). Partial volume correction was used to quantify GM perfusion (279). Each voxel perfusion was calculated using the following formula for PCASL as per the assumptions stated by Alsop et al. (2015) (276):

$$CBF = \frac{6000 \,.\, \lambda \,.\, (SI_{control} - SI_{label}) \,.\, e^{\frac{PLD}{T_{1b}}}}{2 \,.\, \alpha \,.\, T1_b \,.\, SI_{PD} \,.\, (1 - e^{\frac{-\tau}{T_{1b}}})}$$

where λ = 0.9 mL/g (brain/blood barrier partition coefficient);

$SI_{control}$ and SI_{label} = time-averaged signal intensities of control and label images;

PLD = post-labeling delay;

T_{1b} = 1.65 s (longitudinal relaxation time of blood);

α = 0.85 (labeling efficiency);

SI_{PD} = signal intensity of proton density-weighted image;

τ = labeling duration;

The factor of 6000 was used to convert the units from mL/g/s to mL/(100g)/min.

ASL images registered to the T_1-weighted structural space allowed for overlaying of the bilateral HC masks on the ASL perfusion image using 95% threshold to obtain HC perfusion values.

2.2.5 Statistical Analysis

Data were assessed for normality using Shapiro-Wilk test (280) and by examining Q-Q plots. Bivariate Pearson's correlations were performed to identify whether any blood lipid markers were associated with HC viscoelastic properties as well as to examine associations between resting perfusion, CVR and HC viscoelastic properties. Mediation analyses were performed to assess whether CVR mediates the significant association between independent variables (blood lipids) and the dependent variables (HC viscoelastic properties) of interest from the bivariate correlation analyses. We used jamovi software (v.2.3.26) to perform the mediation analyses; standardized effect sizes and confidence intervals (CI) not overlapping 0 were considered as evidence of mediation (281). We used GraphPad Prism 9.0 (GraphPad Sofware Inc., San Diego, CA) for all other statistical analyses. Statistical significance was set at $p < 0.05$.

2.3 Results

Twenty-one adult men and women (8M/13F) between the ages of 30-64 years completed the study. Participants were generally healthy and did not report any overt cardiovascular disease or other chronic diseases. Participant screening characteristics are presented in **Table 2.1**. Participants were young to mid-life, mostly White adults, and were normotensive with a normal BMI. There were four premenopausal, two perimenopausal and seven postmenopausal females enrolled in the study. Participant screening and baseline blood chemistries are presented in **Table 2.2.** Lipid panel values presented are averages of fasted baseline values from the 2 experimental visits of the clinical trial. Participants' mean blood chemistries were within normal limits, except for total and LDL cholesterol, which were clinically within the borderline high range.

Table 2.1 Screening characteristics

Demographic data	
N, M/F	8/13
Race, White/Asian	20/1
Menopause Status, Pre/Peri/Post	4/2/7
Anthropometrics	
Age, yr	48 ± 12.6
Body Mass, kg	68.9 ± 12.0
Height, cm	166.8 ± 10.3
BMI, kg/m^2	24.7 ± 2.9
Hemodynamics	
Systolic BP, mmHg	116 ± 12
Diastolic BP, mmHg	72 ± 6
MAP, mmHg	87 ± 7
Heart rate, bpm	65 ± 9

Data are expressed as mean ± SD. BMI: body mass index; BP: blood pressure; MAP: mean arterial pressure.

Table 2.2 Baseline blood chemistries

Complete Blood Count	
WBC, x $10^3/\mu L$	5.0 ± 1.1
RBC, x $10^6/\mu L$	4.5 ± 0.3
Hemoglobin, g/dL	13.8 ± 0.8
Hematocrit, %	41.5 ± 2.5
Metabolic Panel	
Glucose, mg/dL	89 ± 7.0
BUN, mg/dL	13.9 ± 2.9
Creatinine, mg/dL	0.9 ± 0.1
eGFR, mL/min/1.73	93 ± 15.2
BUN/Creatinine	16.7 ± 3.4
Sodium, mmol/L	141 ± 2.3
Potassium, mmol/L	4.4 ± 0.3
Chloride, mmol/L	102.5 ± 2.6
Lipid Panel	
Total Cholesterol, mg/dL	213 ± 36
Triglycerides, mg/dL	104 ± 76
HDL Cholesterol, mg/dL	64 ± 20
LDL Cholesterol, mg/dL	130 ± 29
VLDL Cholesterol, mg/dL	19 ± 14
ApoE, ε4 Carriers/ ε4 Non-Carriers	6/15

Data are expressed as mean ± SD. ApoE: apolipoprotein E; BUN: blood urea nitrogen; eGFR: estimated glomerular filtration rate; HDL: high-density lipoprotein; LDL: low-density lipoprotein; RBC: red blood cells; VLDL: very low-density lipoprotein; WBC: white blood cells.

2.3.1 Blood Lipids and Hippocampal Tissue Viscoelastic Properties

Bivariate Pearson's correlations between serum lipid markers and their relation to HC viscoelastic properties are presented in Table 2.3. LDL-C was associated with HC stiffness (r=-0.42, p=0.049). Total cholesterol was also associated with HC stiffness (r=-0.44, p=0.047), however, we observed no relation between HDL-C and HC stiffness (r=-0.09, p=0.69), which implied that the relation between total cholesterol and HC stiffness was solely due to the influence of LDL-C. Hence, total cholesterol was not included in further mediation analyses. There was no association between any other lipid markers and HC viscoelastic properties.

Table 2.3 Bivariate correlation between serum lipids and hippocampal tissue viscoelastic properties

		TC	TG	HDL-C	LDL-C	VLDL-C
Hippocampal Stiffness	r	-0.44*	-0.14	-0.09	-0.42*	-0.11
	p	0.047	0.54	0.69	0.049	0.64
Hippocampal Damping Ratio	r	0.08	0.26	0.08	-0.09	0.26
	p	0.75	0.25	0.73	0.69	0.26

HDL-C: high-density lipoprotein cholesterol; LDL-C: low-density lipoprotein cholesterol; TC: total cholesterol; TG: triglycerides; VLDL-C: very low-density lipoprotein cholesterol; r values represent Pearson's correlation coefficients; *p < 0.05; N=21

Serum TGs were not associated with HC stiffness (r=-0.14, p=0.54) or HC damping ratio (r=0.26, p=0.25) in our current cohort. However, because we had previously observed significant associations between elevated blood TGs and HC viscoelastic properties, we examined our data closely and created scatterplots

depicting the association between serum TGs and HC viscoelastic properties. The majority of our participants had clinically normal baseline TGs (< 150 mg/dL) while two participants had borderline high TGs (150-199 mg/dL) and one participant had clinically high TGs (200-499 mg/dL) (circled in red; **Figures 2.1A & B**). When this participant was removed from the analyses, higher TGs were more strongly correlated with lower HC stiffness (r=-0.39, p=0.087; **Figure 2.1C**), although this was not significant. After removing this outlier, higher TGs were also associated with a higher HC damping ratio (r=0.46, p=0.04; **Figure 2.1D**), which confirmed our previous findings.

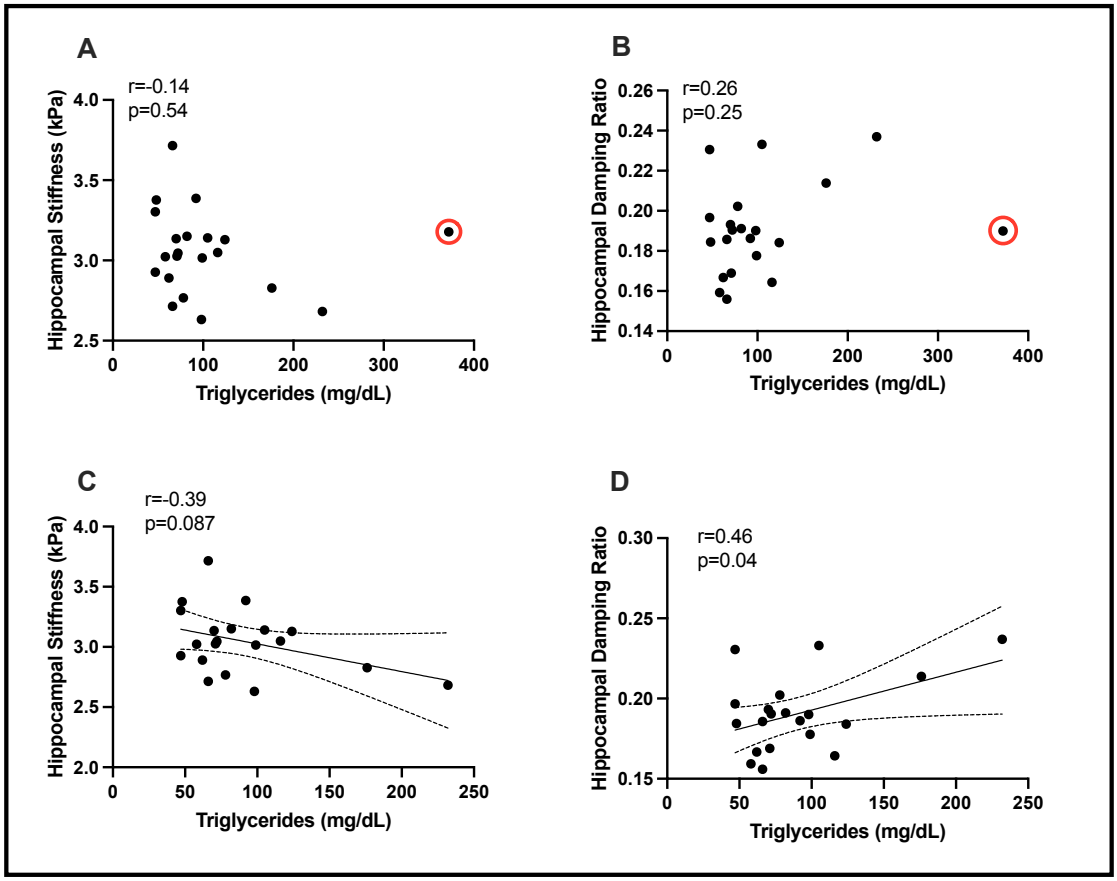

Figure 2.1 Association between serum triglycerides and (**A**) hippocampal stiffness (clinically high TG participant included); N=21; (**B**) hippocampal damping ratio (clinically high TG participant included); N=21; (**C**) hippocampal stiffness (clinically high TG participant removed); N=20; (**D**) hippocampal damping ratio (clinically high TG participant removed); *p < 0.05; N=20; dashed lines represent 95% confidence interval.

2.3.2 Cerebrovascular Function and Hippocampal Tissue Viscoelastic Properties

Resting perfusion and CVR for gray matter (GM) as well as for the HC are presented in Table 2.4. GM perfusion was not associated with HC stiffness (r=0.12, p=0.61). There was a near significant association between GM perfusion and HC damping ratio (r=-0.41, p=0.06). There was no association between HC perfusion and

HC stiffness (r=0.06, p=0.81) and damping ratio (r=-0.24, p=0.31). GM CVR was not associated with HC stiffness (r=-0.08, p=0.72) or HC damping ratio (r=0.05, p=0.84). HC CVR was also not associated with HC stiffness (r=0.13, p=0.56) or HC damping ratio (r=0.15, p=0.53).

Table 2.4 Bivariate correlation matrix between cerebrovascular measures and hippocampal viscoelastic properties

		GM CBF	**HC CBF**	**GM CVR**	**HC CVR**
Hippocampal Stiffness	r	0.12	0.06	-0.08	0.13
	p	0.61	0.81	0.72	0.56
Hippocampal Damping Ratio	r	-0.41	-0.24	0.05	0.15
	p	0.06	0.31	0.84	0.53

CBF: cerebral blood flow; CVR: cerebrovascular reactivity; GM: gray matter; HC: hippocampus; r values represent Pearson's correlation coefficients; *p < 0.05; N=21

2.3.3 Cerebrovascular Function as Mediator of Blood Lipids on Hippocampal Tissue Viscoelastic Properties

Mediation models were performed for each of the following statistically significant associations using GM and HC resting perfusion and CVR as mediators: LDL-C and HC stiffness and TG and HC damping ratio. GM [indirect effect: β=-0.008; 95% CI (-0.00067, 0.00052); **Figure 2.3A**] and HC [indirect effect: β=-0.001; 95% CI (-0.0003, 0.00027); **Figure 2.3B**] perfusion did not mediate the association between LDL-C and HC stiffness. GM [indirect effect: β=0.09; 95% CI (-0.000027, 0.000083); **Figure 2.4A**] and HC [indirect effect: β=-0.001; 95% CI (-0.00005,

0.00005); **Figure 2.4B**] perfusion also did not mediate the association between TG and HC damping ratio.

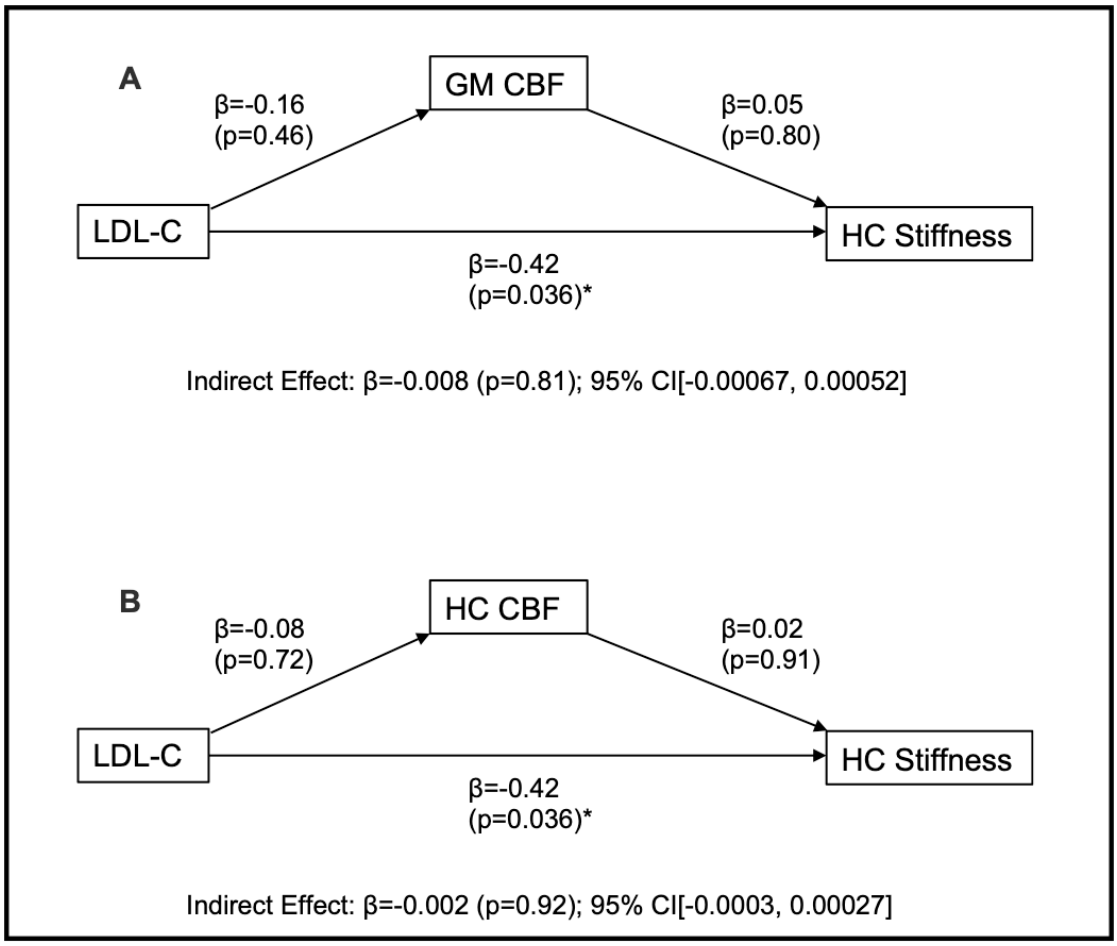

Figure 2.3 Mediation models between LDL-C and hippocampal stiffness showing no mediating effect of (A) gray matter perfusion and (B) hippocampal perfusion; *$p < 0.05$; N=21

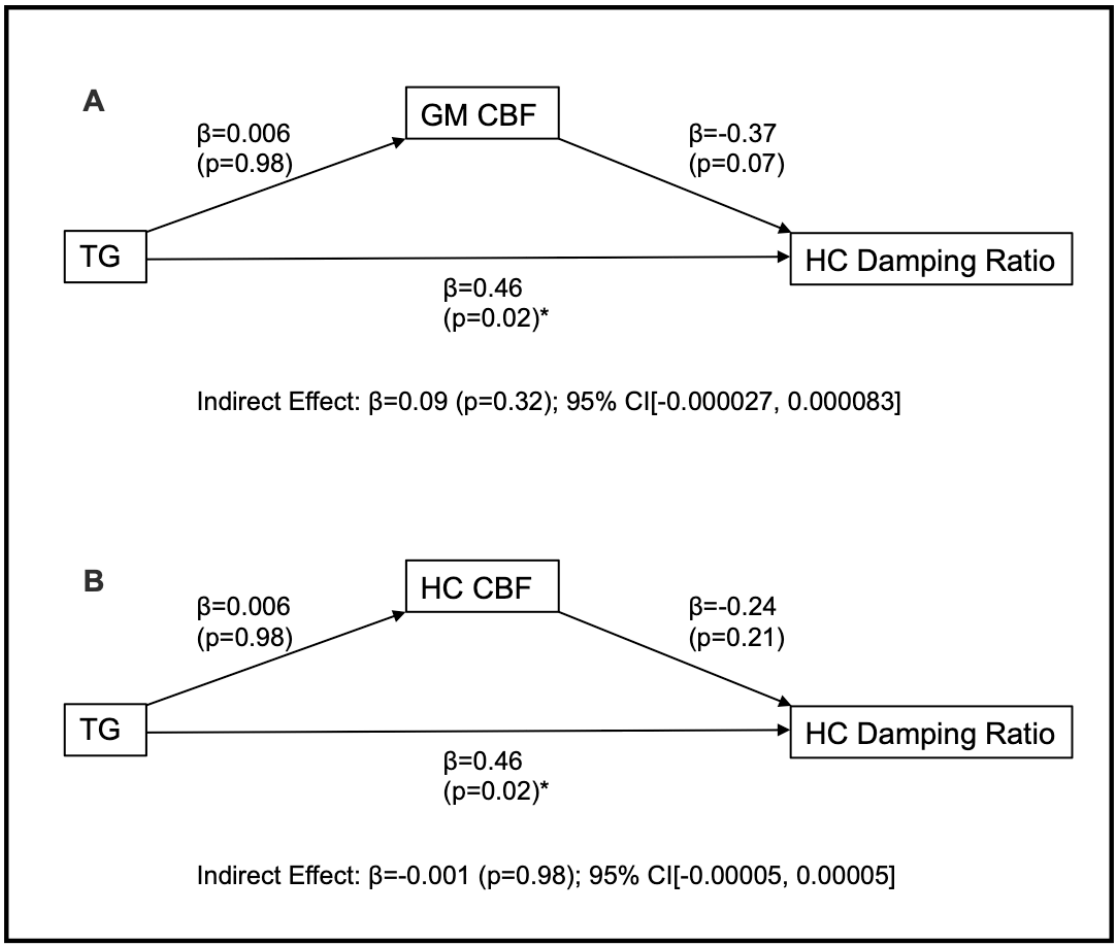

Figure 2.4 Mediation models between triglycerides and hippocampal damping ratio showing no mediating effect of (A) gray matter perfusion and (B) hippocampal perfusion; *p < 0.05; N=20

Both GM [indirect effect: β=0.03; 95% CI (-0.0013, 0.0016); **Figure 2.5A**] and HC [indirect effect: β=0.001; 95% CI (-0.001, 0.001); **Figure 2.5B**] CVR did not mediate the association between LDL-C and HC stiffness. GM [indirect effect: β=-0.05; 95% CI (-0.0003, 0.0002); **Figure 2.6A**] and HC [indirect effect: β=0.01; 95% CI (-0.0001, 0.0001); **Figure 2.6B**] CVR also did not mediate the association between TG and HC damping ratio.

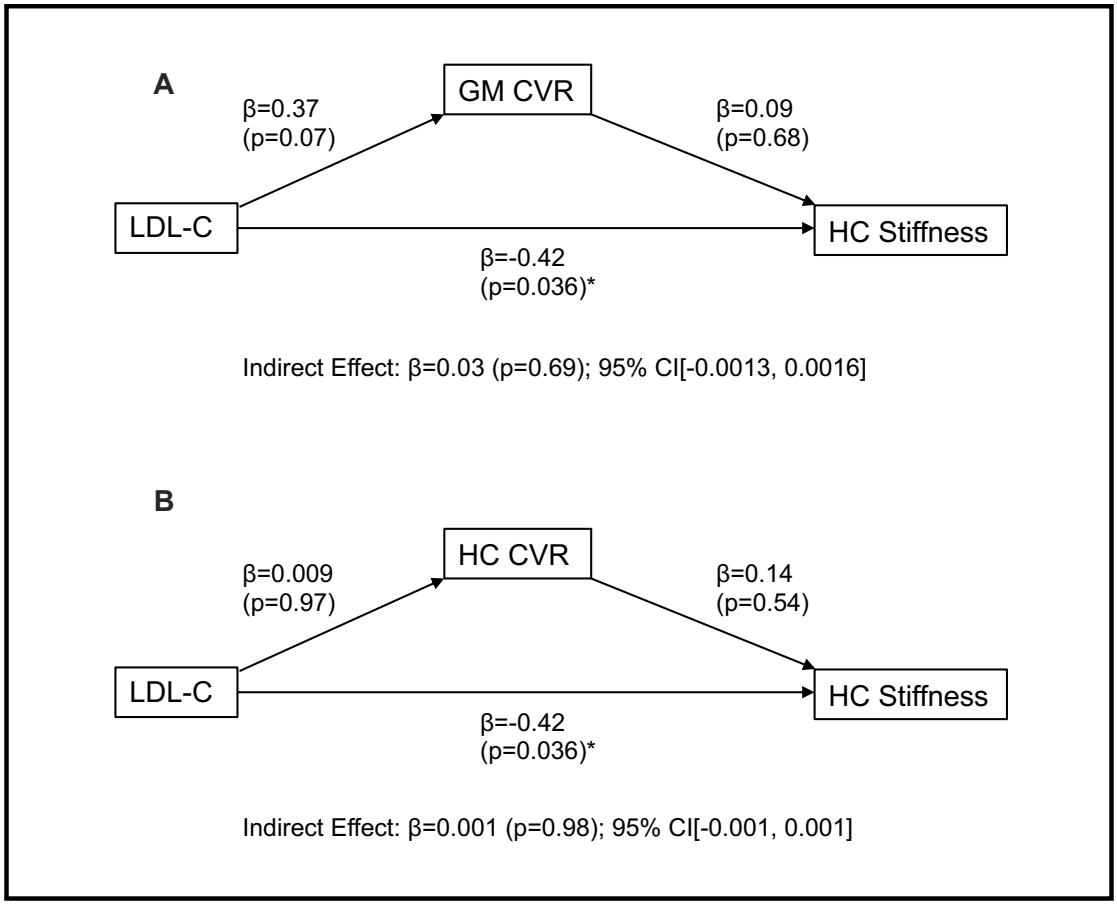

Figure 2.5 Mediation models between LDL-C and hippocampal stiffness showing no mediating effect of (A) gray matter cerebrovascular reactivity and (B) hippocampal cerebrovascular reactivity; *p < 0.05; N=21

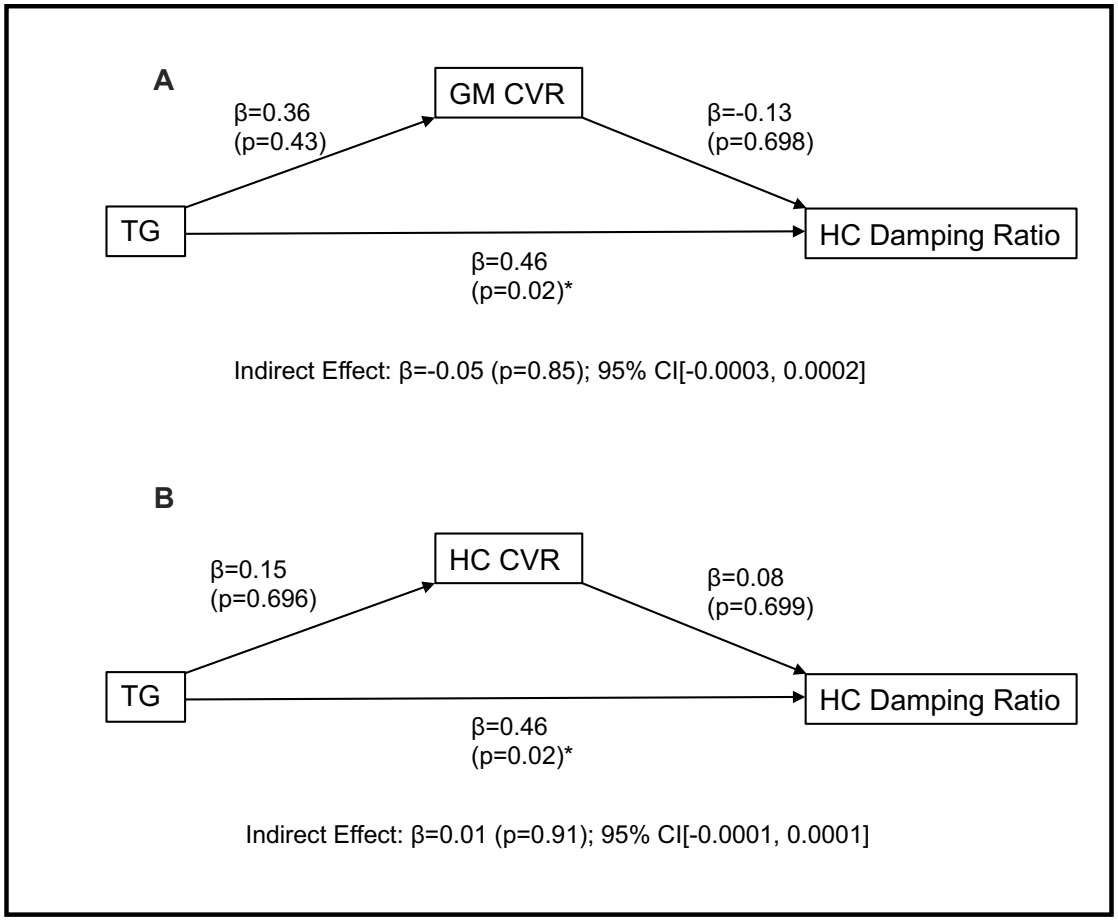

Figure 2.6 Mediation models between triglycerides and hippocampal damping ratio showing no mediating effect of (A) gray matter cerebrovascular reactivity and (B) hippocampal cerebrovascular reactivity; *$p < 0.05$; N=20

2.4 Discussion

The primary aim of this study was to test whether cerebrovascular function mediated the association between increased blood lipids and reduced HC tissue viscoelastic properties, which was observed in our previous findings (6). In this study, we found that elevated serum lipids were associated with reduced HC tissue viscoelastic properties; however, cerebrovascular function did not mediate this

association. We observed that a high LDL-C concentration was associated with a lower HC stiffness and a high TG concentration was associated with a greater HC damping ratio after removing a participant with clinically high TGs from the analyses. Contrary to our hypothesis, we did not find any associations between cerebrovascular function and HC tissue viscoelastic properties.

For this study, we used a high-resolution, noninvasive brain imaging modality - MRE to assess HC tissue viscoelastic properties. These properties include stiffness, which indicates neuronal density, neural network strength and myelin content, and damping ratio, which reflects neuronal organization and connections in animal models (144,167,168). A high damping ratio represents a more viscous fluid with fewer connections, whereas a lower damping ratio represents an elastic solid with dense neuronal connections (144). In contrast, a lower stiffness indicates softer brain tissue with fewer number of neurons in a weaker cellular matrix. Collectively, a lower HC stiffness and higher HC damping ratio represent a reduction in brain tissue integrity, which has been seen with increasing age (147–149,282,283) and in individuals with mild cognitive impairment and AD (151–153). The present study's results align with our previous findings in which we have shown that mildly elevated serum TGs are associated with increased HC damping ratio suggesting that slightly aberrant levels of TGs may play a role in disrupting neuronal connections and organization prior to causing clinically relevant structural damage such as HC tissue atrophy. A novel finding from this study was that LDL-C was associated with reduced HC stiffness, suggesting that LDL-C along with TGs have a role in softening the HC and attenuating HC tissue integrity.

The exact mechanism by which elevated blood lipids are associated with reduced HC tissue integrity is not known. Transport of TGs is carried out by TG-rich lipoproteins (TRLs) such as VLDL particles which, in high abundance, can bind to toll-like receptors on endothelial cells and release pro-inflammatory cytokines and reactive oxygen species (ROS) (14,231). ROS, primarily superoxide, scavenge nitric oxide (NO), reducing its bioavailability, thus leading to vascular endothelial dysfunction. Furthermore, elevated TRL binding leads to the formation of smaller and denser LDL particles that are readily oxidized, and in turn leads to increased pro-inflammatory signaling and binding of monocytes to endothelial cells also causing endothelial dysfunction (12). As such, we hypothesized that reduced cerebrovascular endothelial function may result from elevated blood lipids and be an important mediator of reduced HC tissue viscoelastic properties.

CO_2-mediated CVR reflects cerebrovascular endothelial function, and a reduction in CVR is associated with an increased risk of cognitive aging. Previous studies have found that CO_2-induced CVR results in a transient increase in brain tissue viscoelastic properties (19,20). However, it is important to note that these observations were made using acute manipulations of cerebral hemodynamics that led to a transient change in brain tissue viscoelastic properties. Because of this established acute link between hemodynamic and brain tissue properties, we hypothesized that reduced cerebrovascular function would lead to chronically reduced brain tissue properties and would explain the link between elevated blood lipids and reduced HC stiffness; however, this was not observed. Therefore, it is possible that chronically high or low CVR may play less of a role in regulating HC tissue properties as is reflected by a lack of any associations between cerebrovascular measures and HC tissue viscoelastic

properties in our present cohort. Additionally, our mediation analyses did not reveal a significant effect of LDL-C or TG on cerebrovascular function. This could possibly be due to the fact that our participant cohort consisted of healthy young and mid-life individuals, most of whom habitually had clinically normal serum lipids and therefore, these lipid concentrations were not significant enough to be associated with an alteration in their cerebrovascular function. Therefore, there appears to be a different mechanism than cerebrovascular function that may be related to the association between increased blood lipids and reduced HC tissue properties.

Other determinants of cardiovascular disease risk and brain aging such as large artery stiffness and central pulse pressures could be alternate mechanism by which blood lipids impact HC tissue properties. A review by Wilkinson and Cockcroft (2007) provides a summary of multiple studies that observed significant positive associations among elevated total cholesterol, TGs and LDL-C and measures of arterial stiffness and pulse pressure (284). Additionally, our recent work has found that elevated carotid pulse pressure is associated with a reduced HC stiffness in adults across the lifespan (285). Hence, arterial stiffness and pulse pressure may be potential mediators of the association between elevated blood lipids and HC tissue properties and therefore, should be investigated in future studies.

Poor lifestyle factors such as consumption of a Western-style diet that consists of high added sugar and saturated fats, may be a contributor of the association between elevated lipids and reduced HC tissue properties. Many animal studies have shown the presence of increased neural inflammation (286,287) and reduction of brain-derived neurotrophic factor (BDNF) (288,289) following consumption of Western-style diets. As such, it will be important to conduct randomized-controlled trials to investigate the

effect of added sugars and saturated fats as a mechanistic link for the association between blood lipids and markers of brain health.

Currently there is not enough evidence to support that TGs or other TRLs such as VLDL and LDL can cross the blood-brain barrier (BBB). However, Banks et al. (2018) detected TGs in human cerebrospinal fluid (CSF) and found that radioactive TG triolein could readily cross the BBB in mice (290). The authors also showed that administration of the fenofibrate gemfibrozil lowered serum TGs and improved cognitive function in these mice. Other animal studies suggest that TGs may be involved in the impairment of the N-methyl-D-aspartate component of the long-term synaptic potentiation in the HC (291). Another potential mechanism by which TGs can negatively impact the brain is through the breakdown and release of free fatty acids directly in the brain from adipocytes. The free fatty acid receptor, GPR40, was also detected in the HC (292) along with saturated free fatty acids, palmitic acid and lauric acid, which have been shown to induce a cascade of pro-inflammatory signaling in cultured macrophages and regulating astrocytic and microglial signaling (293–295).

Even though this study was conducted in healthy individuals, our results have important implications in age-related cognitive impairment and dementia risk. Blood lipids, specifically TGs, may play a role in cerebral amyloid-beta (Aβ) deposition. In a longitudinal study, Nagga et al. (2018) found that older individuals with high mid-life serums TGs had an increased risk of Aβ and tau pathology two decades later (296). Although exact pathophysiological effect of TGs was not understood from this study, the authors suggest that TGs could have a direct effect on Aβ homeostasis (297) and Aβ aggression kinetics (298). They also suggest that lipids could contribute to increased membrane fluidity that may trigger secretase-mediated Aβ production (299)

and in addition, TRLs in blood could be Aβ carriers (300). Apolipoprotein E (ApoE) genotype may be involved in the association between increased lipids and reduced HC tissue properties because of its significant role in lipid metabolism and its transport of Aβ (301–303). Individuals with one or more copies of the ε4 variant of the ApoE gene are at an increased risk of AD (304). In our cohort, we had six individuals with one copy of the ε4 variant, however, we did not see a difference in lipid concentration or HC tissue properties in ε4 carriers vs. non-carriers (data not shown). Future studies with an even distribution of ε4 carriers and non-carriers need to be conducted to identify if ApoE genotype has any influence on the association between blood lipids and HC tissue properties.

This study has some limitations with respect to the sample size (N=21), which was powered to detect a change in cerebrovascular function during acute added sugar consumption (Chapter 3) and may have been underpowered for a mediation analysis (305); however, our data still provide useful information as it confirms our previous observation in which elevated blood lipids were associated with reduced HC viscoelastic tissue properties. Due to the small sample size and lack of diversity, we were limited in the generalizability of our findings and the ability to examine the effect of sex on the associations between blood lipids and markers of brain health. Furthermore, even though we reported menopausal status, menstrual cycle in premenopausal females was not controlled for in this study, however, it has been shown that controlling for menstrual cycle phase differences has no effect on peripheral vascular endothelial function (306) and cerebral autoregulation (307), and it is also believed to reduce external validity of physiological findings as it is not reflective of the general population (308). The cross-sectional aspect of this study also

prevents us from deriving a causal link of the associations between blood lipids and HC tissue properties. Even though, we made every effort to recruit participants within a narrow age range, our cohort consisted of individuals in their 30s and 40s, in addition to mid-life adults who were generally healthy and had mostly normal serum lipids. Therefore, it is possible that changes in blood lipids did not yet fully converge to cause changes in cerebrovascular function in a subset of our participants, thus leading to an underestimation of the contribution of cerebrovascular function as the mediator of the association between blood lipids and HC tissue properties. These limitations can be overcome by conducting longitudinal studies with a larger sample size and a tighter window of mid-life individuals when the earliest mechanistic changes in the association between lipids and markers of brain health can be detected.

2.5 Conclusions

In summary, the purpose of this study was to determine if cerebrovascular function mediated the association between elevated blood lipids and reduced HC tissue viscoelastic properties. Our primary findings indicate that serum LDL-C is associated with a lower HC stiffness and serum TGs are associated with a higher HC damping ratio. We did not find any direct associations between cerebrovascular function and lipids or cerebrovascular function with HC tissue properties. We also did not see a mediating effect of cerebrovascular function on the association between lipids and HC tissue properties. Despite not finding significant effects of cerebrovascular function on the relation between lipids and brain tissue properties, this study confirmed our previous findings that even mildly elevated blood lipids are associated with reductions in HC tissue properties. This finding provides an important premise of targeting cardiometabolic risk factors such as blood lipids as a potential

therapeutic to prevent or delay future cognitive aging. Further randomized-controlled trials investigating the effect of poor lifestyle factors such as diet and its associated inflammation along with other measures of vascular function need to be conducted via longitudinal studies with a tighter age range in order to identify the mechanistic association between lipids and brain health.

Chapter 3

ACUTE EFFECTS OF DIETARY ADDED SUGARS ON CEREBROVASCULAR FUNCTION AND BRAIN TISSUE VISCOELASTIC PROPERTIES

3.1 Introduction

Alzheimer's disease (AD), the most common form of dementia characterized by neurodegeneration and irreversible memory loss, shares many of the same modifiable risk factors as cardiometabolic diseases (4). Poor lifestyle factors such as consumption of a Western diet contribute to elevated cardiometabolic risk parameters due, in part, to the high abundance of added sugars (5,21). Dietary added sugars are caloric sweeteners that are added to foods and beverages during processing and preparation (22). The most common form of added sugar is fructose, which is mostly added to processed foods in the form of high-fructose corn syrup (HFCS) (55% of fructose and 45% of glucose), or as sucrose (table sugar), which consists of glucose and fructose linked by a glycosidic bond. While glucose is converted and stored by the liver as glycogen or is transported in blood to other tissues to generate ATP, excess dietary fructose is metabolized by the liver to form triglycerides (TGs) by a process called *de novo* lipogenesis (11,24,181,205). TGs are packaged and transported in blood within very low-density lipoprotein (VLDL) particles for energy production or long-term storage in adipose tissue. Accumulation of TG-rich VLDL particles causes them to bind to receptors in vascular endothelial cells, resulting in the activation of transcription factor, nuclear factor kappa B (NFκB), which promotes the release of

reactive oxygen species (ROS) (12,14). These ROS scavenge endothelial nitric oxide (NO), therefore, reducing its bioavailability and leading to peripheral vascular endothelial dysfunction (228).

The metabolism of fructose also leads to the generation of uric acid from the rapid phosphorylation of fructose by the enzyme fructokinase C which results in a reduction in ATP (8,10). The reduction of ATP and uric acid generation leads to activation of nicotinamide adenine dinucleotide phosphate (NADPH) oxidase, triggering a cascade that results in the production of mitochondrial superoxide (O_2^-), and a subsequent reduction in endothelial NO bioavailability, ultimately resulting in peripheral vascular endothelial dysfunction (9,237,238,309). Although the effects of blood lipids and uric acid on vascular endothelial dysfunction may occur over a long period of time as a result of chronic exposure, it has also been shown that increased acute added sugar intake is associated with an increase in serum TGs (203,206,208,210,214) and a reduction in peripheral vascular endothelial function (25–29,33). Limited research has also shown that acute fructose intake is associated with a reduction in cerebral blood flow (CBF) (30,31) and middle cerebral artery blood velocity (32). However, these studies focused primarily on the acute effect of added sugars from soft drinks or fructose infusions on other brain pathways such as appetite and reward behavior. Moreover, studies investigating the effect of added sugars on peripheral vascular endothelial function focused on the hyperglycemic response instead of the effects of fructose in added sugars. Hence, it is unknown whether added sugars found in solid foods in a typical Western-style meal affect brain health.

Our previous findings have shown that elevated blood lipids, particularly TGs, are cross-sectionally associated with reduced memory performance and neuronal tissue viscoelastic properties of the hippocampus (HC) (6), a brain structure essential for memory encoding and recall (7). Furthermore, prior studies have observed that an increase in CO_2-induced cerebrovascular reactivity (CVR) results in a transient increase in brain tissue properties (19,20). Since the associations among added sugar intake, elevated blood lipids, and peripheral vascular endothelial function are well-established, it is possible that added sugars may affect the cerebral vasculature and brain tissue in a similar manner. Therefore, understanding the link between acute added sugar consumption and markers of brain health may provide insight into the underlying mechanisms by which chronic consumption of a Western diet accelerates risk for cognitive aging. The rationale behind this study was to investigate the effects of a single meal containing high vs. low added sugars on CVR and brain tissue viscoelastic properties prior to- and 3 hours postprandial. Whether the changes to these brain health measures were related to changes in blood lipids, uric acid and markers of ROS were also examined. Furthermore, measures of cognitive (executive) function on a subset of participants in response to either meal was examined. We hypothesized that the high-sugar meal would acutely lower CVR, brain tissue viscoelastic properties and cognitive function, and these reductions will be associated with an increase in blood lipids, uric acid, and markers of ROS. Based on the findings that high baseline TGs are associated with reduced brain tissue viscoelastic properties and high acute added sugar intake is associated with elevated blood TG production and reduced peripheral vascular endothelial function, we hypothesized that individuals with high baseline serum TGs would exhibit the greatest reduction in CVR and brain tissue

viscoelastic properties in response to the high-sugar meal compared to the low-sugar meal.

3.2 Methods

The study was approved by University of Delaware's (UD) Institutional Review Board (1718585) and registered as a randomized-controlled clinical trial (ClinicalTrials.gov Identifier: NCT05408338). Experimental procedures and protocols outlined in this study conformed to the standards outlined in the latest revisions of the Declaration of Helsinki (revised 1983). The study purpose, along with the possible benefits and risks, were explained to all study participants and written and verbal informed consent was obtained from participants prior to participation. All measurements were made at UD's Neurovascular Aging Laboratory and the Center for Biomedical and Brain Imaging between June 2022 and April 2023.

3.2.1 Study Protocol

The study consisted of three in-person visits, including one consent and screening visit (Visit 1) and two identical experimental visits distinguished by either a high-sugar (HS) meal or a low-sugar (LS) meal (Visits 2 and 3). Participants completed medical history, family history, MRI safety, menstrual history (females only), and diet history (DHQ-III) questionnaires during the screening visit. Height (cm) and body mass (kg) were measured using a stadiometer and electronic scale from which body mass index (BMI; kg/m^2) was calculated. Seated resting blood pressures were assessed after 10 minutes of quiet rest using a semi-automated blood pressure device (ADView 2®, American Diagnostic Corporation, Hauppauge, NY). Participants' non-dominant arm was used to make repeat measurements with 2 min of

quiet rest between each measurement until three blood pressure values were within 5 mmHg of each other. The values were averaged to determine resting systolic and diastolic blood pressure (SBP, DBP).

After the screening visit, participants were randomized to either the HS meal or the LS meal condition after which they crossed over to the other meal on two separate days. A blocked randomization stratified by biological sex created by a biostatistician was used for randomization. Each visit was separated by a washout period of at least 7 days and took place at the same time of day. Participants refrained from over-the-counter medications for 48 h, vigorous aerobic exercise and alcohol for 24 h and food and beverages (except water), including caffeine for 12 h before each experimental visit. Participants completed a 24-hour dietary assessment (ASA24) questionnaire to ensure they consumed similar diets prior to their experimental study visits as well as diets similar to their habitual diet (assessed with DHQ-III during screening) to minimize variability between these visits. Primary outcomes were assessed at baseline and at 3 hours postprandial (i.e., time at which substantial increase in TG occurs compared to baseline), and included measures of CVR, brain tissue viscoelastic properties, and executive function and processing speed. Serum TG, LDL-C, HDL-C, VLDL, uric acid, total antioxidant capacity (TAC) and oxidative stress were measured at baseline and 3 hours postprandial and were used to determine if direct changes in primary outcomes, following each meal, were associated with changes in blood markers.

3.2.2 Study Participants

We recruited twenty-two young and mid-life adult men and women (9M/15F) between the ages of 30 – 64 years from the greater Newark/Wilmington, DE area.

Participants were generally healthy with normal liver and renal function and without stage 2 hypertension (SBP < 140 mmHg; DBP < 90) and morbid obesity (BMI < 40 kg/m^2). Participants were also free from chronic diseases (e.g., heart disease, kidney disease, type 1 or 2 diabetes, cancer) and major psychological and neurological disorders as assessed by their medical history, complete blood count, and comprehensive metabolic panel. We excluded participants who were smokers and/or tobacco product users, who were on lipid-lower medications (e.g., statins), who consumed more than 10-15% of their total calories from added sugars (assessed from DHQ-III), who were intolerant or allergic to any of the study meal ingredients (e.g. gluten, lactose, nuts), who were unable to have an MRI scan (e.g., metal implants) and females who were pregnant or breastfeeding.

3.2.3 Study Meals

Participants were provided a single meal high in added sugars (HS: 61 g,) and a single meal low in added sugars (LS: 16 g). The meals were chosen in consultation with a registered dietician and were similar in total energy (HS: 1260 kcal; LS: 1301 kcal) and macronutrient content (HS: Carbohydrates: 150 g; Total fat: 60 g; Protein: 30 g; LS: Carbohydrates: 155 g; Total fat: 61 g; Protein: 33 g) but differed in saturated fatty acids (SFA) (HS: 26 g vs. LS: 12 g), poly- (PUFA) (HS: 12 g vs. LS: 16 g) and monounsaturated fatty acids (MUFA) (HS: 22 g vs. LS: 33 g), and fiber content (HS: 5 g vs. LS: 19 g). Added sugars and fatty acid amounts of the meals were selected from previous literature that had observed a robust increase in blood TGs 3 hours postprandial (203,208).

3.2.4 Blood Analysis

Venous blood samples were drawn from the participants' antecubital vein by a laboratory member trained in phlebotomy. A standard serum lipid panel, consisting of total cholesterol, TG, LDL-C, HDL-C, and very low-density lipoprotein cholesterol (VLDL-C), and serum uric acid were assessed (Labcorp, Burlington, NC) Additionally, whole blood and plasma samples were stored for measuring oxidative stress and antioxidant capacity.

3.2.4.1 Measurement of Oxidative Stress

Oxidative stress was assessed by quantifying ROS, specifically free radicals such as O_2^- from whole blood samples using electron parametric resonance (EPR) spectroscopy (310) using EMXnano (Bruker, Billerica, MA). Whole blood was incubated for 10 minutes at 37°C, immediately after collection, in a buffer solution containing 0.2 mM of 1-hydroxy-3-methoxycarbonyl-2,2,5,5-tetramethylpyrrolidine (CMH) spin probe and 100 μM of phosphate buffer saline (PBS) in diethylenetriamine acid (DTPA). The CMH spin probe allows for the detection of O_2^- as it is oxidized by O_2^- to form 3-methoxycarbonyl-proxyl nitroxide (CM), which is paramagnetic and is able to be easily detected by EPR (311). Since O_2^- is highly reactive with a short half-life (312), DTPA is used as a chelating agent to prevent O_2^- from reacting with ferrous compounds. Blood samples incubated in CMH and DTPA were pipetted into polytetrafluoroethylene (PTFE) tubes and flash frozen in liquid nitrogen and stored in -80°C freezer for batch analysis by EPR using acquisition parameters described in previous literature (313). The sample O_2^- concentration was assessed as molarity (mol/L) and number of spins that represent number of O_2^- or free radicals.

3.2.4.2 Measurement of Total Antioxidant Capacity

We used a Trolox equivalent antioxidant capacity assay kit (catalogue# ab65329, Abcam, BioVision) to measure total antioxidant capacity (TAC). All reagents and samples were allowed to equilibrate to room temperature before use. 1 μL of plasma sample was adjusted to 100 μL of ddH_20 and 100 μL of Cu^{2+} solution and added onto standard and sample wells of a 96-well microtiter plate. An orbital plate shaker was used to incubate the light-protected plate at room temperature for 90 min. Optical density was measured at 570 nm on a microplate reader. TAC was assessed as a function of Trolox concentration using the equation:

$\frac{S_a}{S_v}$ in mM Trolox equivalent

where S_a = sample amount (nmol) from the standard curve;

S_v = undiluted sample volume added to wells

3.2.5 Cerebrovascular Reactivity

We assessed cerebrovascular reactivity (CVR) as the maximal change (from rest) in cerebral perfusion measured with arterial-spin labeling (ASL) during 3-minutes of hypercapnia in 20 participants. An MR-compatible prospective end-tidal targeting system, which allows for precise and repeatable manipulation of end-tidal partial pressure of carbon dioxide ($P_{ET}CO_2$) on a breath-by-breath basis using a computerized gas blender (RespirAct™, Thornhill Research, Ontario, Canada), was used to induce hypercapnia (132,136,273). Participants had a rubber face-mask fitted onto their faces with adhesive tape (Tegaderm, 3M, St. Paul, MN) prior to the ASL scan to ensure there were no air leaks. After the face-mask was connected to the gas-delivery system, participants were asked to breathe at a steady rate (15 breaths per minute) for ~ 3 minutes to allow oxygen (O_2) consumption and CO_2 production to

achieve a steady state. Four input gases were supplied to the gas blender from customized gas tanks (Airgas, Air Liquide, Radnor, PA): (1) gas A 10/90% O_2/N_2; (2) gas B 10/90% O_2/CO_2; (3) pure oxygen (100% O_2); (4) calibration gas (10/9% CO_2/O_2/balance N_2). Target $P_{ET}CO_2$ was set at 9 mmHg above resting values, whereas $P_{ET}O_2$ remained at resting levels. ASL images were acquired over 9 minutes including 3 minutes of resting, 3 minutes of hypercapnia, and 3 minutes of recovery scans. CVR was calculated using the formula:

$$CVR = \frac{CBF_{hypercapnia} - CBF_{resting}}{CBF_{resting}\,(P_{ET}CO_{2.hypercapnia} - P_{ET}CO_{2.resting})} \times 100\%$$

3.2.5.1 Measurement of Cerebral Perfusion

We used a pseudo-continuous arterial spin labeling (PCASL) scan sequence, obtained from the Human Connectome Project (275) and modified according to Alsop et al.'s (2015) "white paper" for clinical ASL implementations (276) to quantify cerebral perfusion (274). Imaging parameters used for the scan were: TR/TE: 4510/20 ms; voxel size: 2.5 x 2.5 x 2.3 mm^3; flip angle: 90°; 215 x 215 mm^2 FOV; 86 x 86 matrix; 60 slices; slice thickness: 2.27 mm; labeling duration: 1.8 s; post-labeling delay (PLD): 1.8 s; 60 pairs of control/label images; total acquisition time: 9 minutes and 27 seconds. Signal readout was implemented using multi-band 2D gradient echo-planar imaging (EPI) using partial Fourier = 6/8 and SMS acceleration factor = 6. Two equilibrium echo magnetization (M_0) images were acquired at the end of the scan and were averaged to produce a calibration image.

The segmented T_1 MPRAGE image, collected prior to the MRE scan (described in section 3.1.5) were registered onto the ASL space using the FLIRT tool in FSL. Perfusion was quantified with a standard kinetic- model inversion using the

Bayesian algorithm (277). Perfusion maps were calibrated onto the proton density-weighted M_0 image using voxel-wise calibration mode with a sequence TR=8 s and a calibration gain of 1. Motion correction and spatial regularization of the estimated perfusion image were used on the ASL time-series (278). Partial volume correction was used to quantify GM perfusion (279). Perfusion in each voxel was calculated using the following formula for PCASL as per the assumptions stated by Alsop et al. (2015) (276):

$$CBF = \frac{6000 \,.\, \lambda \,.\, (SI_{control} - SI_{label}) \,.\, e^{\frac{PLD}{T_{1b}}}}{2 \,.\, \alpha \,.\, T1_b \,.\, SI_{PD} \,.\, (1 - e^{\frac{-\tau}{T_{1b}}})}$$

where λ = 0.9 mL/g (brain/blood barrier partition coefficient);

$SI_{control}$ and SI_{label} = time-averaged signal intensities of control and label images;

PLD = post-labeling delay;

T_{1b} = 1.65 s (longitudinal relaxation time of blood);

α = 0.85 (labeling efficiency);

SI_{PD} = signal intensity of proton density-weighted image;

τ = labeling duration;

The factor of 6000 was used to convert the units from mL/g/s to mL/(100g)/min.

ASL images registered to the T_1-weighted structural space allowed for overlaying of the bilateral HC masks on the ASL perfusion image using 95% threshold to obtain HC perfusion values.

3.2.6 Brain Tissue Viscoelastic Properties

A 3T Magnetom Prisma MRI scanner (Siemens, Erlangen, Germany) with a 64-channel head coil was used to perform all MRI measurements. We performed a T_1-weighted magnetization-prepared rapid echo (MPRAGE) scan (repetition time (TR)/echo time (TE): 2300/2.32 ms; flip angle: 8°; 240 x 240 mm^2 FOV; 256 x 256 matrix; 192 slices; slice thickness: 0.9 mm) to obtain bilateral HC masks that were segmented using FreeSurfer 6.0 (6) and registered from the T_1 anatomical space into the magnetic resonance elastography (MRE) space using the FLIRT tool in FSL (FMRIB Software Library v. 6.0.0) (272). The HC masks provided information about the HC viscoelastic properties.

A high-resolution (1.25 mm^3 isotropic) 3D multiband, multishot spiral MRE sequence with a total scan time of 4 minutes and 29 seconds was used to assess viscoelastic properties of the whole brain. The imaging parameters were: TR/TE: 140/76 ms; flip angle: 90°; 240 x 240 mm^2 field-of-view (FOV); 160 x 160 matrix; 80 slices; slice thickness: 1.5 mm. A pneumatic actuator system (Resoundant, Rochester, MN) and a soft pillow driver generated shear waves synchronously with the scan at 50 Hz to the participant's head (161). The resulting motion and displacement data were used to estimate maps of the viscoelastic complex shear modulus, which were used to calculate the viscoelastic properties that include shear stiffness and damping ratio (159,160,164–166) as previously described by our group (6).

3.2.7 Cognitive Tasks

Cognitive measures of executive function and processing speed were assessed in a subset of participants (N=10) using NIH Toolbox Cognition Battery (NIHTB-CB; v. 1.26.7141) on an iPad. Age, sex, education, race, and ethnicity were normalized

across all tests. The trials on these tests were mixed and standardized on each day (HS meal vs LS meal day) and time-point (baseline and postprandial) for each participant. Participants received instructions orally by the same experimenter and visually from the iPad. Inhibitory control and attention were assessed using the Flanker test. During the Flanker test, participants focused on a visual target and selected one of two buttons on the iPad screen that matched the direction where a middle arrow was pointing, while ignoring other side stimuli called flanking. Participants received congruent trials in which all arrows pointed in the same direction as the middle arrow and incongruent trials in which the arrows pointed in the opposite direction as the middle arrow. Mean accuracy and reaction times were scored.

Cognitive flexibility was assessed using the Dimensional Change Card Sort test. During this test, participants matched a target stimulus to one of two choice stimuli according to a word cue (e.g. shape or color). Participants received a mix of "repeat" trials in which one dimension (e.g. color) is relevant for majority of the trials with occasional changes to the other dimension (e.g. shape) and "switch" trials in which the dimension from preceding trials must be changed (e.g. from shape to color). This test was also scored for mean accuracy and reaction time.

Processing speed was assessed using the Pattern Comparison Processing Speed test. Participants identified whether two visual patterns were the "same" or "not the same". The test was scored as the number of correct items selected in 90 seconds.

3.2.8 Statistical Analysis

The primary outcomes of this study were CVR and brain tissue viscoelastic properties in response to a HS and a LS meal. We performed an *a priori* power analysis based on a study by Rudolph et al. (2007) that aimed to examine the acute

effects of fast-food meals on peripheral vascular endothelial function assessed by brachial flow-mediated dilation (FMD. This study found that an effect size of d=0.70 was achieved to detect a minimum of 30% difference in the primary target variables of the mean diet-induced changes in FMD between 2 meals in a sample size of 24 participants with an α=0.05 and power=0.80 (314). Based on the results of this study, we determined that to detect a significant main effect of meal on the primary outcomes and to achieve significance at α=0.05 and power=0.90, we would need 19 participants. We targeted a sample size of N=20 to have equal number of males and females. Data were analyzed using a two-way repeated measures ANOVA (meal x time). We used Tukey's post hoc comparison tests when needed. Postprandial changes in primary outcomes and blood variables comparing HS vs. LS meals were assessed using paired t-tests. We also performed an exploratory sensitivity analysis to determine whether baseline cardiometabolic risk assessed with baseline TGs affected the responsiveness to the HS meal. Postprandial changes in primary outcomes were correlated to postprandial changes in serum TGs to assess if individuals with higher baseline TGs exhibited a greater response than those with lower baseline TGs due to the HS meal compared to the LS meal. Data were assessed for normality using Shapiro-Wilk test (280) and by examining Q-Q plots. When non-normal datasets were present, we performed nonparametric analyses. Data are expressed as mean±SD. Statistical significance was set at $p < 0.05$. We used GraphPad Prism 9.0 (GraphPad Sofware Inc., San Diego, CA) for all statistical analyses.

3.3 Results

Twenty-two adult men and women (9M/13F) between the ages of 30-64 years completed this study. Participants were generally healthy and did not report any overt

cardiovascular disease or other chronic diseases. Participant screening characteristics are presented in **Table 3.1**. Participants were young to mid-life, mostly White adults, who were normotensive and had normal BMI. There were four premenopausal, two perimenopausal and seven postmenopausal females enrolled in the study. Participant screening and baseline blood chemistries are presented in **Table 3.2**. Lipid panel values presented are averages of fasted baseline values from the 2 experimental visits of the clinical trial. Participants' mean blood chemistries were within normal limits, except for total and LDL cholesterol, which were clinically within the borderline high range.

Participants' habitual dietary intake and diet recalls 24 hours prior to each experimental visit (HS vs. LS) are presented in **Table 3.3**. There were no significant differences between energy, macronutrients and micronutrients consumed habitually and before each experimental except for alcohol intake as participants were asked to refrain from alcohol 24 hours prior to the experimental visits.

Table 3.1 Screening characteristics

Demographic data	
N, M/F	9/13
Race, White/Asian	21/1
Menopause Status, Pre/Peri/Post	4/2/7
Anthropometrics	
Age, yr	48 ± 12
Body Mass, kg	70 ± 12
Height, cm	167 ± 11
BMI, kg/m^2	24.7 ± 2.8
Hemodynamics	
Systolic BP, mmHg	116 ± 11
Diastolic BP, mmHg	73 ± 6
MAP, mmHg	87 ± 7
Heart rate, bpm	64 ± 9

Data are expressed as mean ± SD. BMI: body mass index; BP: blood pressure; MAP: mean arterial pressure.

Table 3.2 Baseline blood chemistries

Complete Blood Count	
WBC, x $10^3/\mu L$	5.0 ± 1.1
RBC, x $10^6/\mu L$	4.5 ± 0.3
Hemoglobin, g/dL	13.8 ± 0.8
Hematocrit, %	41.4 ± 2.5
Metabolic Panel	
Glucose, mg/dL	89 ± 7.0
BUN, mg/dL	13.8 ± 2.9
Creatinine, mg/dL	0.9 ± 0.1
eGFR, mL/min/1.73	93 ± 15.2
BUN/Creatinine	16.5 ± 3.4
Sodium, mmol/L	141 ± 2.3
Potassium, mmol/L	4.4 ± 0.3
Chloride, mmol/L	102.4 ± 2.6
Lipid Panel	
Total Cholesterol, mg/dL	216 ± 37
Triglycerides, mg/dL	105 ± 74
HDL Cholesterol, mg/dL	65 ± 20
LDL Cholesterol, mg/dL	132 ± 30
VLDL Cholesterol, mg/dL	19 ± 14

Data are expressed as mean ± SD. BUN: blood urea nitrogen; eGFR: estimated glomerular filtration rate; HDL: high-density lipoprotein; LDL: low-density lipoprotein; RBC: red blood cells; VLDL: very low-density lipoprotein; WBC: white blood cells.

Table 3.3 Dietary intake

	Habitual	**24-hr HS**	**24-hr LS**	**P-value**
Energy intake, kcal/day	1626 ± 658	1857 ± 608	1907 ± 834	0.38
Total carbohydrate, g/day	193 ± 89	210 ± 92	227 ± 112	0.52
Total protein, g/day	74 ± 35	79 ± 25	77 ± 37	0.89
Total fat, g/day	62 ± 23	79 ± 35	79 ± 38	0.13
Added sugars, g/day	43 ± 26	40 ± 32	46 ± 38	0.83
Total fiber, g/day	20 ± 13	20 ± 10	22 ± 12	0.74
Saturated fat, g/day	20 ± 9	27 ± 18	26 ± 17	0.23
Sodium, mg/day	2731 ± 1107	3545 ± 1409	3307 ± 1907	0.19
Potassium, mg/day	2755 ± 1390	2686 ± 1243	2814 ± 1408	0.95
Calcium, mg/day	1032 ± 532	1053 ± 595	1018 ± 587	0.98
Magnesium, mg/day	333 ± 166	301 ± 103	330 ± 172	0.73
Vitamin A (RAE), mcg/day	950 ± 746	907 ± 881	1053 ± 808	0.83
Vitamin C, mg/day	100 ± 88	77 ± 58	92 ± 77	0.60
Iron, mg/day	14 ± 7	15 ± 7	17 ± 10	0.48
Zinc, mg/day	10 ± 5	11 ± 6	11 ± 7	0.95
Alcohol, g/day	5 ± 6	0 ± 0	0 ± 0	<0.001*

Data are mean ± SD; 24-hr HS: dietary intake 24 hours prior to high-sugar meal; 24-hr LS: dietary intake 24 hours prior to low-sugar meal; *$p < 0.05$; N=22

3.3.1 Serum Lipids and Uric Acid

Serum lipids in response to each meal are presented in **Table 3.4**. Total cholesterol concentration was higher compared to baseline after consumption of both HS and LS meals. TG (**Figure 3.1A**) and VLDL-C concentrations were higher compared to baseline after consumption of both HS and LS meals. Due to a trending interaction effect of time x meal ($p=0.07$) on TG concentration, we further examined if the postprandial changes in TG concentration differed between the HS and LS meals. Increase in TGs following the HS meal tended to be greater than the increase following the LS meal, although this was not statistically significant ($p=0.06$; **Figure 3.1B**). There was a main effect of time and a near significant interaction effect of time x meal on HDL-C concentration in which HDL-C was lower compared to baseline following consumption of both HS and LS meals. A post hoc test revealed that HDL-C following HS meal consumption was significantly lower compared to baseline ($p=0.02$), while there was no significant difference in postprandial HDL-C concentration following the LS meal. LDL-C concentration was lower compared to baseline following both HS and LS meals.

Table 3.4 Serum lipids

	HS		LS	
	PRE	**POST**	**PRE**	**POST**
Total Cholesterol, mg/dL	215 ± 40	221 ± 41*	220 ± 35	224 ± 36*
Triglycerides, mg/dL	104 ± 78	215 ± 140*	108 ± 77	191 ± 115*
HDL-Cholesterol, mg/dL	64 ± 21	62 ± 20*	65 ± 20	64 ± 20
LDL-Cholesterol, mg/dL	131 ± 32	120 ± 29*	136 ± 28	126 ± 26*
VLDL-Cholesterol, mg/dL	19 ± 15	38 ± 26*	19 ± 15	36 ± 23*

Data are mean ± SD; HS: high-sugar meal; LS: low-sugar meal; $P_{ET}CO_2$: end-tidal carbon dioxide; PRE: baseline; POST: postprandial; *p < 0.05 vs. baseline; N=22

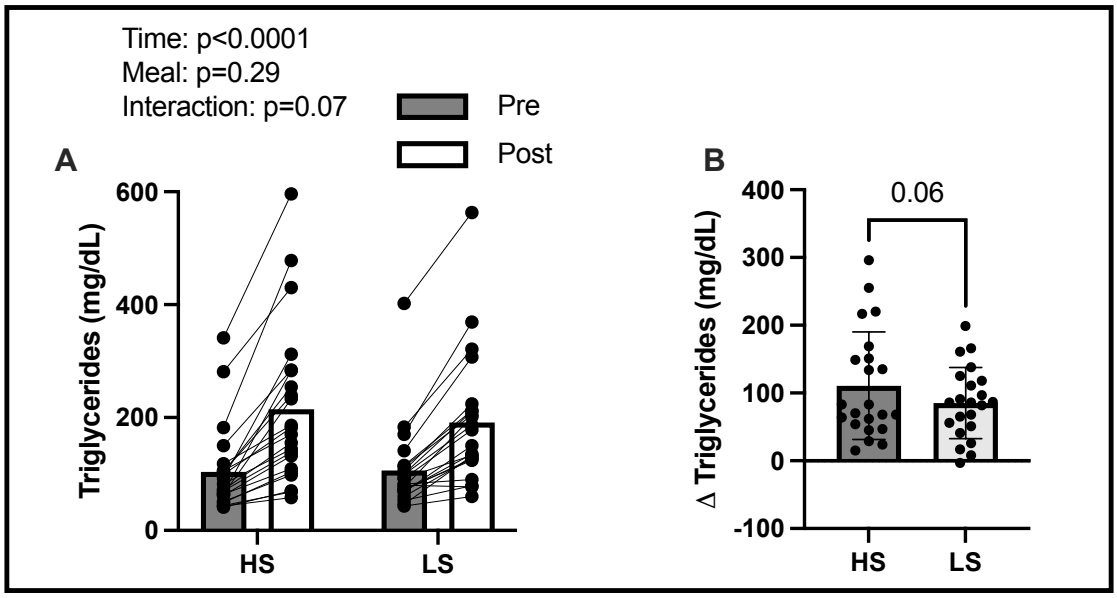

Figure 3.1 (**A**) Triglyceride concentration at baseline and 3-hours postprandial following high-sugar and low-sugar meal. (**B**) Change in triglyceride concentration following high-sugar and low-sugar meal. HS: high-sugar meal; LS: low-sugar meal; PRE: baseline; POST: postprandial; *p < 0.05; N=22

Uric acid concentration (**Figure 3.2A**) was lower compared to baseline following both HS and LS meals. A post hoc test showed that the reduction in uric acid concentration (relative to baseline) following the HS meal was greater than that of the LS meal ($p<0.001$; **Figure 3.2B**).

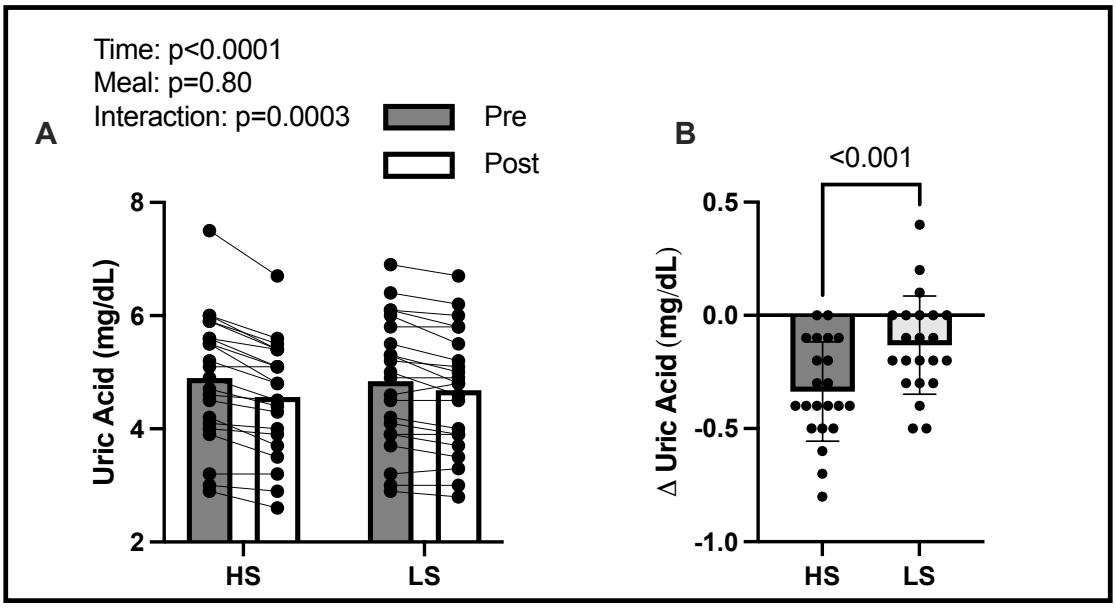

Figure 3.2 (**A**) Uric acid concentration at baseline and 3-hours postprandial following high-sugar and low-sugar meal. (**B**) change in uric acid concentration following high-sugar and low-sugar meal. HS: high-sugar meal; LS: low-sugar meal; PRE: baseline; POST: postprandial; *p < 0.05; N=22

3.3.2 Oxidative Stress and Total Antioxidant Capacity

Oxidative stress was assessed by quantifying ROS as concentration (molarity) and number (spins) of O_2^- or free radicals. Concentration (**Figure 3.3A**) and number of free radicals (**Figure 3.3B**) were lower compared to baseline following both the HS and LS meals.

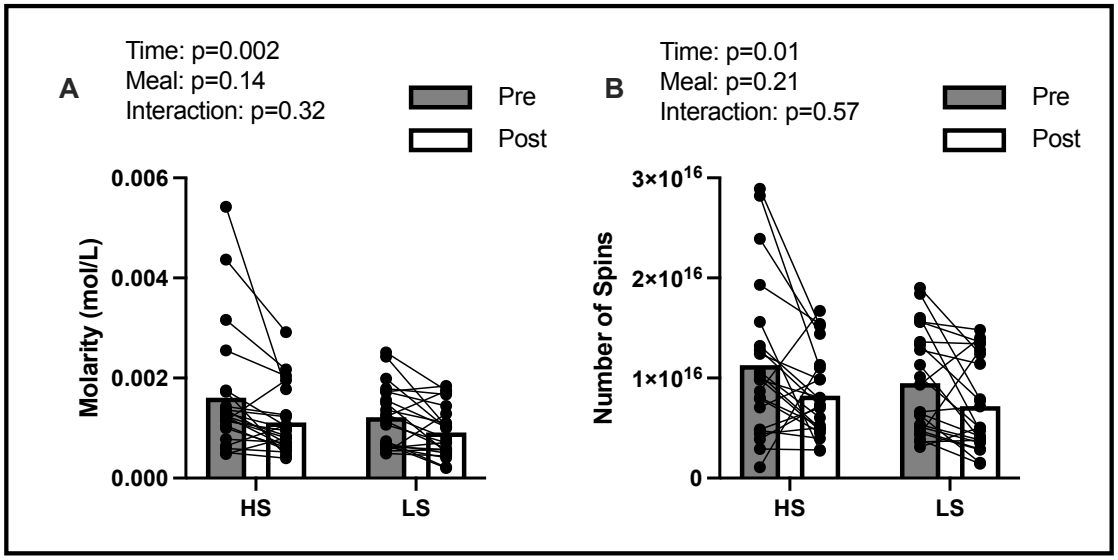

Figure 3.3 Superoxide (**A**) concentration and (**B**) number following high-sugar and low-sugar meal. HS: high-sugar meal; LS: low-sugar meal; PRE: baseline; POST: postprandial; *p < 0.05; N=22

We performed a total antioxidant capacity (TAC) assay on 20 participants on two separate dates (N=10 on each day) with different assay kit lot numbers. TAC did not differ following either the HS or LS meal (**Figure 3.4A**). Due to the difference in assay lot kit numbers, there was a batch effect which is why the postprandial changes in TAC following HS and LS meals are depicted in **Figure 3.4B**. Postprandial changes in TAC did not differ in response to HS or LS meal (p=0.18).

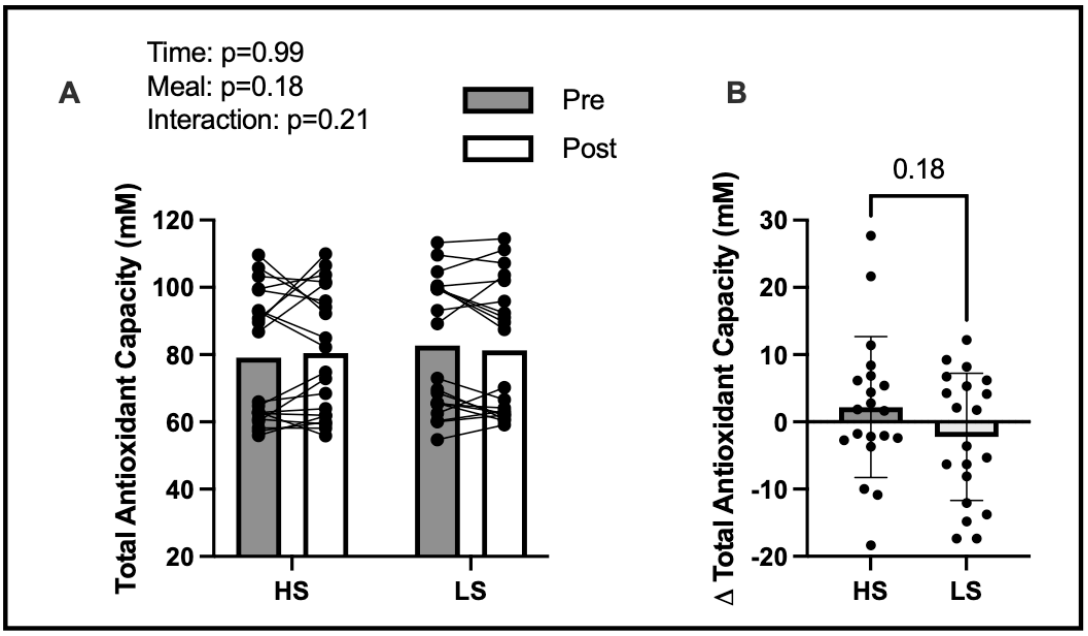

Figure 3.4 (**A**) Total antioxidant capacity at baseline and 3-hours postprandial following high-sugar and low-sugar meal. (**B**) change in total antioxidant capacity following high-sugar and low-sugar meal. HS: high-sugar meal; LS: low-sugar meal; *p < 0.05; N=20

3.3.3 Vascular Properties and Cerebrovascular Reactivity

SBP did not differ following either the HS or LS meal (**Figure 3.5A**). DBP was lower 3-hours postprandial compared to baseline following both HS and LS meals (**Figure 3.5B**).

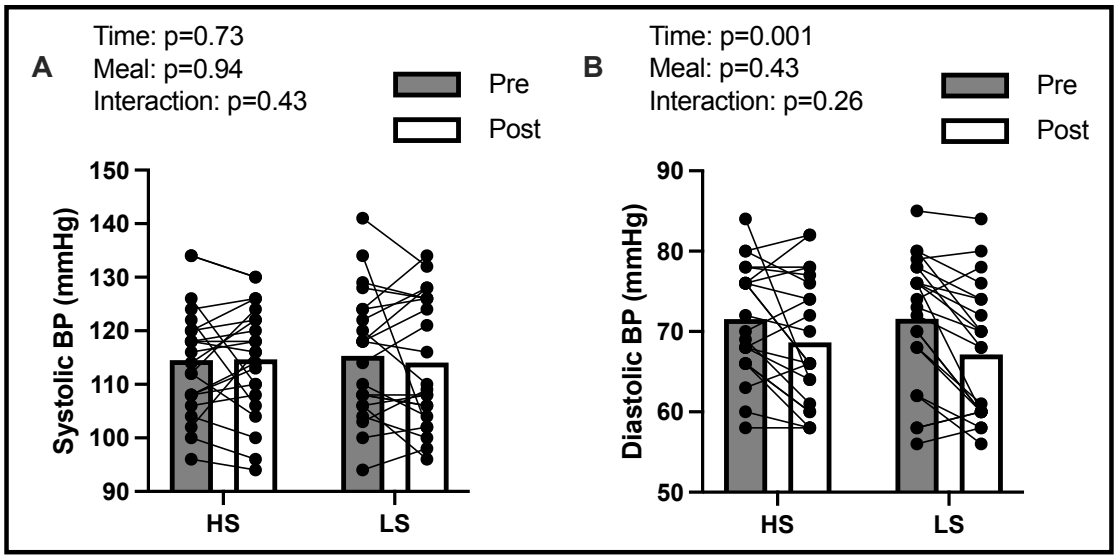

Figure 3.5 Systolic (**A**) and diastolic (**B**) blood pressure at baseline and 3-hours postprandial following high-sugar and low-sugar meal. HS: high-sugar meal; LS: low-sugar meal; PRE: baseline; POST: postprandial; *p < 0.05; N=22

Cerebrovascular variables of gray matter (GM), HC perfusion and $P_{ET}CO_2$ at rest and during hypercapnia in response to each meal are presented in **Table 3.5**. GM or HC perfusion at rest did not differ following the HS meal compared to the LS meal. Furthermore, GM and HC perfusion also did not differ following either meal during hypercapnia. $P_{ET}CO_2$ at rest was higher following both meals compared to baseline. $P_{ET}CO_2$ during hypercapnia was not different following the HS meal compared to the LS meal.

Table 3.5 Cerebrovascular variables

	HS		LS	
	PRE	**POST**	**PRE**	**POST**
Rest				
GM CBF mL/100g/min	71.2 ± 15.8	72.5 ± 13.2	71.0 ± 13.4	72.7 ± 12.6
HC CBF, mL/100g/min	46.4 ± 8.1	48.4 ± 12.0	44.6 ± 10.1	44.7 ± 7.8
$P_{ET}CO_2$, mmHg	41.4 ± 4.8	42.7 ± 3.5*	41.6 ± 4.2	41.9 ± 3.6*
Hypercapnia				
GM CBF, mL/100g/min	92.8 ± 22.3	98.1 ± 18.0	90.3 ± 17.9	94.0 ± 15.8
HC CBF, mL/100g/min	56.1 ± 13.8	59.5 ± 14.7	55.4 ± 9.9	55.0 ± 10.0
$P_{ET}CO_2$, mmHg	48.6 ± 5.4	50.4 ± 3.7	49.5 ± 4.7	49.8 ± 3.7

Data are mean ± SD; CBF: cerebral blood flow; GM: gray matter; HC: hippocampus; HS: high-sugar meal; LS: low-sugar meal; $P_{ET}CO_2$: end-tidal carbon dioxide; PRE: baseline; POST: postprandial; *$p < 0.05$ vs. baseline; N=20

Twenty participants completed the full CVR protocol for HS and LS meal conditions. GM and HC CVR did not differ from baseline following either HS or LS meal (**Figure 3.6**).

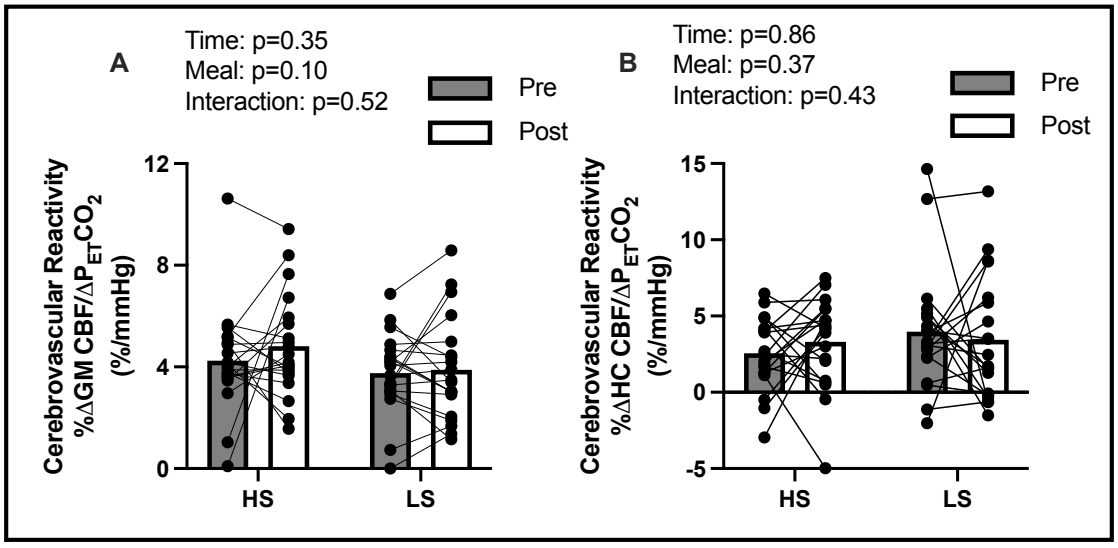

Figure 3.6 (**A**) Gray matter and (**B**) hippocampal cerebrovascular reactivity at baseline and 3-hours postprandial following high-sugar and low-sugar meal. CBF: cerebral blood flow; GM: gray matter; HC: hippocampus; HS: high-sugar meal; LS: low-sugar meal; PRE: baseline; POST: postprandial; *$p < 0.05$; N=20

3.3.4 Whole Brain and Hippocampal Tissue Viscoelastic Properties

We have complete datasets for whole brain (WB) and HC tissue viscoelastic properties that include stiffness and damping ratio in seventeen participants. There was no statistical significance in WB stiffness following either HS or LS meal, however, WB stiffness tended to be lower following both HS and LS meals (**Figure 3.7A**). WB damping ratio was higher compared to baseline after consumption of both HS and LS meals (**Figure 3.7B**).

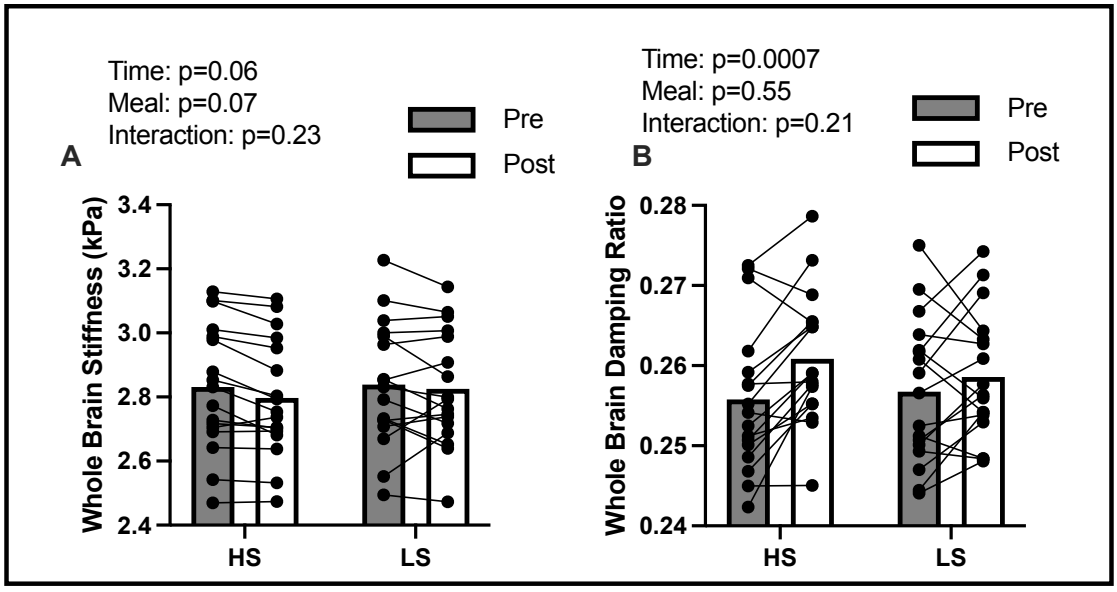

Figure 3.7 Whole brain (**A**) stiffness and (**B**) damping ratio at baseline and 3-hours postprandial following high-sugar and low-sugar meal. HS: high-sugar meal; LS: low-sugar meal; PRE: baseline; POST: postprandial; *p < 0.05; N=17

HC stiffness was reduced following both HS and LS meals (**Figure 3.8A**). HC damping ratio did not differ following either HS or LS meal (**Figure 3.8B**).

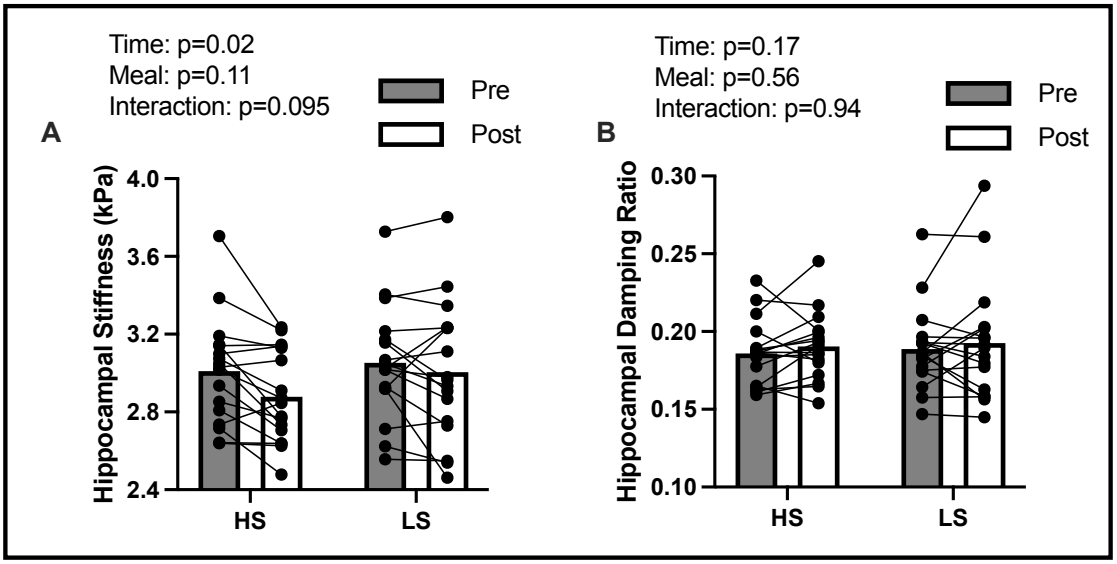

Figure 3.8 Hippocampal (**A**) stiffness and (**B**) damping ratio at baseline and 3-hours postprandial following high-sugar and low-sugar meal. HS: high-sugar meal; LS: low-sugar meal; PRE: baseline; POST: postprandial; *p < 0.05; N=17

3.3.5 Cognitive Tasks

A subset of ten participants completed cognitive measures of executive function and processing speed. Pattern Comparison Processing Speed test scores were higher compared to baseline following both HS and LS meals with no interaction effect (**Figure 3.9A**). There was a significant effect of meal which was observed due to the differences in baseline scores before consumption of either meal (p=0.04). Dimensional Change Card Sort test scores were higher compared to baseline following both HS and LS meals (**Figure 3.9B**). There was only an interaction effect on Flanker test scores following the HS and LS meals (**Figure 3.9C**). Post hoc test revealed no significant differences between time and meal conditions, however, participants scored higher following the HS meal, while they scored lower following the LS meal when compared to baseline (HS: Δ 4.8 ± 2.8 vs. LS: Δ -6.8 ± 2.8).

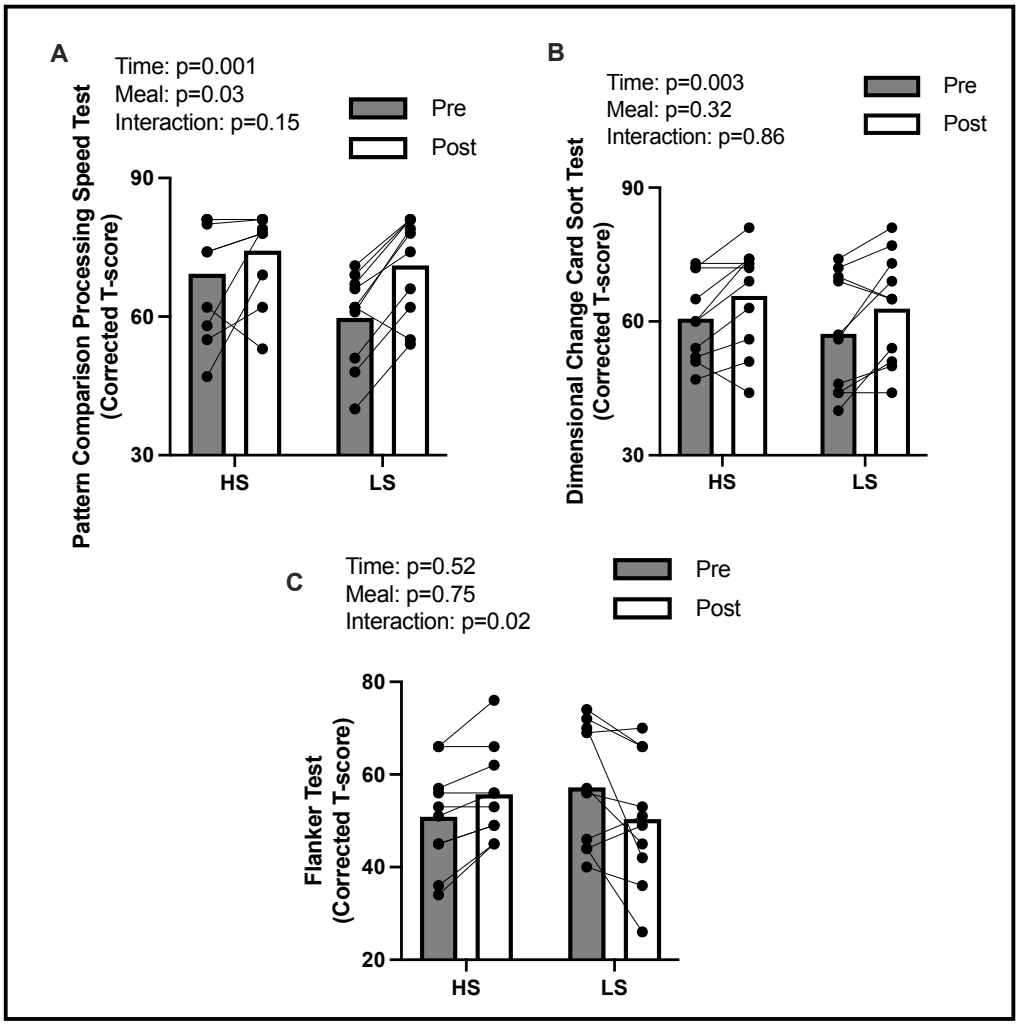

Figure 3.9 (**A**) Pattern Comparison Processing Speed (**B**) Dimensional Change Card Sort (**C**) Flanker Inhibitory Control and Attention test corrected T-scores at baseline and 3-hours postprandial following high-sugar and low-sugar meal. HS: high-sugar meal; LS: low-sugar meal; PRE: baseline; POST: postprandial; *p < 0.05; N=10

3.3.6 Responsiveness to Meals

To assess whether individuals with high baseline serum TGs had a more robust response in CVR and brain tissue viscoelastic properties due to the HS meal compared to the LS meal, we correlated baseline TG concentration to postprandial changes of

both HS and LS meals (**Figure 3.10**). Higher baseline TGs were significantly associated with an increase in postprandial TG concentration after consumption of both HS (r=0.61; p=0.003) and LS (r=0.65; p=0.001) meals. The slope of the change in TGs following both meals were not different (p=0.40). Postprandial changes in TG concentration in response to either HS or LS meal were not significantly associated with CVR (data not shown). There were no associations between postprandial changes in TGs and brain tissue properties in response to either HS or LS meal (data not shown).

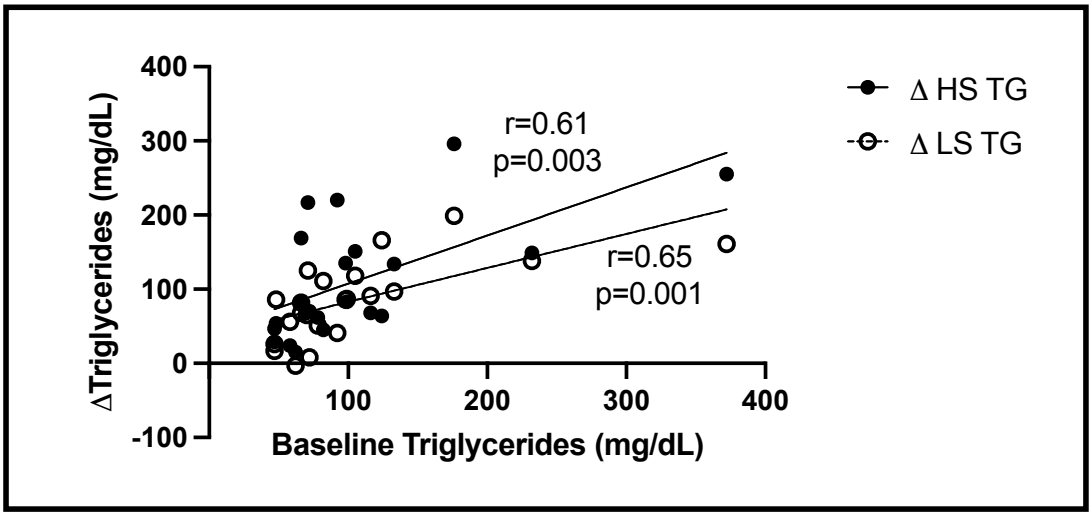

Figure 3.10 Association between baseline triglycerides and 3-hours postprandial changes in triglyceride concentration following a high-sugar and low-sugar meal; HS: high-sugar meal; LS: low-sugar meal; TG: triglycerides; *p < 0.05; N=22

3.4 Discussion

The primary aim of this study was to examine the effects of acute added sugar intake from a single HS meal on cerebrovascular function and HC tissue viscoelastic

properties and identify whether a HS vs. LS meal impacts blood lipids, uric acid, and ROS. We found that cerebrovascular function did not change following either meal whereas there was an increase in whole brain damping ratio and a decrease in HC stiffness after consumption of both meals. Serum TG concentration was higher after both meals, where the increase in TG tended to be greater following the HS meal than the LS meal. Our sensitivity analyses showed that higher baseline serum TG concentration was correlated to an increase in postprandial TG concentration. However, no significant robust response in cerebrovascular function or brain tissue properties was observed in response to either meal. Contrary to our hypothesis, serum uric acid concentration was lower following both meals where the reduction was greater following the HS meal. Concentration and number of O_2^- were also lower following both meals, while there was no significant difference in TAC after either meal. We also examined executive function in a subset of participants and observed that participants exhibited improved executive function after both meals, where there was an increase in Flanker test scores following the HS meal and a decrease following the LS meal.

This study's hypotheses were based off our previous findings in which high serum TGs were associated with reduced HC tissue viscoelastic properties. Prior literature has shown that acute fructose intake is associated with an increase serum TGs (203,206,208,210,214) and impaired peripheral vascular endothelial function (25–29). Increased fructose intake has been shown to be associated with increases in serum uric acid which in turn is associated with oxidative stress and peripheral vascular endothelial dysfunction (9,237,238,309), therefore, we had hypothesized that a meal high in added sugars would similarly lower CVR and HC tissue viscoelastic

properties. In the present study, we observed an increase in serum TGs and a reduction in brain tissue properties, however, the increase was not dependent on added sugar content. In contrast, we observed opposing findings in which serum uric acid concentration was reduced followed by a reduction in O_2^- with no change in CVR, where the reduction in uric acid was greater following the HS meal.

Possible reasons for these conflicting results could be due to the varying role of uric acid acting as a pro-oxidant or an antioxidant. Uric acid has a paradoxical effect on oxidative stress. During fructose metabolism, xanthine oxidase acts on xanthine to produce uric acid (8,9) and O_2^- (242,243); however, uric acid also accounts for over 60% of free radical scavenging activity in human serum (315) and exerts greater antioxidant effects than Vitamins C and E (316). A study by Cardona et al. (2008) observed an increase in serum TG concentration and a decrease in serum uric acid and circulating antioxidant defenses in individuals 3 hours after consumption of a high-fat meal (317). The authors hypothesized that the high-fat meal causes uric acid to exert its antioxidant effects in which it scavenges free radicals, specifically O_2^- while being oxidized to allantoin and other products of oxidation (318). These findings align with ours in that we observed a significant decrease in serum uric acid concentration 3 hours after consumption of both meals that consisted high amounts of total fat, with the greatest decrease following the HS meal, which may have implications in the increased added sugar content of the meal. Nevertheless, we did not observe any significant changes in TAC following either meal. Additionally, we did not measure allantoin or other products of uric acid oxidation and we did not measure uric acid (in serum or urine) or oxidative stress earlier than the 3-hour timepoint that may have given more information about the antioxidant properties of uric acid in our cohort.

In our cohort, we did not observe any significant changes in CVR following either the HS or LS meal. Moreover, there were no postprandial changes in CVR in response to the HS meal in individuals who had higher baseline serum TGs. A possible reason on why there were no changes in cerebrovascular endothelial function could be due to the lack of an increase in oxidative stress 3 hours after meal consumption. Prior studies that observed a reduction in peripheral vascular endothelial function (25–29) due to acute added sugar intake, primarily examined the hyperglycemia-mediated increases in oxidative stress and assessed endothelium-dependent vascular function during the timepoint when participants' blood glucose concentration peaks (~40 min postprandial). However, the purpose of our study was to examine fructose-mediated hyperuricemia and hypertriglyceridemia for which reason we assessed cerebrovascular function 3 hours postprandial during the time when blood TGs are substantially elevated compared to baseline. Therefore, it is possible that we missed the timepoint during which hyperglycemia-mediated oxidative stress may have occurred. Furthermore, our enrolled participants were healthy young and mid-life individuals, with only three individuals who had clinically high baseline serum TG concentrations. Therefore, the majority of participants in our cohort did not have baseline TGs that were high enough to cause a robust response in cerebrovascular function.

In this study, we found that brain tissue viscoelastic properties were reduced after consumption of both meals, regardless of added sugar content. Specifically, whole brain damping ratio increased whereas HC stiffness decreased after consumption of both meals. Previous studies have shown that acute manipulation of cerebral perfusion through hypercapnia (19,20) and increased flux rate through the

capillary bed (319) and cerebral arterial pulsation during the systolic phase of the cardiac cycle (320) transiently changes brain tissue viscoelastic properties, suggesting that these acute changes in viscoelastic properties may reflect changes in the cerebral microvascular bed. We did not observe any changes in CO_2-induced CVR and cerebral perfusion, however, cerebral perfusion pressures were not accounted for during our measurements as we were not able to acquire beat-to-beat blood pressures during each cardiac cycle, thereby, missing important cerebrovascular hemodynamic variables that may have contributed to the change in brain tissue viscoelastic properties.

In this study, elevated TG concentration from both HS and LS meals that also consisted of high amounts of total fat could be associated with neuroinflammation, which in turn may be associated with a reduction in brain tissue properties. Studies in rodents have shown that a chronic high-sugar and high-fat diet is associated with increased pro-inflammatory cytokines in the brain and a reduction in brain-derived neurotropic factor (BDNF) along with impaired hippocampal-dependent memory function (286–289,321). It has been suggested that lipids from the ingestion of a high-sugar/high-fat meal may cross the blood-brain barrier (BBB) by the presence of TGs in human cerebrospinal fluid (CSF) and by an experiment that showed that radioactive TG triolein could readily cross the BBB in mice (290). TGs have also been observed to be involved in the breakdown and release from adipocytes into free fatty acids directly in the brain. The free fatty acid receptor, GPR40, was detected in the HC (292) along with saturated free fatty acids, palmitic acid and lauric acid, which have been shown to induce a cascade of pro-inflammatory signaling in cultured macrophages and regulating astrocytic and microglial signaling (293–295). It is unclear whether these changes can occur in the human brain acutely after consumption

of a single high-sugar/high-fat meal as the aforementioned studies examined chronic (~30 days) effects of these diets in rodents. However, it is important to measure systemic inflammation after acute consumption of a high-sugar/high-fat meal as studies have shown that acute systemic inflammation exacerbates neuroinflammation and drives HC neuronal network dysfunction in human and mice AD brains (322).

We had hypothesized that our observed results that showed an increase in serum TGs and a decrease in brain tissue properties would be greater following the HS meal due to the presence of high added sugar content in addition to high fat content. However, we saw a main effect of time meaning that they were observed after consumption of both meals. This is because the experimental LS meal in our study was comprised of similar amounts of total fat as the HS meal in order to match its energy and macronutrient content. These fats were mostly PUFA and MUFA while the HS meal comprised of mostly SFA. High levels of SFA directly increase blood lipids and have been shown to be associated with increased cardiovascular disease and AD risk (323), while high levels of PUFA and MUFA reduce blood lipid levels and were found to be beneficial for vascular and brain health (324). A high amount of SFA chosen for the HS meal is translatable to how added sugars are consumed from a Western-style diet (325), therefore, we acknowledge that any changes observed in our primary outcomes in response to the meals may not be specifically due to the influence of fructose. Interestingly, the increase in TGs and the reduction in HC stiffness tended to be greater following the HS meal in our cohort but did not reach statistical significance.

In this study, it was observed that HDL-C concentration decreased following the HS meal, LDL-C concentration decreased, and VLDL-C and total cholesterol

increased after consumption of both meals. These results align with the acute postprandial response of these lipoproteins after a high-sugar/high-fat meal. In the postprandial state, there is an increase in TGs, which are carried in TG-rich lipoproteins (TRLs) such as VLDL whose concentration also increases significantly (326). There is an increased transfer of cholesteryl esters from HDL and LDL particles with the TRLs due to the increased activity of the cholesteryl ester transfer protein (326,327). This transfer leads to the decrease in concentration of HDL-C and LDL-C. Additionally, the catabolic activity of hepatic lipase also increases, which breaks down the HDL and LDL particles into smaller and denser remnant cholesterol particles (326) that probably explains the increase in postprandial total cholesterol (328).

Contrary to our hypothesis, we also observed an increase in executive function and processing speed after both meals. These results may have been related to the fact that baseline measurements were made in the fasted states while both diets contained glucose, which is the brain's predominant energy source (329). However, these postprandial increases are more likely due to practice effects, which are test score improvements in response to repeated exposure to the testing material. Similar practice effects were observed in a study by Parsey et al. (2021) where the authors found that fluid cognitive scores from the NIHTB-CB that were administered 3 hours postprandial of either a high- or low-fat meal, were higher in healthy older adults on second administration (330). Also similar to our analyses, this study did not account for the order in which the meal was received when assessing cognitive results. This may explain the differences in baseline test scores in our cohort, suggesting that baseline scores were higher for the second meal group due to practice effects. Other studies have observed practice effects with the NIHTB-CB tests in adults across the

lifespan over longer intervals (331–333). Interestingly, we observed a reduction in Flanker test scores after the LS meal, which tests attention and inhibitory control. The exact meaning of this finding is unclear. Studies have shown that executive function, after acute hypoglycemia declines if blood sugar reaches below 54 mg/dL (334–336); however, it is unlikely that our participants experienced hypoglycemia 3 hours after consumption of a LS meal, which was enriched in carbohydrates and fats. These findings need to be tested in a larger sample size to assess if they can be replicated or if this was a random observation.

This study had some limitations. We did not meet our targeted sample size of N=20 for measures of brain tissue viscoelastic properties due to missing data from equipment malfunction and inadequate brain imaging quality. However, our current sample size of N=17 for these measures achieved statistical power as an *a priori* power analysis revealed that a sample size of N=15 was needed in order to achieve at least 80% power. Despite this limitation, we observed significant changes in brain tissue viscoelastic properties due to both meals; however, we were unable to detect a robust interaction effect, which may have been due to sample size. We also did not assess pro-inflammatory cytokines; hence, we are unable to determine if increased inflammation was responsible for the reduction in brain tissue properties due to increased TGs from the meals. Additionally, we did not measure blood biomarkers and measures of brain health past the 3-hour timepoint due to participant time constraints and limitations in availability of the MRI. Therefore, we may have missed the timepoint during which TG concentration peaks in the blood (4-6 h postprandial) and subsequent changes in markers of brain health during those timepoints. Finally, due to our small sample size and lack of diversity, we are unable to determine

generalizability in our findings and sex differences in primary outcomes in response to the meals. Furthermore, even though we reported menopausal status, menstrual cycle phase in premenopausal females was not controlled for this study. It has been shown that controlling for menstrual cycle phase differences has no effect on peripheral vascular endothelial function (306) and cerebral autoregulation (307), and it is also believed to reduce external validity of physiological findings as it is not reflective of the general population (308). Future randomized-controlled trials investigating the chronic effects of a Western-style diet and the subsequent role of neural inflammation need to be performed in order to assess the mechanism behind the changes in cerebrovascular function and brain tissue properties in response to an unhealthy diet enriched in added sugars and saturated fats.

3.5 Conclusions

The primary findings of the present study showed an increase in serum TGs and a reduction in brain tissue viscoelastic properties 3 hours after meal consumption, regardless of the amount of added sugars. We also found that serum uric acid concentration along with ROS decreased after both meals, however, we did not observe any changes in cerebrovascular function due to either the experimental HS or the control LS meal. Furthermore, in a subset of participants, it was observed that measures of executive function increased following both meals, whereas participants' measures of attention and inhibitory control were increased following the HS meal and was decreased following the LS meal. Studies examining the chronic effects of Western-style diets on blood markers, cerebrovascular function and brain tissue properties need to be conducted to better assess the mechanism by which unhealthy diets affect brain health and are a risk factor of cognitive aging.

Chapter 4

CONCLUSION

4.1 Summary

Elevated blood lipids are modifiable risk factors common to cardiovascular and cerebrovascular disease and age-related cognitive decline (4). An increased concentration of blood lipids are associated with a reduction in HC tissue viscoelastic properties and memory performance (6). Elevated blood lipids are also associated with peripheral vascular endothelial dysfunction, which is partially mediated via increased oxidative stress and systemic inflammation (8–12). Peripheral vascular endothelial function is correlated with cerebrovascular endothelial function (15,16) and an impairment in peripheral endothelial function contributes to the development of atherosclerosis and cognitive aging (13,14). Therefore, there could be a potential role of cerebrovascular function as a potential mediator of the association between lipids and HC tissue properties.

Additionally, high dietary added sugar intake from a Western-style diet (5,21), is associated with elevated cardiometabolic risk parameters (8), including high serum TGs and uric acid (22,23). Specifically, acute added sugar intake have been shown to attenuate CBF and peripheral vascular endothelial function (25–33), while manipulations in CO_2-induced CBF is also associated with transient changes in brain tissue properties (19,20). However, these studies examined hyperglycemia-mediated peripheral vascular endothelial dysfunction using sugar-sweetened beverages (SSB) as interventions or explored brain pathways unrelated to cerebrovascular or memory

function. Thus, the direct effects of acute added sugar intake from solid foods typically present in a Western-style meal on cerebrovascular function and brain health are unclear. In this study, we examined if cerebrovascular function mediated the association between elevated blood lipids and brain tissue properties. We also sought to investigate the effects of acute added sugar intake on serum lipid and uric acid and associated oxidative stress, cerebrovascular function and brain tissue properties.

Our previous finding of a relation between blood lipids and HC tissue properties were reinforced as we observed that elevated serum TGs were associated with a higher HC damping ratio while elevated serum LDL-C was associated with a lower HC stiffness. However, there was no mediating effect of CVR on this association. These findings suggest that there may be alternative mechanistic explanations behind the association between aberrant blood lipids and reduced HC tissue properties. These mechanisms could be examined through investigation of other vascular measures such as arterial stiffness and through randomized-controlled trials that would examine the role of poor lifestyle factors such as a Western diet consumption and associated inflammation on brain health. Future longitudinal studies should also be conducted in mid-life adults with a narrower age range in which their blood lipids, cerebrovascular function and HC tissue properties would be monitored throughout several years.

When the effects of acute added sugar intake were examined, we observed that there was an increase in serum TGs and a reduction in brain tissue viscoelastic properties 3 hours after consumption of meals that were high and low in added sugar, and were comprised of high amounts of fat. It was also observed that serum uric acid concentration along with ROS decreased after the meals, however, there were no

significant changes in cerebrovascular function following either the HS or LS meals. These findings suggest that acute modulations in serum lipids via a single Western-style meal high in added sugars and saturated fat leads to changes in brain tissue properties. These observed changes were independent of changes in cerebrovascular function and changes in uric acid and oxidative stress as these variables decreased following the meals, specifically the HS meal. The decrease in uric acid and ROS appear to be a transient compensatory mechanism in response to an acute HS meal. Further studies investigating the chronic effects of a Western diet along with subsequent role of inflammation in the association between serum TGs and brain tissue properties need to be examined.

4.2 Perspectives

There is a current surge in the global population of older adults as well as the incidence of age-related cognitive impairment and AD. It is expected that the number of adults over the age of 65 years with dementia and/or AD will more than double in the next thirty years (2,269). Currently, there is an extremely low success rate in AD clinical trials (270). It has also been observed that individuals with lower social determinants of health, which includes social and economic factors such as access to education, healthy nutrition and overall healthcare, are at an increased risk of AD (337). Therefore, there is an urgent need to target modifiable lifestyle factors as an alternative approach to delaying and preventing cognitive aging. We have shown that elevated serum lipids, habitually and due to a single meal high in added sugars and saturated fats, are negatively associated with brain tissue properties. Further studies need to be conducted in order to understand the mechanism behind these associations. These findings may provide critical information by which clinical and nutritional

guidelines can better inform the public to make healthier lifestyle choices to prevent future incidence of age-related cognitive impairment and/or AD.

REFERENCES

1. James BD, Leurgans SE, Hebert LE, Scherr PA, Yaffe K, Bennett DA. Contribution of Alzheimer disease to mortality in the United States. Neurology. 2014;

2. Hebert LE, Weuve J, Scherr PA, Evans DA. Alzheimer disease in the United States (2010-2050) estimated using the 2010 census. Neurology. 2013;80(19):1778–83.

3. Wong W. Economic burden of Alzheimer disease and managed care considerations. Am J Manag Care. 2020;

4. Santos CY, Snyder PJ, Wu W-C, Zhang M, Echeverria A, Alber J. Pathophysiologic relationship between Alzheimer's disease, cerebrovascular disease, and cardiovascular risk: A review and synthesis. Alzheimer's Dement Diagnosis, Assess Dis Monit. 2017;7:69–87.

5. Virani SS, Alonso A, Aparicio HJ, Benjamin EJ, Bittencourt MS, Callaway CW, et al. Heart Disease and Stroke Statistics—2021 Update. Circulation. 2021 Feb 23;143(8):e254–743.

6. Sanjana F, Delgorio PL, Hiscox L V, DeConne TM, Hobson JC, Cohen ML, et al. Blood lipid markers are associated with hippocampal viscoelastic properties and memory in humans. J Cereb Blood Flow Metab. 2020 Oct 26;0271678X20968032.

7. Eichenbaum H, Yonelinas AP, Ranganath C. The Medial Temporal Lobe and Recognition Memory. Annu Rev Neurosci. 2007;

8. Johnson RJ, Nakagawa T, Sanchez-Lozada LG, Shafiu M, Sundaram S, Le M, et al. Sugar, uric acid, and the etiology of diabetes and obesity. Diabetes. 2013.

9. Kanellis J, Kang DH. Uric acid as a mediator of endothelial dysfunction, inflammation, and vascular disease. Semin Nephrol. 2005;

10. Jia G, Aroor AR, Whaley-Connell AT, Sowers JR. Fructose and uric acid: is there a role in endothelial function? Curr Hypertens Rep. 2014;16(6):434.

11. Schwarz JM, Neese R, Shackleton C, Hellerstein MK. De Novo Lipogenesis (DNL) During Fasting And Oral Fructose In Lean And Obese Hyperinsulinimic Subjects. In: Diabetes. AMER DIABETES ASSOC 1660 DUKE ST, ALEXANDRIA, VA 22314; 1993. p. A39–A39.

12. Welty FK. How do elevated triglycerides and low HDL-cholesterol affect inflammation and atherothrombosis? Current Cardiology Reports. 2013.

13. Targonski P V, Bonetti PO, Pumper GM, Higano ST, Holmes DR, Lerman A. Coronary Endothelial Dysfunction Is Associated With an Increased Risk of Cerebrovascular Events. Circulation. 2003 Jun 10;107(22):2805–9.

14. Donato AJ, Pierce GL, Lesniewski LA, Seals DR. Role of NFkappaB in age-related vascular endothelial dysfunction in humans. Aging (Albany NY). 2009 Aug 10;1(8):678–80.

15. Ainslie PN, Murrell C, Peebles K, Swart M, Skinner MA, Williams MJA, et al. Early morning impairment in cerebral autoregulation and cerebrovascular CO2 reactivity in healthy humans: relation to endothelial function. Exp Physiol. 2007;92(4):769–77.

16. Lavi S, Gaitini D, Milloul V, Jacob G. Impaired cerebral CO2 vasoreactivity: association with endothelial dysfunction. Am J Physiol Circ Physiol. 2006 Oct 1;291(4):H1856–61.

17. Glodzik L, Randall C, Rusinek H, de Leon MJ. Cerebrovascular reactivity to carbon dioxide in Alzheimer's disease. J Alzheimers Dis. 2013;35(3):427–40.

18. Sabayan B, Jansen S, Oleksik AM, Van Osch MJP, Van Buchem MA, Van Vliet P, et al. Cerebrovascular hemodynamics in Alzheimer's disease and vascular dementia: A meta-analysis of transcranial Doppler studies. Ageing Research Reviews. 2012.

19. Kreft B, Tzschätzsch H, Schrank F, Bergs J, Streitberger K-J, Wäldchen S, et al. Time-Resolved Response of Cerebral Stiffness to Hypercapnia in Humans. Ultrasound Med Biol. 2020;46(4):936–43.

20. Hetzer S, Dittmann F, Bormann K, Hirsch S, Lipp A, Wang DJJ, et al. Hypercapnia increases brain viscoelasticity. J Cereb Blood Flow Metab. 2019;

21. van de Rest O, Berendsen AAM, Haveman-Nies A, de Groot LC. Dietary Patterns, Cognitive Decline, and Dementia: A Systematic Review. Adv Nutr. 2015 Mar 1;6(2):154–68.

22. Johnson RK, Appel LJ, Brands M, Howard B V, Lefevre M, Lustig RH, et al. Dietary sugars intake and cardiovascular health: a scientific statement from the American Heart Association. Circulation. 2009/08/24. 2009 Sep;120(11):1011–20.

23. Johnson RJ, Gomez-Pinilla F, Nagel M, Nakagawa T, Rodriguez-Iturbe B, Sanchez-Lozada LG, et al. Cerebral Fructose Metabolism as a Potential Mechanism Driving Alzheimer's Disease. Front Aging Neurosci. 2020;

24. Chong MFF, Fielding BA, Frayn KN. Mechanisms for the acute effect of fructose on postprandial lipemia. Am J Clin Nutr. 2007;

25. Loader J, Meziat C, Watts R, Lorenzen C, Sigaudo-Roussel D, Stewart S, et al. Effects of Sugar-Sweetened Beverage Consumption on Microvascular and Macrovascular Function in a Healthy Population. Arterioscler Thromb Vasc Biol. 2017 Jun 1;37(6):1250–60.

26. Bock JM, Iwamoto E, Horak JG, Feider AJ, Hanada S, Casey DP. Aerobic exercise offsets endothelial dysfunction induced by repetitive consumption of sugar-sweetened beverages in young healthy men. Am J Physiol Integr Comp Physiol. 2020 May 13;319(1):R11–8.

27. Loader J, Montero D, Lorenzen C, Watts R, Méziat C, Reboul C, et al. Acute hyperglycemia impairs vascular function in healthy and cardiometabolic diseased subjects: Systematic review and meta-analysis. Arterioscler Thromb Vasc Biol. 2015;

28. Varsamis P, Walther G, Share B, Taylor F, Stewart S, Lorenzen C, et al. Transient endothelial dysfunction induced by sugar-sweetened beverage consumption may be attenuated by a single bout of aerobic exercise. Microvasc Res. 2018;115:8–11.

29. Lavi T, Karasik A, Koren-Morag N, Kanety H, Feinberg MS, Shechter M. The acute effect of various glycemic index dietary carbohydrates on endothelial function in nondiabetic overweight and obese subjects. J Am Coll Cardiol. 2009;

30. Purnell JQ, Klopfenstein BA, Stevens AA, Havel PJ, Adams SH, Dunn TN, et al. Brain functional magnetic resonance imaging response to glucose and fructose infusions in humans. Diabetes, Obes Metab. 2011;

31. Page KA, Chan O, Arora J, Belfort-DeAguiar R, Dzuira J, Roehmholdt B, et al. Effects of fructose vs glucose on regional cerebral blood flow in brain regions involved with appetite and reward pathways. JAMA - J Am Med Assoc. 2013;

32. Reed EL, Worley ML, Kueck PJ, Pietrafasa LD, Schlader ZJ, Johnson BD. Cerebral vascular function following the acute consumption of caffeinated artificially- and sugar sweetened soft drinks in healthy adults. Front Hum Neurosci. 2022;

33. Greenshields JT, Keeler JM, Freemas JA, Baker TB, Johnson BD, Carter SJ, et al. Cutaneous microvascular vasodilatory consequences of acute consumption of a caffeinated soft drink sweetened with high-fructose corn syrup. Physiol Rep. 2021;

34. Hoiland RL, Fisher JA, Ainslie PN. Regulation of the cerebral circulation by arterial carbon dioxide. Compr Physiol. 2019;

35. Zarrinkoob L, Ambarki K, Wåhlin A, Birgander R, Eklund A, Malm J. Blood flow distribution in cerebral arteries. J Cereb Blood Flow Metab. 2015;

36. Alpers BJ, Berry RG, Paddison RM. Anatomical Studies of the Circle of Willis in Normal Brain. Arch Neurol Psychiatry. 1959;

37. Nishimura N, Schaffer CB, Friedman B, Lyden PD, Kleinfeld D. Penetrating arterioles are a bottleneck in the perfusion of neocortex. Proc Natl Acad Sci U S A. 2007;

38. Wong AD, Ye M, Levy AF, Rothstein JD, Bergles DE, Searson PC. The blood-brain barrier: An engineering perspective. Frontiers in Neuroengineering. 2013.

39. Ballabh P, Braun A, Nedergaard M. The blood-brain barrier: An overview: Structure, regulation, and clinical implications. Neurobiology of Disease. 2004.

40. Grieb P, Forster RE, Strome D. O2 exchange between blood and brain tissues studied with 18O2 indicator-dilution technique. J Appl Physiol. 1985;

41. Pardridge WM, Eisenberg J, Yang J. Human Blood—Brain Barrier Insulin Receptor. J Neurochem. 1985;

42. Engelhardt S, Patkar S, Ogunshola OO. Cell-specific blood-brain barrier regulation in health and disease: A focus on hypoxia. British Journal of Pharmacology. 2014.

43. Ainslie PN, Duffin J. Integration of cerebrovascular CO2 reactivity and chemoreflex control of breathing: Mechanisms of regulation, measurement, and interpretation. American Journal of Physiology - Regulatory Integrative and Comparative Physiology. 2009.

44. McDonald DA. Blood flow in arteries. Edward Arnold Publ. 1974;

45. Olufsen MS, Nadim A, Lipsitz LA. Dynamics of cerebral blood flow regulation explained using a lumped parameter model. Am J Physiol - Regul Integr Comp Physiol. 2002;

46. Kety SS, Schmidt CF. The nitrous oxide method for the quantitative determination of cerebral blood flow in man: theory, procedure and normal values. J Clin Invest. 1948;

47. Kety SS, Schmidt CF. The determination of cerebral blood flow in man by the use of nutrous oxide in low concentrations. Am J Physiol Content. 1945;

48. Golay X, Hendrikse J, Lim TCC. Perfusion Imaging Using Arterial Spin Labeling. Topics in Magnetic Resonance Imaging. 2004.

49. Wolf RL, Detre JA. Clinical Neuroimaging Using Arterial Spin-Labeled Perfusion Magnetic Resonance Imaging. Neurotherapeutics. 2007;

50. Petersen ET, Lim T, Golay X. Model-free arterial spin labeling quantification approach for perfusion MRI. Magn Reson Med. 2006;

51. Chappell M, Macintosh B, Okell T. Introduction to perfusion quantification using arterial spin labelling. Introduction to Perfusion Quantification using Arterial Spin Labelling. 2017.

52. Pollock JM, Tan H, Kraft RA, Whitlow CT, Burdette JH, Maldjian JA. Arterial Spin-Labeled MR Perfusion Imaging: Clinical Applications. Magnetic Resonance Imaging Clinics of North America. 2009.

53. Liu TT, Brown GG. Measurement of cerebral perfusion with arterial spin labeling: Part 1. Methods. Journal of the International Neuropsychological Society. 2007.

54. Ferré JC, Bannier E, Raoult H, Mineur G, Carsin-Nicol B, Gauvrit J-Y. Arterial spin labeling (ASL) perfusion: Techniques and clinical use. Diagn Interv Imaging. 2013;94(12):1211–23.

55. Detre JA, Alsop BC, Vives LR, Maccotta L, Teener JW, Raps EC. Noninvasive MRI evaluation of cerebral blood flow in cerebrovascular disease. Neurology. 1998;

56. Chen J, Licht DJ, Smith SE, Agner SC, Mason S, Wang S, et al. Arterial spin labeling perfusion MRI in pediatric arterial ischemic stroke: Initial experiences.

J Magn Reson Imaging. 2009;

57. Du AT, Jahng GH, Hayasaka S, Kramer JH, Rosen HJ, Gorno-Tempini ML, et al. Hypoperfusion in frontotemporal dementia and Alzheimer disease by arterial spin labeling MRI. Neurology. 2006;

58. Chao LL, Buckley ST, Kornak J, Schuff N, Madison C, Yaffe K, et al. ASL perfusion MRI predicts cognitive decline and conversion from MCI to dementia. Alzheimer Dis Assoc Disord. 2010;

59. Engelhorn T, Doerfler A, Weise J, Baehr M, Forsting M, Hufnagel A. Cerebral perfusion alterations during the acute phase of experimental generalized status epilepticus: Prediction of survival by using perfusion-weighted MR imaging and histopathology. Am J Neuroradiol. 2005;

60. Wolf RL, Wang J, Detre JA, Zager EL, Hurst RW. Arteriovenous shunt visualization in arteriovenous malformations with arterial spin-labeling MR imaging. Am J Neuroradiol. 2008;

61. Warmuth C, Günther M, Zimmer C. Quantification of blood flow in brain tumors: Comparison of arterial spin labeling and dynamic susceptibility-weighted contrast-enhanced MR imaging. Radiology. 2003;

62. Petcharunpaisan S. Arterial spin labeling in neuroimaging. World J Radiol. 2010;

63. Purkayastha S, Sorond F. Transcranial doppler ultrasound: Technique and application. Semin Neurol. 2012;32(4):411–20.

64. Serrador JM, Picot PA, Rutt BK, Shoemaker JK, Bondar RL. MRI Measures of Middle Cerebral Artery Diameter in Conscious Humans During Simulated Orthostasis. Stroke. 2000 Jul 1;31(7):1672–8.

65. Verbree J, Bronzwaer ASGT, Ghariq E, Versluis MJ, Daemen MJAP, Van Buchem MA, et al. Assessment of middle cerebral artery diameter during hypocapnia and hypercapnia in humans using ultra-high-field MRI. J Appl Physiol. 2014;

66. Coverdale NS, Gati JS, Opalevych O, Perrotta A, Shoemaker JK. Cerebral blood flow velocity underestimates cerebral blood flow during modest hypercapnia and hypocapnia. J Appl Physiol. 2014;

67. Harper AM, Bell RA. The effect of metabolic acidosis and alkalosis on the blood flow through the cerebral cortex. J Neurol Neurosurg Psychiatry. 1963;

68. Kety SS, Schmidt CF. The effects of active and passive hyperventilation on cerebral blood flow, cerebral oxygen consumption, cardiac output, and blood pressure of normal young men. J Clin Invest. 1946;

69. Coverdale NS, Lalande S, Perrotta A, Shoemaker JK. Heterogeneous patterns of vasoreactivity in the middle cerebral and internal carotid arteries. Am J Physiol - Hear Circ Physiol. 2015;

70. Willie CK, Macleod DB, Shaw AD, Smith KJ, Tzeng YC, Eves ND, et al. Regional brain blood flow in man during acute changes in arterial blood gases. J Physiol. 2012;

71. Howarth C, Sutherland B, Choi HB, Martin C, Lind BL, Khennouf L, et al. A critical role for astrocytes in hypercapnic vasodilation in brain. J Neurosci. 2017;

72. Lennox WG, Gibbs EL. The Blood Flow In The Brain And The Leg Of Man, And The Changes Induced By Alteration Of Blood Gases. J Clin Invest. 1932;

73. Xu H, Cui N, Yang Z, Wu J, Giwa LR, Abdulkadir L, et al. Direct Activation of Cloned KATP Channels by Intracellular Acidosis. J Biol Chem. 2001;

74. Kinoshita H, Katusic ZS. Role of potassium channels in relaxations of isolated canine basilar arteries to acidosis. Stroke. 1997;

75. Jackson WF. Potassium channels in the peripheral microcirculation. Microcirculation. 2005.

76. Parfenova H, Shibata M, Zuckerman S, Leffler CW. CO2 and cerebral circulation in newborn pigs: Cyclic nucleotides and prostanoids in vascular regulation. Am J Physiol - Hear Circ Physiol. 1994;

77. Leffler CW, Mirro R, Pharris LJ, Shibata M. Permissive role of prostacyclin in cerebral vasodilation to hypercapnia in newborn pigs. Am J Physiol - Hear Circ Physiol. 1994;

78. Fleming I, Hecker M, Busse R. Intracellular alkalinization induced by bradykinin sustains activation of the constitutive nitric oxide synthase in endothelial cells. Circ Res. 1994;

79. Caggiano AO, Kraig RP. Neuronal nitric oxide synthase expression is induced in neocortical astrocytes after spreading depression. J Cereb Blood Flow Metab. 1998;

80. Lindauer U, Kunz A, Schuh-Hofer S, Vogt J, Dreier JP, Dirnagl U. Nitric oxide from perivascular nerves modulates cerebral arterial pH reactivity. Am J Physiol - Hear Circ Physiol. 2001;

81. Iadecola C. Does nitric oxide mediate the increases in cerebral blood flow elicited by hypercapnia? Proc Natl Acad Sci U S A. 1992;

82. Wang Q, Paulson OB, Lassen NA. Effect of Nitric Oxide Blockade by NG-Nitro-l-Arginine on Cerebral Blood Flow Response to Changes in Carbon Dioxide Tension. J Cereb Blood Flow Metab. 1992 Nov 1;12(6):947–53.

83. Iadecola C, Zhang F, Xu X. Role of nitric oxide synthase-containing vascular nerves in cerebrovasodilation elicited from cerebellum. Am J Physiol Integr Comp Physiol. 1993 Apr 1;264(4):R738–46.

84. Iadecola C, Li J, Ebner TJ, Xu X. Nitric oxide contributes to functional hyperemia in cerebellar cortex. Am J Physiol - Regul Integr Comp Physiol. 1995;

85. Fathi AR, Yang C, Bakhtian KD, Qi M, Lonser RR, Pluta RM. Carbon dioxide influence on nitric oxide production in endothelial cells and astrocytes: Cellular mechanisms. Brain Res. 2011;1386:50–7.

86. Mashour GA, Boock RJ. Effects of shear stress on nitric oxide levels of human cerebral endothelial cells cultured in an artificial capillary system. Brain Res. 1999;

87. Peebles K, Celi L, McGrattan K, Murrell C, Thomas K, Ainslie PN. Human cerebrovascular and ventilatory CO2 reactivity to end-tidal, arterial and internal jugular vein PCO2. J Physiol. 2007;

88. Lavi S, Egbarya R, Lavi R, Jacob G. Role of Nitric Oxide in the Regulation of Cerebral Blood Flow in Humans. Circulation. 2003 Apr 15;107(14):1901–5.

89. Hoiland RL, Smith KJ, Carter HH, Lewis NCS, Tymko MM, Wildfong KW, et al. Shear-mediated dilation of the internal carotid artery occurs independent of hypercapnia. Am J Physiol - Hear Circ Physiol. 2017;

90. Smith KJ, Hoiland RL, Grove R, McKirdy H, Naylor L, Ainslie PN, et al. Matched increases in cerebral artery shear stress, irrespective of stimulus, induce similar changes in extra-cranial arterial diameter in humans. J Cereb Blood Flow Metab. 2019;

91. Carter HH, Atkinson CL, Heinonen IHA, Haynes A, Robey E, Smith KJ, et al.

Evidence for shear stress-mediated dilation of the internal carotid artery in humans. Hypertension. 2016;

92. Ide K, Worthley M, Anderson T, Poulin MJ. Effects of the nitric oxide synthase inhibitor L-NMMA on cerebrovascular and cardiovascular responses to hypoxia and hypercapnia in humans. J Physiol. 2007;

93. Davis RJ, Murdoch CE, Ali M, Purbrick S, Ravid R, Baxter GS, et al. EP4 prostanoid receptor-mediated vasodilatation of human middle cerebral arteries. Br J Pharmacol. 2004;

94. Parsons AA, Whalley ET. Effects of prostanoids on human and rabbit basilar arteries precontracted in vitro. Cephalalgia. 1989;

95. Paul KS, Whalley ET, Forster BC, Lye R, Dutton J. Prostacyclin and cerebral vessel relaxation. J Neurosurg. 1982;

96. Boullin D, Bunting S, Blaso W, Hunt T, Moncada S. Responses of human and baboon arteries to prostaglandin endoperoxides and biologically generated and synthetic prostacyclin: their relevance to cerebral arterial spasm in man. Br J Clin Pharmacol. 1979;

97. Leffler CW, Busija DW, Armstead WM, Shanklin DR, Mirro R, Thelin O. Activated oxygen and arachidonate effects on newborn cerebral arterioles. Am J Physiol - Hear Circ Physiol. 1990;

98. Leffler CW, Mirro R, Shibata M, Parfenova H, Armstead WM, Zuckerman S. Effects of indomethacin on cerebral vasodilator responses to arachidonic acid and hypercapnia in newborn pigs. Pediatr Res. 1993;

99. Kontos HA, Wei EP, Povlishock JT, Christman CW. Oxygen radicals mediate the cerebral arteriolar dilation from arachidonate and bradykinin in cats. Circ Res. 1984;

100. Parfenova H, Leffler CW. Effects of hypercapnia on prostanoid and cAMP production by cerebral microvascular cell cultures. Am J Physiol - Cell Physiol. 1996;

101. Hoiland RL, Ainslie PN, Wildfong KW, Smith KJ, Bain AR, Willie CK, et al. Indomethacin-induced impairment of regional cerebrovascular reactivity: Implications for respiratory control. J Physiol. 2015;

102. St. Lawrence KS, Ye FQ, Lewis BK, Weinberger DR, Frank JA, McLaughlin AC. Effects of indomethacin on cerebral blood flow at rest and during

hypercapnia: An arterial spin tagging study in humans. J Magn Reson Imaging. 2002;

103. Hoiland RL, Tymko MM, Bain AR, Wildfong KW, Monteleone B, Ainslie PN. Carbon dioxide-mediated vasomotion of extra-cranial cerebral arteries in humans: a role for prostaglandins? J Physiol. 2016;

104. Sobczyk O, Duffin J, Fisher JA, Mikulis DJ. The Physiological Basis of Cerebrovascular ReactivityCerebrovascular reactivity (CVR) Measurements BT - Cerebrovascular Reactivity: Methodological Advances and Clinical Applications. In: Chen J, Fierstra J, editors. New York, NY: Springer US; 2022. p. 1–18.

105. Ringelstein EB, Sievers C, Ecker S, Schneider PA, Otis SM. Noninvasive assessment of CO2-induced cerebral vasomotor response in normal individuals and patients with internal carotid artery occlusions. Stroke. 1988 Aug 1;19(8):963–9.

106. Gupta A, Chazen JL, Hartman M, Delgado D, Anumula N, Shao H, et al. Cerebrovascular reserve and stroke risk in patients with carotid stenosis or occlusion: A systematic review and meta-analysis. Stroke. 2012.

107. Widder B, Kleiser B, Krapf H. Course of cerebrovascular reactivity in patients with carotid artery occlusions. Stroke. 1994;

108. Reinhard M, Schwarzer G, Briel M, Altamura C, Palazzo P, King A, et al. Cerebrovascular reactivity predicts stroke in high-grade carotid artery disease. Neurology. 2014;

109. Markus H, Cullinane M. Severely impaired cerebrovascular reactivity predicts stroke and TIA risk in patients with carotid artery stenosis and occlusion. Brain. 2001;

110. Marshall O, Lu H, Brisset JC, Xu F, Liu P, Herbert J, et al. Impaired cerebrovascular reactivity in multiple sclerosis. JAMA Neurol. 2014;

111. Marshall O, Chawla S, Lu H, Pape L, Ge Y. Cerebral blood flow modulation insufficiency in brain networks in multiple sclerosis: A hypercapnia MRI study. J Cereb Blood Flow Metab. 2016;

112. Dandona P, James IM, Newbury PA, Woollard ML, Beckett AG. Cerebral blood flow in diabetes mellitus: Evidence of abnormal cerebrovascular reactivity. Br Med J. 1978;

113. Fulesdi B, Limburg M, Bereczki D, Michels RPJ, Neuwirth G, Legemate D, et al. Impairment of cerebrovascular reactivity in long-term type 1 diabetes. Diabetes. 1997;

114. Frosch OH, Yau PL, Osorio RS, Rusinek H, Storey P, Convit A. Insulin resistance among obese middle-aged is associated with decreased cerebrovascular reactivity. Neurology. 2017;89(3):249–55.

115. Xie A, Skatrud JB, Morgan B, Chenuel B, Khayat R, Reichmuth K, et al. Influence of cerebrovascular function on the hypercapnic ventilatory response in healthy humans. J Physiol. 2006 Nov 15;577(1):319–29.

116. Xie A, Skatrud JB, Khayat R, Dempsey JA, Morgan B, Russell D. Cerebrovascular Response to Carbon Dioxide in Patients with Congestive Heart Failure. Am J Respir Crit Care Med. 2005 Aug 1;172(3):371–8.

117. Ide K, Eliasziw M, Poulin MJ. Relationship between middle cerebral artery blood velocity and end-tidal PCO2 in the hypocapnic-hypercapnic range in humans. J Appl Physiol. 2003 Jul 1;95(1):129–37.

118. Park CW, Sturzenegger M, Douville CM, Aaslid R, Newell DW. Autoregulatory response and CO2 reactivity of the basilar artery. Stroke. 2003;

119. Ramsay SC, Murphy K, Shea SA, Friston KJ, Lammertsma AA, Clark JC, et al. Changes in global cerebral blood flow in humans: effect on regional cerebral blood flow during a neural activation task. J Physiol. 1993;

120. Thomas BP, Liu P, Park DC, Van Osch MJP, Lu H. Cerebrovascular reactivity in the brain white matter: Magnitude, temporal characteristics, and age effects. J Cereb Blood Flow Metab. 2014;

121. Bhogal AA, Philippens MEP, Siero JCW, Fisher JA, Petersen ET, Luijten PR, et al. Examining the regional and cerebral depth-dependent BOLD cerebrovascular reactivity response at 7T. Neuroimage. 2015;

122. Mandell DM, Han JS, Poublanc J, Crawley AP, Kassner A, Fisher JA, et al. Selective Reduction of Blood Flow to White Matter During Hypercapnia Corresponds With Leukoaraiosis. Stroke. 2008 Jul 1;39(7):1993–8.

123. Meadows GE, Dunroy HMA, Morrell MJ, Corfield DR. Hypercapnic cerebral vascular reactivity is decreased, in humans, during sleep compared with wakefulness. J Appl Physiol. 2003 Jun 1;94(6):2197–202.

124. Rasmussen P, Stie H, Nielsen B, Nybo L. Enhanced cerebral CO2 reactivity

during strenuous exercise in man. Eur J Appl Physiol. 2006;96(3):299–304.

125. Ogoh S, Hayashi N, Inagaki M, Ainslie PN, Miyamoto T. Interaction between the ventilatory and cerebrovascular responses to hypo- and hypercapnia at rest and during exercise. J Physiol. 2008 Sep 1;586(17):4327–38.

126. Conroy DA, Spielman AJ, Scott RQ. Daily rhythm of cerebral blood flow velocity. J Circadian Rhythms. 2005;3(1):3.

127. Bassetti C, Aldrich M. Night time versus daytime transient ischaemic attack and ischaemic stroke: A prospective study of 110 patients. J Neurol Neurosurg Psychiatry. 1999;

128. Marler JR, Price TR, Clark GL, Muller JE, Robertson T, Mohr JP, et al. Morning increase in onset of ischemic stroke. Stroke. 1989 Apr 1;20(4):473–6.

129. Manfredini R, Boari B, Smolensky MH, Salmi R, la Cecilia O, Maria Malagoni A, et al. Circadian Variation in Stroke Onset: Identical Temporal Pattern in Ischemic and Hemorrhagic Events. Chronobiol Int. 2005 Jan 1;22(3):417–53.

130. Lu H, Liu P, Yezhuvath U, Cheng Y, Marshall O, Ge Y. MRI Mapping of Cerebrovascular Reactivity via Gas Inhalation Challenges. JoVE. 2014;(94):e52306.

131. Tancredi FB, Lajoie I, Hoge RD. A simple breathing circuit allowing precise control of inspiratory gases for experimental respiratory manipulations. BMC Res Notes. 2014;

132. Fisher JA. The CO2 stimulus for cerebrovascular reactivity: Fixing inspired concentrations vs. targeting end-tidal partial pressures. Vol. 36, Journal of Cerebral Blood Flow and Metabolism. 2016. p. 1004–11.

133. Duffin J. Measuring the respiratory chemoreflexes in humans. Respiratory Physiology and Neurobiology. 2011.

134. Wise RG, Pattinson KTS, Bulte DP, Chiarelli PA, Mayhew SD, Balanos GM, et al. Dynamic forcing of end-tidal carbon dioxide and oxygen applied to functional magnetic resonance imaging. J Cereb Blood Flow Metab. 2007;

135. Slessarev M, Han J, Mardimae A, Prisman E, Preiss D, Volgyesi G, et al. Prospective targeting and control of end-tidal CO2 and O2 concentrations. J Physiol. 2007;

136. Mark CI, Slessarev M, Ito S, Han J, Fisher JA, Pike GB. Precise control of end-

tidal carbon dioxide and oxygen improves BOLD and ASL cerebrovascular reactivity measures. Magn Reson Med. 2010;

137. Ito S, Mardimae A, Han J, Duffin J, Wells G, Fedorko L, et al. Non-invasive prospective targeting of arterial PCO2 in subjects at rest. J Physiol. 2008;

138. Squire LR. The Legacy of Patient H.M. for Neuroscience. Neuron. 2009.

139. Knierim JJ. The hippocampus. Curr Biol. 2015;25(23):R1116–21.

140. Duvernoy HM, Cattin F, Risold PY, Vannson JL, Gaudron M. The human hippocampus: Functional anatomy, vascularization and serial sections with MRI, fourth edition. The Human Hippocampus: Functional Anatomy, Vascularization and Serial Sections with MRI, Fourth Edition. 2013.

141. Wiltgen BJ, Zhou M, Cai Y, Balaji J, Karlsson MG, Parivash SN, et al. The Hippocampus Plays a Selective Role in the Retrieval of Detailed Contextual Memories. Curr Biol. 2010 Aug;20(15):1336–44.

142. Lazarov O, Marr RA. Neurogenesis and Alzheimer's disease: At the crossroads. Experimental Neurology. 2010.

143. Muthupillai R, Lomas DJ, Rossman PJ, Greenleaf JF, Manduca A, Ehman RL. Magnetic resonance elastography by direct visualization of propagating acoustic strain waves. Science (80-). 1995 Sep 29;269(5232):1854 LP – 1857.

144. Sack I, Jöhrens K, Würfel J, Braun J. Structure-sensitive elastography: On the viscoelastic powerlaw behavior of in vivo human tissue in health and disease. Soft Matter. 2013;

145. Riek K, Millward JM, Hamann I, Mueller S, Pfueller CF, Paul F, et al. Magnetic resonance elastography reveals altered brain viscoelasticity in experimental autoimmune encephalomyelitis. NeuroImage Clin. 2012;

146. Schregel K, Wuerfel nee Tysiak E, Garteiser P, Gemeinhardt I, Prozorovski T, Aktas O, et al. Demyelination reduces brain parenchymal stiffness quantified in vivo by magnetic resonance elastography. Proc Natl Acad Sci. 2012;

147. Hiscox L V., Schwarb H, McGarry MDJ, Johnson CL. Aging brain mechanics: Progress and promise of magnetic resonance elastography. NeuroImage. 2021.

148. Delgorio PL, Hiscox L V, Daugherty AM, Sanjana F, Pohlig RT, Ellison JM, et al. Effect of Aging on the Viscoelastic Properties of Hippocampal Subfields Assessed with High-Resolution MR Elastography. Cereb Cortex. 2021 Jun

1;31(6):2799–811.

149. Arani A, Murphy MC, Glaser KJ, Manduca A, Lake DS, Kruse SA, et al. Measuring the effects of aging and sex on regional brain stiffness with MR elastography in healthy older adults. Neuroimage. 2015;

150. Millward JM, Guo J, Berndt D, Braun J, Sack I, Infante-Duarte C. Tissue structure and inflammatory processes shape viscoelastic properties of the mouse brain. NMR Biomed. 2015;28(7):831–9.

151. Hiscox L V, Johnson CL, McGarry MDJ, Marshall H, Ritchie CW, van Beek EJR, et al. Mechanical property alterations across the cerebral cortex due to Alzheimer's disease. Brain Commun. 2019 Dec 17;2(1).

152. Murphy MC, Jones DT, Jack CR, Glaser KJ, Senjem ML, Manduca A, et al. Regional brain stiffness changes across the Alzheimer's disease spectrum. NeuroImage Clin. 2016;

153. Murphy MC, Huston J, Jack CR, Glaser KJ, Manduca A, Felmlee JP, et al. Decreased brain stiffness in Alzheimer's disease determined by magnetic resonance elastography. J Magn Reson Imaging. 2011;

154. Lipp A, Trbojevic R, Paul F, Fehlner A, Hirsch S, Scheel M, et al. Cerebral magnetic resonance elastography in supranuclear palsy and idiopathic Parkinson's disease. NeuroImage Clin. 2013;

155. Lipp A, Skowronek C, Fehlner A, Streitberger K-J, Braun J, Sack I. Progressive supranuclear palsy and idiopathic Parkinson's disease are associated with local reduction of in vivo brain viscoelasticity. Eur Radiol. 2018;28(8):3347–54.

156. Wuerfel J, Paul F, Beierbach B, Hamhaber U, Klatt D, Papazoglou S, et al. MR-elastography reveals degradation of tissue integrity in multiple sclerosis. Neuroimage. 2010;49(3):2520–5.

157. Romano A, Guo J, Prokscha T, Meyer T, Hirsch S, Braun J, et al. In vivo waveguide elastography: Effects of neurodegeneration in patients with amyotrophic lateral sclerosis. Magn Reson Med. 2014 Dec 1;72(6):1755–61.

158. Streitberger KJ, Sack I, Krefting D, Pfüller C, Braun J, Paul F, et al. Brain viscoelasticity alteration in chronic-progressive multiple sclerosis. PLoS One. 2012;

159. Hiscox L V, Johnson CL, McGarry MDJ, Schwarb H, van Beek EJR, Roberts N, et al. Hippocampal viscoelasticity and episodic memory performance in

healthy older adults examined with magnetic resonance elastography. Brain Imaging Behav. 2020;14(1):175–85.

160. Schwarb H, Johnson CL, McGarry MDJ, Cohen NJ. Medial temporal lobe viscoelasticity and relational memory performance. Neuroimage. 2016;

161. Johnson CL, Holtrop JL, McGarry MDJ, Weaver JB, Paulsen KD, Georgiadis JG, et al. 3D multislab, multishot acquisition for fast, whole-brain MR elastography with high signal-to-noise efficiency. Magn Reson Med. 2014 Feb 1;71(2):477–85.

162. Van Houten EEW, Miga MI, Weaver JB, Kennedy FE, Paulsen KD. Three-dimensional subzone-based reconstruction algorithm for MR elastography. Magn Reson Med. 2001 May 1;45(5):827–37.

163. McGarry MDJ, Van Houten EEW, Johnson CL, Georgiadis JG, Sutton BP, Weaver JB, et al. Multiresolution MR elastography using nonlinear inversion. Med Phys. 2012 Oct 1;39(10):6388–96.

164. Hiscox L V, Johnson CL, McGarry MDJ, Perrins M, Littlejohn A, van Beek EJR, et al. High-resolution magnetic resonance elastography reveals differences in subcortical gray matter viscoelasticity between young and healthy older adults. Neurobiol Aging. 2018;65:158–67.

165. Schwarb H, Johnson CL, Daugherty AM, Hillman CH, Kramer AF, Cohen NJ, et al. Aerobic fitness, hippocampal viscoelasticity, and relational memory performance. Neuroimage. 2017;

166. Johnson CL, Schwarb H, McGarry MDJ, Anderson AT, Huesmann GR, Sutton BP, et al. Viscoelasticity of subcortical gray matter structures. Hum Brain Mapp. 2016 Dec 1;37(12):4221–33.

167. Weickenmeier J, de Rooij R, Budday S, Steinmann P, Ovaert TC, Kuhl E. Brain stiffness increases with myelin content. Acta Biomater. 2016;

168. Freimann FB, Müller S, Streitberger KJ, Guo J, Rot S, Ghori A, et al. MR elastography in a murine stroke model reveals correlation of macroscopic viscoelastic properties of the brain with neuronal density. NMR Biomed. 2013;

169. Farias ST, Mungas D, Reed BR, Harvey D, DeCarli C. Progression of mild cognitive impairment to dementia in clinic- vs community-based cohorts. Arch Neurol. 2009;

170. Tzschätzsch H, Kreft B, Schrank F, Bergs J, Braun J, Sack I. In vivo time-

harmonic ultrasound elastography of the human brain detects acute cerebral stiffness changes induced by intracranial pressure variations. Sci Rep. 2018;

171. Panagiotakos DB, Pitsavos C, Arvaniti F, Stefanadis C. Adherence to the Mediterranean food pattern predicts the prevalence of hypertension, hypercholesterolemia, diabetes and obesity, among healthy adults; the accuracy of the MedDietScore. Prev Med (Baltim). 2007;

172. Sacks FM, Moore TJ, Appel LJ, Obarzanek E, Cutler JA, Vollmer WM, et al. A dietary approach to prevent hypertension: A review of the dietary approaches to stop hypertension (DASH) study. Clin Cardiol. 1999;

173. Martínez-Lapiscina EH, Clavero P, Toledo E, Estruch R, Salas-Salvadó J, San Julián B, et al. Mediterranean diet improves cognition: The PREDIMED-NAVARRA randomised trial. J Neurol Neurosurg Psychiatry. 2013;

174. Smith PJ, Blumenthal JA, Babyak MA, Craighead L, Welsh-Bohmer KA, Browndyke JN, et al. Effects of the dietary approaches to stop hypertension diet, exercise, and caloric restriction on neurocognition in overweight adults with high blood pressure. Hypertension. 2010;

175. Morris MC, Tangney CC, Wang Y, Sacks FM, Barnes LL, Bennett DA, et al. MIND diet slows cognitive decline with aging. Alzheimer's Dement. 2015;

176. Morris MC, Tangney CC, Wang Y, Sacks FM, Bennett DA, Aggarwal NT. MIND diet associated with reduced incidence of Alzheimer's disease. Alzheimer's Dement. 2015;

177. Kanoski SE, Davidson TL. Western diet consumption and cognitive impairment: Links to hippocampal dysfunction and obesity. Physiol Behav. 2011;103(1):59–68.

178. Berrino F. Western diet and Alzheimer's disease. Epidemiologia e prevenzione. 2002.

179. Więckowska-Gacek A, Mietelska-Porowska A, Wydrych M, Wojda U. Western diet as a trigger of Alzheimer's disease: From metabolic syndrome and systemic inflammation to neuroinflammation and neurodegeneration. Ageing Research Reviews. 2021.

180. Tappy L, Lê K-A. Metabolic Effects of Fructose and the Worldwide Increase in Obesity. Physiol Rev. 2010 Jan 1;90(1):23–46.

181. Tappy L. Fructose-containing caloric sweeteners as a cause of obesity and

metabolic disorders. J Exp Biol. 2018 Mar 7;221(Suppl 1):jeb164202.

182. Rödel W. J. S. Fruton: Molecules and Life – Historical Essays on the Interplay of Chemistry and Biology. 579 Seiten. Wiley-Interscience, New York, London, Sydney, Toronto 1972. Preis: 8,95 £. Food / Nahrung. 1974 Jan 1;18(4):471–2.

183. Douard V, Ferraris RP. Regulation of the fructose transporter GLUT5 in health and disease. Am J Physiol Metab. 2008 Aug 1;295(2):E227–37.

184. Corpe CP, Burant CF, Hoekstra JH. Intestinal Fructose Absorption: Clinical and Molecular Aspects. J Pediatr Gastroenterol Nutr. 1999;28(4).

185. Kneepkens CM, Vonk RJ, Fernandes J. Incomplete intestinal absorption of fructose. Arch Dis Child. 1984 Aug 1;59(8):735 LP – 738.

186. Ravich WJ, Bayless TM, Thomas M. Fructose: Incomplete Intestinal Absorption in Humans. Gastroenterology. 1983;84(1):26–9.

187. Pekin N, Keelan M, Jarocka-Cyrta E, Clandinin MT, Thomson ABR. Ontogeny of intestinal adaptation in rats in response to isocaloric changes in dietary lipids. Am J Physiol. 1997;

188. Colville CA, Seatter MJ, Jess TJ, Gould GW, Thomas HM. Kinetic analysis of the liver-type (GLUT2) and brain-type (GLUT3) glucose transporters in Xenopus oocytes: substrate specificities and effects of transport inhibitors. Biochem J. 1993 Mar 15;290(3):701–6.

189. Cheeseman CI. GLUT2 is the transporter for fructose across the rat intestinal basolateral membrane. Gastroenterology. 1993;105(4):1050–6.

190. Adelman RC, Ballard FJ, Weinhouse S. Purification and Properties of Rat Liver Fructokinase. J Biol Chem. 1967 Jul 25;242(14):3360–5.

191. Cori GT, Ochoa S, Slein MW, Cori CF. The metabolism of fructose in liver. Isolation of fructose-1-phosphate and inorganic pyrophosphate. BBA - Biochim Biophys Acta. 1951;

192. Mayes PA. Intermediary metabolism of fructose. American Journal of Clinical Nutrition. 1993.

193. Samuel VT. Fructose induced lipogenesis: From sugar to fat to insulin resistance. Trends in Endocrinology and Metabolism. 2011.

194. Fushinobu S, Nishimasu H, Hattori D, Song HJ, Wakagi T. Structural basis for the bifunctionality of fructose-1,6-bisphosphate aldolase/phosphatase. Nature.

2011;

195. Johnson RJ, Sanchez-Lozada LG, Nakagawa T. The Effect of Fructose on Renal Biology and Disease. J Am Soc Nephrol. 2010;21(12).

196. Timlin MT, Parks EJ. Temporal pattern of de novo lipogenesis in the postprandial state in healthy men. Am J Clin Nutr. 2005 Jan 1;81(1):35–42.

197. Donnelly KL, Smith CI, Schwarzenberg SJ, Jessurun J, Boldt MD, Parks EJ. Sources of fatty acids stored in liver and secreted via lipoproteins in patients with nonalcoholic fatty liver disease. J Clin Invest. 2005 May 2;115(5):1343–51.

198. Faeh D, Minehira K, Schwarz J-M, Periasamy R, Park S, Tappy L. Effect of Fructose Overfeeding and Fish Oil Administration on Hepatic De Novo Lipogenesis and Insulin Sensitivity in Healthy Men. Diabetes. 2005 Jul 1;54(7):1907–13.

199. Vedala A, Wang W, Neese RA, Christiansen MP, Hellerstein MK. Delayed secretory pathway contributions to VLDL-triglycerides from plasma NEFA, diet, and de novo lipogenesis in humans. J Lipid Res. 2006;

200. Hudgins LC, Hellerstein MK, Seidman CE, Neese RA, Tremaroli JD, Hirsch J. Relationship between carbohydrate-induced hypertriglyceridemia and fatty acid synthesis in lean and obese subjects. J Lipid Res. 2000;

201. Silbernagel G, Machann J, Unmuth S, Schick F, Stefan N, Häring HU, et al. Effects of 4-week very-high-fructose/glucose diets on insulin sensitivity, visceral fat and intrahepatic lipids: an exploratory trial. Br J Nutr. 2011/03/14. 2011;106(1):79–86.

202. Lê K-A, Faeh D, Stettler R, Ith M, Kreis R, Vermathen P, et al. A 4-wk high-fructose diet alters lipid metabolism without affecting insulin sensitivity or ectopic lipids in healthy humans. Am J Clin Nutr. 2006 Dec 1;84(6):1374–9.

203. Gallagher C, Keogh JB, Pedersen E, Clifton PM. Fructose acute effects on glucose, insulin, and triglyceride after a solid meal compared with sucralose and sucrose in a randomized crossover study. Am J Clin Nutr. 2016 Jun 1;103(6):1453–7.

204. Stanhope KL, Bremer AA, Medici V, Nakajima K, Ito Y, Nakano T, et al. Consumption of Fructose and High Fructose Corn Syrup Increase Postprandial Triglycerides, LDL-Cholesterol, and Apolipoprotein-B in Young Men and Women. J Clin Endocrinol Metab. 2011 Oct 1;96(10):E1596–605.

205. Bantle JP, Raatz SK, Thomas W, Georgopoulos A. Effects of dietary fructose on plasma lipids in healthy subjects. Am J Clin Nutr. 2000 Nov 1;72(5):1128–34.

206. Stanhope KL, Griffen SC, Bair BR, Swarbrick MM, Keim NL, Havel PJ. Twenty-four-hour endocrine and metabolic profiles following consumption of high-fructose corn syrup-, sucrose-, fructose-, and glucose-sweetened beverages with meals. Am J Clin Nutr. 2008 May;87(5):1194–203.

207. Stanhope KL, Medici V, Bremer AA, Lee V, Lam HD, Nunez M V, et al. A dose-response study of consuming high-fructose corn syrup-sweetened beverages on lipid/lipoprotein risk factors for cardiovascular disease in young adults. Am J Clin Nutr. 2015/04/22. 2015 Jun;101(6):1144–54.

208. Abraha A, Humphreys SM, Clark ML, Matthews DR, Frayn KN. Acute effect of fructose on postprandial lipaemia in diabetic and non-diabetic subjects. Br J Nutr. 2007/03/09. 1998;80(2):169–75.

209. West S, Smail O, Bond B. The acute influence of sucrose consumption with and without vitamin C co-ingestion on microvascular reactivity in healthy young adults. Microvasc Res. 2019;126:103906.

210. Teff KL, Elliott SS, Tschöp M, Kieffer TJ, Rader D, Heiman M, et al. Dietary Fructose Reduces Circulating Insulin and Leptin, Attenuates Postprandial Suppression of Ghrelin, and Increases Triglycerides in Women. J Clin Endocrinol Metab. 2004 Jun 1;89(6):2963–72.

211. Bar-On H, Stein Y. Effect of Glucose and Fructose Administration on Lipid Metabolism in the Rat. J Nutr. 1968 Jan 1;94(1):95–105.

212. Topping DL, Mayes PA. The immediate effects of insulin and fructose on the metabolism of the perfused liver. Changes in lipoprotein secretion, fatty acid oxidation and esterification, lipogenesis and carbohydrate metabolism. Biochem J. 1972 Jan 1;126(2):295–311.

213. Clark DG, Rognstad R, Katz J. Lipogenesis in rat hepatocytes. J Biol Chem. 1974;

214. Parks EJ, Skokan LE, Timlin MT, Dingfelder CS. Dietary Sugars Stimulate Fatty Acid Synthesis in Adults. J Nutr. 2008;

215. Da Silva LA, De Marcucci OL, Carmona A. Adaptive changes in total pyruvate dehydrogenase activity in lipogenic tissues of rats fed high-sucrose or high-fat diets. Comp Biochem Physiol Part A Physiol. 1992;103(2):407–11.

216. Carmona A, Freedland RA. Comparison among the Lipogenic Potential of various Substrates in Rat Hepatocytes: The Differential Effects of Fructose-Containing Diets on Hepatic Lipogenesis. J Nutr. 1989 Sep 1;119(9):1304–10.

217. Park OJ, Cesar D, Faix D, Wu K, Shackleton CHL, Hellerstein MK. Mechanisms of fructose-induced hypertriglyceridaemia in the rat. Activation of hepatic pyruvate dehydrogenase through inhibition of pyruvate dehydrogenase kinase. Biochem J. 1992 Mar 15;282(3):753–7.

218. Matsuzaka T, Shimano H, Yahagi N, Amemiya-Kudo M, Okazaki H, Tamura Y, et al. Insulin-Independent Induction of Sterol Regulatory Element-Binding Protein-1c Expression in the Livers of Streptozotocin-Treated Mice. Diabetes. 2004 Mar 1;53(3):560–9.

219. Shimomura I, Bashmakov Y, Horton JD. Increased levels of nuclear SREBP-1c associated with fatty livers in two mouse models of diabetes mellitus. J Biol Chem. 1999;

220. Denechaud P-D, Dentin R, Girard J, Postic C. Role of ChREBP in hepatic steatosis and insulin resistance. FEBS Lett. 2008;582(1):68–73.

221. Koo H-Y, Wallig MA, Chung BH, Nara TY, Cho BHS, Nakamura MT. Dietary fructose induces a wide range of genes with distinct shift in carbohydrate and lipid metabolism in fed and fasted rat liver. Biochim Biophys Acta - Mol Basis Dis. 2008;1782(5):341–8.

222. Alves-Bezerra M, Cohen DE. Triglyceride metabolism in the liver. Compr Physiol. 2018;

223. Gordon DA, Wetterau JR, Gregg RE. Microsomal triglyceride transfer protein: a protein complex required for the assembly of lipoprotein particles. Trends Cell Biol. 1995;5(8):317–21.

224. Cohen DE, Fisher EA. Lipoprotein metabolism, dyslipidemia, and nonalcoholic fatty liver disease. Semin Liver Dis. 2013;

225. Miller M, Stone NJ, Ballantyne C, Bittner V, Criqui MH, Ginsberg HN, et al. Triglycerides and Cardiovascular Disease. Circulation. 2011 May 24;123(20):2292–333.

226. Kajikawa M, Higashi Y. Triglycerides and endothelial function: Molecular biology to clinical perspective. Current Opinion in Lipidology. 2019.

227. Sandoo A, Veldhuijzen van Zanten JJCS, Metsios GS, Carroll D, Kitas GD.

The Endothelium and Its Role in Regulating Vascular Tone. Open Cardiovasc Med J. 2015;4(1):302–12.

228. Villar IC, Francis S, Webb A, Hobbs AJ, Ahluwalia A. Novel aspects of endothelium-dependent regulation of vascular tone. Kidney International. 2006.

229. LaRocca TJ, Martens CR, Seals DR. Nutrition and other lifestyle influences on arterial aging. Ageing Res Rev. 2016/09/28. 2017 Oct;39:106–19.

230. Fleming I, Busse R. Molecular mechanisms involved in the regulation of the endothelial nitric oxide synthase. American Journal of Physiology - Regulatory Integrative and Comparative Physiology. 2003.

231. Donato AJ, Morgan RG, Walker AE, Lesniewski LA. Cellular and molecular biology of aging endothelial cells. Journal of Molecular and Cellular Cardiology. 2015.

232. Hansson GK, Hermansson A. The immune system in atherosclerosis. Nature Immunology. 2011.

233. Moore KJ, Tabas I. Macrophages in the pathogenesis of atherosclerosis. Cell. 2011.

234. Bekkering S, Quintin J, Joosten LAB, Van Der Meer JWM, Netea MG, Riksen NP. Oxidized low-density lipoprotein induces long-term proinflammatory cytokine production and foam cell formation via epigenetic reprogramming of monocytes. Arterioscler Thromb Vasc Biol. 2014;

235. Toth PP. Triglyceride-rich lipoproteins as a causal factor for cardiovascular disease. Vasc Health Risk Manag. 2016 May 6;12:171–83.

236. Lanaspa MA, Sanchez-Lozada LG, Choi Y-J, Cicerchi C, Kanbay M, Roncal-Jimenez CA, et al. Uric Acid Induces Hepatic Steatosis by Generation of Mitochondrial Oxidative Stress. J Biol Chem. 2012;

237. Sánchez-Lozada LG, Lanaspa MA, Cristóbal-García M, García-Arroyo F, Soto V, Cruz-Robles D, et al. Uric acid-induced endothelial dysfunction is associated with mitochondrial alterations and decreased intracellular ATP concentrations. Nephron - Exp Nephrol. 2013;

238. Lanaspa MA, Sanchez-Lozada LG, Cicerchi C, Li N, Roncal-Jimenez CA, Ishimoto T, et al. Uric Acid Stimulates Fructokinase and Accelerates Fructose Metabolism in the Development of Fatty Liver. PLoS One. 2012;

239. Samuel VT, Petersen KF, Shulman GI. Lipid-induced insulin resistance: unravelling the mechanism. The Lancet. 2010.

240. Baldwin W, McRae S, Marek G, Wymer D, Pannu V, Baylis C, et al. Hyperuricemia as a mediator of the proinflammatory endocrine imbalance in the adipose tissue in a murine model of the metabolic syndrome. Diabetes. 2011;

241. Sautin YY, Nakagawa T, Zharikov S, Johnson RJ. Adverse effects of the classic antioxidant uric acid in adipocytes: NADPH oxidase-mediated oxidative/nitrosative stress. Am J Physiol - Cell Physiol. 2007;

242. Porras AG, Olson JS, Palmer G. The reaction of reduced xanthine oxidase with oxygen. Kinetics of peroxide and superoxide formation. J Biol Chem. 1981;

243. Fridovich I. Superoxide dismutases: defence against endogenous superoxide radical. Ciba Found Symp. 1978;

244. George J, Carr E, Davies J, Belch JJF, Struthers A. High-dose allopurinol improves endothelial function by profoundly reducing vascular oxidative stress and not by lowering uric acid. Circulation. 2006;

245. Maruhashi T, Hisatome I, Kihara Y, Higashi Y. Hyperuricemia and endothelial function: From molecular background to clinical perspectives. Atherosclerosis. 2018 Nov;278:226–31.

246. Gersch C, Palii SP, Kim KM, Angerhofer A, Johnson RJ, Henderson GN. Inactivation of nitric oxide by uric acid. Nucleosides, Nucleotides and Nucleic Acids. 2008;

247. Imaram W, Gersch C, Kim KM, Johnson RJ, Henderson GN, Angerhofer A. Radicals in the reaction between peroxynitrite and uric acid identified by electron spin resonance spectroscopy and liquid chromatography mass spectrometry. Free Radic Biol Med. 2010;

248. Santos CXC, Anjos EI, Augusto O. Uric acid oxidation by peroxynitrite: Multiple reactions, free radical formation, and amplification of lipid oxidation. Arch Biochem Biophys. 1999;

249. Zharikov S, Krotova K, Hu H, Baylis C, Johnson RJ, Block ER, et al. Uric acid decreases NO production and increases arginase activity in cultured pulmonary artery endothelial cells. Am J Physiol - Cell Physiol. 2008;

250. Schwartz IF, Grupper A, Chernichovski T, Grupper A, Hillel O, Engel A, et al.

Hyperuricemia attenuates aortic nitric oxide generation, through inhibition of arginine transport, in rats. J Vasc Res. 2011;

251. Maples KR, Mason RP. Free radical metabolite of uric acid. J Biol Chem. 1988;

252. Weiss EP, Arif H, Villareal DT, Marzetti E, Holloszy JO. Endothelial function after high-sugar-food ingestion improves with endurance exercise performed on the previous day. Am J Clin Nutr. 2008 Jul;88(1):51–7.

253. Kato T, Inoue T, Node K. Postprandial endothelial dysfunction in subjects with new-onset type 2 diabetes: An acarbose and nateglinide comparative study. Cardiovasc Diabetol. 2010;

254. Duckrow RB, Beard DC, Brennan RW. Regional cerebral blood flow decreases during chronic and acute hyperglycemia. Stroke. 1987;

255. Harik SI, LaManna JC. Vascular Perfusion and Blood-Brain Glucose Transport in Acute and Chronic Hyperglycemia. J Neurochem. 1988;

256. Duckrow RB. Decreased cerebral blood flow during acute hyperglycemia. Brain Res. 1995;

257. Page KA, Melrose AJ. Brain, hormone and appetite responses to glucose versus fructose. Current Opinion in Behavioral Sciences. 2016.

258. Morton GJ, Cummings DE, Baskin DG, Barsh GS, Schwartz MW. Central nervous system control of food intake and body weight. Nature. 2006.

259. Smeets PAM, De Graaf C, Stafleu A, Van Osch MJP, Van Der Grond J. Functional MRI of human hypothalamic responses following glucose ingestion. Neuroimage. 2005;

260. Matsuda M, Liu Y, Mahankali S, Pu Y, Mahankali A, Wang J, et al. Altered hypothalamic function in response to glucose ingestion in obese humans. Diabetes. 1999;

261. Liu Y, Jia-Hong G, Liu HL, Fox PT. The temporal response of the brain after eating revealed by functional MRI. Nature. 2000;

262. Rorabaugh JM, Stratford JM, Zahniser NR. A relationship between reduced nucleus accumbens shell and enhanced lateral hypothalamic orexin neuronal activation in long-term fructose bingeing behavior. PLoS One. 2014;

263. Anderson EA, Mark AL. Flow-mediated and reflex changes in large peripheral artery tone in humans. Circulation. 1989;

264. Kelleher RJ, Soiza RL. Evidence of endothelial dysfunction in the development of Alzheimer's disease: Is Alzheimer's a vascular disorder? Am J Cardiovasc Dis. 2013;

265. Togo T, Katsuse O, Iseki E. Nitric oxide pathways in Alzheimer's disease and other neurodegenerative dementias. Neurol Res. 2004;

266. Hoth KF, Tate DF, Poppas A, Forman DE, Gunstad J, Moser DJ, et al. Endothelial function and white matter hyperintensities in older adults with cardiovascular disease. Stroke. 2007;

267. Isaka Y, Okamoto M, Ashida K, Imaizumi M. Decreased cerebrovascular dilatory capacity in subjects with asymptomatic periventricular hyperintensities. Stroke. 1994;

268. Bakker SLM, De Leeuw FE, De Groot JC, Hofman A, Koudstaal PJ, Breteler MMB. Cerebral vasomotor reactivity and cerebral white matter lesions in the elderly. Neurology. 1999;

269. 2020 Alzheimer's disease facts and figures. Alzheimer's Dement. 2020;

270. Cummings J, Lee G, Ritter A, Sabbagh M, Zhong K. Alzheimer's disease drug development pipeline: 2020. Alzheimer's Dement Transl Res Clin Interv. 2020 Jan 1;6(1):e12050.

271. McGarry MDJ, Van Houten EEW, Perrĩez PR, Pattison AJ, Weaver JB, Paulsen KD. An octahedral shear strain-based measure of SNR for 3D MR elastography. Phys Med Biol. 2011;

272. Jenkinson M, Beckmann CF, Behrens TEJ, Woolrich MW, Smith SM. FSL. Neuroimage. 2012;62(2):782–90.

273. Winter JD, Fierstra J, Dorner S, Fisher JA, Lawrence KS, Kassner A. Feasibility and precision of cerebral blood flow and cerebrovascular reactivity MRI measurements using a computer-controlled gas delivery system in an anesthetised juvenile animal model. J Magn Reson Imaging. 2010;

274. Zhou Y, Rodgers ZB, Kuo AH. Cerebrovascular reactivity measured with arterial spin labeling and blood oxygen level dependent techniques. Magn Reson Imaging. 2015 Jun;33(5):566–76.

275. Juttukonda MR, Li B, Almaktoum R, Stephens KA, Yochim KM, Yacoub E, et al. Characterizing cerebral hemodynamics across the adult lifespan with arterial spin labeling MRI data from the Human Connectome Project-Aging.

Neuroimage. 2021;

276. Alsop DC, Detre JA, Golay X, Günther M, Hendrikse J, Hernandez-Garcia L, et al. Recommended implementation of arterial spin-labeled Perfusion mri for clinical applications: A consensus of the ISMRM Perfusion Study group and the European consortium for ASL in dementia. Magn Reson Med. 2015;

277. Chappell MA, Groves AR, Whitcher B, Woolrich MW. Variational Bayesian Inference for a Nonlinear Forward Model. IEEE Trans Signal Process. 2009;57(1):223–36.

278. Groves AR, Chappell MA, Woolrich MW. Combined spatial and non-spatial prior for inference on MRI time-series. Neuroimage. 2009;45(3):795–809.

279. Chappell MA, Groves AR, MacIntosh BJ, Donahue MJ, Jezzard P, Woolrich MW. Partial volume correction of multiple inversion time arterial spin labeling MRI data. Magn Reson Med. 2011 Apr 1;65(4):1173–83.

280. Shapiro SS, Wilk MB. An Analysis of Variance Test for Normality (Complete Samples). Biometrika. 1965 Apr 27;52(3/4):591–611.

281. Hayes AF, Scharkow M. The Relative Trustworthiness of Inferential Tests of the Indirect Effect in Statistical Mediation Analysis: Does Method Really Matter? Psychol Sci. 2013;

282. Sack I, Streitberger K-J, Krefting D, Paul F, Braun J. The influence of physiological aging and atrophy on brain viscoelastic properties in humans. PLoS One. 2011/09/12. 2011;6(9):e23451–e23451.

283. Sack I, Beierbach B, Wuerfel J, Klatt D, Hamhaber U, Papazoglou S, et al. The impact of aging and gender on brain viscoelasticity. Neuroimage. 2009;

284. Wilkinson I, Cockcroft JR. Cholesterol, lipids and arterial stiffness. Advances in Cardiology. 2007.

285. Sanjana F, Delgorio PL, DeConne TM, Hiscox L V, Pohlig RT, Johnson CL, et al. Vascular determinants of hippocampal viscoelastic properties in healthy adults across the lifespan. J Cereb Blood Flow Metab. 2023 Jul 3;0271678X231186571.

286. Hsu TM, Konanur VR, Taing L, Usui R, Kayser BD, Goran MI, et al. Effects of sucrose and high fructose corn syrup consumption on spatial memory function and hippocampal neuroinflammation in adolescent rats. Hippocampus. 2015;

287. Pistell PJ, Morrison CD, Gupta S, Knight AG, Keller JN, Ingram DK, et al. Cognitive impairment following high fat diet consumption is associated with brain inflammation. J Neuroimmunol. 2010;

288. Wu A, Molteni R, Ying Z, Gomez-Pinilla F. A saturated-fat diet aggravates the outcome of traumatic brain injury on hippocampal plasticity and cognitive function by reducing brain-derived neurotrophic factor. Neuroscience. 2003;

289. Kanoski SE, Meisel RL, Mullins AJ, Davidson TL. The effects of energy-rich diets on discrimination reversal learning and on BDNF in the hippocampus and prefrontal cortex of the rat. Behav Brain Res. 2007;

290. Banks WA, Farr SA, Salameh TS, Niehoff ML, Rhea EM, Morley JE, et al. Triglycerides cross the blood-brain barrier and induce central leptin and insulin receptor resistance. Int J Obes. 2018;

291. Farr SA, Yamada KA, Butterfield DA, Abdul HM, Xu L, Miller NE, et al. Obesity and Hypertriglyceridemia Produce Cognitive Impairment. Endocrinology. 2008 May 1;149(5):2628–36.

292. Ma D, Lu L, Boneva NB, Warashina S, Kaplamadzhiev DB, Mori Y, et al. Expression of free fatty acid receptor GPR40 in the neurogenic niche of adult monkey hippocampus. Hippocampus. 2008;

293. Patil S, Chan C. Palmitic and stearic fatty acids induce Alzheimer-like hyperphosphorylation of tau in primary rat cortical neurons. Neurosci Lett. 2005;384(3):288–93.

294. Aronis A, Madar Z, Tirosh O. Lipotoxic effects of triacylglycerols in J774.2 macrophages. Nutrition. 2008;24(2):167–76.

295. Laine PS, Schwartz EA, Wang Y, Zhang W-Y, Karnik SK, Musi N, et al. Palmitic acid induces IP-10 expression in human macrophages via NF-κB activation. Biochem Biophys Res Commun. 2007;358(1):150–5.

296. Nägga K, Gustavsson A-M, Stomrud E, Lindqvist D, van Westen D, Blennow K, et al. Increased midlife triglycerides predict brain β-amyloid and tau pathology 20 years later. Neurology. 2018 Jan 2;90(1):e73 LP-e81.

297. Burgess BL, McIsaac SA, Naus KE, Chan JY, Tansley GHK, Yang J, et al. Elevated plasma triglyceride levels precede amyloid deposition in Alzheimer's disease mouse models with abundant Aβ in plasma. Neurobiol Dis. 2006;24(1):114–27.

298. Hellstrand E, Sparr E, Linse S. Retardation of Aβ fibril formation by phospholipid vesicles depends on membrane phase behavior. Biophys J. 2010;

299. Araki W, Tamaoka A. Amyloid beta-protein and lipid rafts: Focused on biogenesis and catabolism. Frontiers in Bioscience - Landmark. 2015.

300. Mamo JCL, Jian L, James AP, Flicker L, Esselmann H, Wiltfang J. Plasma lipoprotein β-amyloid in subjects with Alzheimer's disease or mild cognitive impairment. Ann Clin Biochem. 2008 Jul 1;45(4):395–403.

301. Deane R, Sagare A, Hamm K, Parisi M, Lane S, Finn MB, et al. apoE isoform-specific disruption of amyloid β peptide clearance from mouse brain. J Clin Invest. 2008;

302. Hawkes CA, Sullivan PM, Hands S, Weller RO, Nicoll JAR, Carare RO. Disruption of arterial perivascular drainage of amyloid-β from the brains of mice expressing the human APOE ε4 allele. PLoS One. 2012;

303. Verghese PB, Castellano JM, Garai K, Wang Y, Jiang H, Shah A, et al. ApoE influences amyloid-β (Aβ) clearance despite minimal apoE/Aβ association in physiological conditions. Proc Natl Acad Sci U S A. 2013;

304. Castellano JM, Kim J, Stewart FR, Jiang H, DeMattos RB, Patterson BW, et al. Human apoE Isoforms Differentially Regulate Brain Amyloid-β Peptide Clearance. Sci Transl Med. 2011 Jun 29;3(89):89ra57 LP-89ra57.

305. Maxwell SE. The persistence of underpowered studies in psychological research: Causes, consequences, and remedies. Psychol Methods. 2004;

306. Shenouda N, Priest SE, Rizzuto VI, MacDonald MJ. Brachial artery endothelial function is stable across a menstrual and oral contraceptive pill cycle but lower in premenopausal women than in age-matched men. Am J Physiol - Hear Circ Physiol. 2018;

307. Favre ME, Serrador JM. Sex differences in cerebral autoregulation are unaffected by menstrual cycle phase in young, healthy women. Am J Physiol - Hear Circ Physiol. 2019;

308. Stanhewicz AE, Wong BJ. Counterpoint: Investigators should not control for menstrual cycle phase when performing studies of vascular control that include women. Journal of Applied Physiology. 2020.

309. Lanaspa MA, Cicerchi C, Garcia G, Li N, Roncal-Jimenez CA, Rivard CJ, et al. Counteracting Roles of AMP Deaminase and AMP Kinase in the Development

of Fatty Liver. PLoS One. 2012;

310. A. Abdel-Rahman E, Mahmoud AM, Khalifa AM, Ali SS. Physiological and pathophysiological reactive oxygen species as probed by EPR spectroscopy: the underutilized research window on muscle ageing. Journal of Physiology. 2016.

311. Berg K, Ericsson M, Lindgren M, Gustafsson H. A high precision method for quantitative measurements of reactive oxygen species in frozen biopsies. PLoS One. 2014;

312. Hayyan M, Hashim MA, AlNashef IM. Superoxide Ion: Generation and Chemical Implications. Chem Rev. 2016 Mar 9;116(5):3029–85.

313. Elajaili HB, Hernandez-Lagunas L, Ranguelova K, Dikalov S, Nozik-Grayck E. Use of electron paramagnetic resonance in biological samples at ambient temperature and 77 K. J Vis Exp. 2019;

314. Rudolph TK, Ruempler K, Schwedhelm E, Tan-Andresen J, Riederer U, Böger RH, et al. Acute effects of various fast-food meals on vascular function and cardiovascular disease risk markers: The Hamburg Burger Trial. Am J Clin Nutr. 2007;

315. Maxwell SRJ, Thomason H, Sandler D, Leguen C, Baxter MA, Thorpe GHG, et al. Antioxidant status in patients with uncomplicated insulin-dependent and non-insulin-dependent diabetes mellitus. Eur J Clin Invest. 1997;

316. Buettner GR. The Pecking Order of Free Radicals and Antioxidants: Lipid Peroxidation, α-Tocopherol, and Ascorbate. Arch Biochem Biophys. 1993;

317. Cardona F, Túnez I, Tasset I, Garrido-Sánchez L, Collantes E, Tinahones FJ. Circulating antioxidant defences are decreased in healthy people after a high-fat meal. Br J Nutr. 2008;

318. Kaur H, Halliwell B. Action of biologically-relevant oxidizing species upon uric acid. Identification of uric acid oxidation products. Chem Biol Interact. 1990;

319. Hetzer S, Birr P, Fehlner A, Hirsch S, Dittmann F, Barnhill E, et al. Perfusion alters stiffness of deep gray matter. J Cereb Blood Flow Metab. 2018;

320. Schrank F, Warmuth C, Tzschätzsch H, Kreft B, Hirsch S, Braun J, et al. Cardiac-gated steady-state multifrequency magnetic resonance elastography of the brain: Effect of cerebral arterial pulsation on brain viscoelasticity. J Cereb Blood Flow Metab. 2020;

321. White CL, Pistell PJ, Purpera MN, Gupta S, Fernandez-Kim SO, Hise TL, et al. Effects of high fat diet on Morris maze performance, oxidative stress, and inflammation in rats: Contributions of maternal diet. Neurobiol Dis. 2009;

322. Lopez-Rodriguez AB, Hennessy E, Murray CL, Nazmi A, Delaney HJ, Healy D, et al. Acute systemic inflammation exacerbates neuroinflammation in Alzheimer's disease: IL-1β drives amplified responses in primed astrocytes and neuronal network dysfunction. Alzheimer's Dement. 2021;

323. Sacks FM, Lichtenstein AH, Wu JHY, Appel LJ, Creager MA, Kris-Etherton PM, et al. Dietary fats and cardiovascular disease: A presidential advisory from the American Heart Association. Circulation. 2017.

324. Lunn J, Theobald HE. The health effects of dietary unsaturated fatty acids. Nutr Bull. 2006;

325. Rakhra V, Galappaththy SL, Bulchandani S, Cabandugama PK. Obesity and the western diet: How we got here. Mo Med. 2020;117(6):536.

326. Wojczynski MK, Glasser SP, Oberman A, Kabagambe EK, Hopkins PN, Tsai MY, et al. High-fat meal effect on LDL, HDL, and VLDL particle size and number in the Genetics of Lipid-Lowering drugs and diet network (GOLDN): an interventional study. Lipids Health Dis. 2011;10(1):181.

327. Chung BH, Liang P, Doran S, Cho BHS, Franklin F. Postprandial chylomicrons: Potent vehicles for transporting cholesterol from endogenous LDL+HDL and cell membranes to the liver via LCAT and CETP. J Lipid Res. 2004;

328. Nordestgaard B, Freiberg J. Clinical Relevance of Non-Fasting and Postprandial Hypertriglyceridemia and Remnant Cholesterol. Curr Vasc Pharmacol. 2011;

329. Gailliot MT, Baumeister RF. The physiology of willpower: Linking blood glucose to self-control. Personal Soc Psychol Rev. 2007;

330. Parsey CM, Bagger JE, Trittschuh EH, Hanson AJ. Utility of the iPad NIH Toolbox Cognition Battery in a clinical trial of older adults. J Am Geriatr Soc. 2021;

331. Scott EP, Sorrell A, Benitez A. Psychometric Properties of the NIH Toolbox Cognition Battery in Healthy Older Adults: Reliability, Validity, and Agreement with Standard Neuropsychological Tests. J Int Neuropsychol Soc. 2019/07/01. 2019;25(8):857–67.

332. Kuzmuk LE, Rebchuk AD, Deptuck HM, Cairncross M, Silverberg ND, Field TS. Three-month Practice Effect of the National Institutes of Health Toolbox Cognition Battery in Young Healthy Adults. Can J Neurol Sci. 2022/07/08. 2022;1–4.

333. Heaton RK, Akshoomoff N, Tulsky D, Mungas D, Weintraub S, Dikmen S, et al. Reliability and validity of composite scores from the NIH toolbox cognition battery in adults. J Int Neuropsychol Soc. 2014;

334. Graveling AJ, Deary IJ, Frier BM. Acute hypoglycemia impairs executive cognitive function in adults with and without type 1 diabetes. Diabetes Care. 2013;

335. Maran A, Lomas J, Macdonald IA, Amiel SA. Lack of preservation of higher brain function during hypoglycaemia in patients with intensively-treated IDDM. Diabetologia. 1995;

336. Mitrakou A, Ryan C, Veneman T, Mokan M, Jenssen T, Kiss I, et al. Hierarchy of glycemic thresholds for counterregulatory hormone secretion, symptoms, and cerebral dysfunction. Am J Physiol - Endocrinol Metab. 1991;

337. Majoka MA, Schimming C. Effect of Social Determinants of Health on Cognition and Risk of Alzheimer Disease and Related Dementias. Clinical Therapeutics. 2021.

Appendix

IRB APPROVAL LETTER

Institutional Review Board
210H Hullihen Hall
Newark, DE 19716
Phone: 302-831-2137
Fax: 302-831-2828

DATE:	March 1, 2021
TO:	Faria Sanjana, M.S.
FROM:	University of Delaware IRB
STUDY TITLE:	[1718585-1] Acute effects of added sugar intake from sugar-sweetened beverages on cerebrovascular function and brain integrity
SUBMISSION TYPE:	New Project
ACTION:	APPROVED
APPROVAL DATE:	March 1, 2021
EXPIRATION DATE:	February 16, 2022
REVIEW TYPE:	Full Committee Review

Thank you for your New Project submission to the University of Delaware Institutional Review Board (UD IRB). The UD IRB has reviewed and APPROVED the proposed research and submitted documents via Full Committee Review in compliance with the pertinent federal regulations.

As the Principal Investigator for this study, you are responsible for and agree that:

- All research must be conducted in accordance with the protocol and all other study forms as approved in this submission. Any revisions to the approved study procedures or documents must be reviewed and approved by the IRB prior to their implementation. Please use the UD amendment form to request the review of any changes to approved study procedures or documents.
- Informed consent is a process that must allow prospective participants sufficient opportunity to discuss and consider whether to participate. IRB-approved and stamped consent documents must be used when enrolling participants and a written copy shall be given to the person signing the informed consent form.
- Unanticipated problems, serious adverse events involving risk to participants, and all non-compliance issues must be reported to this office in a timely fashion according with the UD requirements for reportable events. All sponsor reporting requirements must also be followed.

Oversight of this study by the UD IRB REQUIRES the submission of a CONTINUING REVIEW seeking the renewal of this IRB approval, which will expire on February 16, 2022. A continuing review/progress report form and up-to-date copies of the protocol form and all other approved study materials must be submitted to the UD IRB at least 45 days prior to the expiration date to allow for the required IRB review of that report.

If you have any questions, please contact the UD IRB Office at (302) 831-2137 or via email at hsrb-research@udel.edu. Please include the study title and reference number in all correspondence with this office.

INSTITUTIONAL REVIEW BOARD

Generated on IRBNet